08822 2

1.0 2.8 2.5

3.2 2.2

3.6

4.0 2.0

1.1

1.8

1.25 1.4 1.6
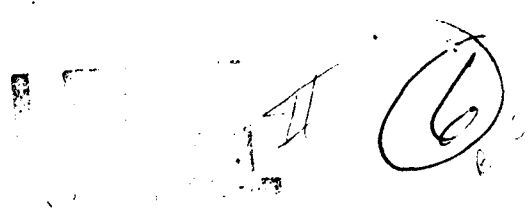
MICROCOPY RESOLUTION TEST CHART
NATIONAL BUREAU OF STANDARDS 1963 A

NSWC TR 79–325
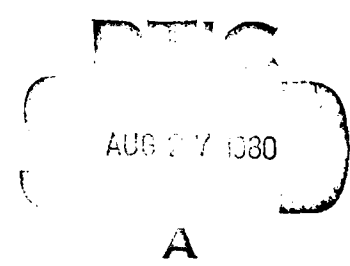
PRESSURE AND HEAT TRANSFER MEASUREMENTS ON LARGE INDENTED NOSETIPS

BY   ROBERT KAVETSKY

STRATEGIC SYSTEMS DEPARTMENT

JUNE 1979

AUG 7 1980

A

NAVAL SURFACE WEAPONS CENTER

Dahlgren, Virginia 22448 ● Silver Spring, Maryland 20910

80 8 27 006

REPORT DOCUMENTATION PAGE	READ INSTRUCTIONS BEFORE COMPLETING FORM

1. REPORT NUMBER NSWC/TR-79-325	2. GOVT ACCESSION NO. AD-A088 272	3. RECIPIENT'S CATALOG NUMBER

4. TITLE (and Subtitle) Pressure & Heat Transfer Measurements on Large Indented Nosetips.	5. TYPE OF REPORT & PERIOD COVERED Final
	6. PERFORMING ORG. REPORT NUMBER

7. AUTHOR(s) A. M. Morrison, W. C. Ragsdale, R. A. Kavetsky	8. CONTRACT OR GRANT NUMBER(s)

9. PERFORMING ORGANIZATION NAME AND ADDRESS Naval Surface Weapons Center White Oak Silver Spring, Maryland 20910	10. PROGRAM ELEMENT, PROJECT, TASK AREA & WORK UNIT NUMBERS 8N645A4; B0003 B0003, CA07QA

11. CONTROLLING OFFICE NAME AND ADDRESS	12. REPORT DATE June 1979
	13. NUMBER OF PAGES 119

14. MONITORING AGENCY NAME & ADDRESS(if different from Controlling Office)	15. SECURITY CLASS. (of this report) UNCLASSIFIED
	15a. DECLASSIFICATION/DOWNGRADING SCHEDULE

16. DISTRIBUTION STATEMENT (of this Report)

Approved for public release; distribution unlimited.

17. DISTRIBUTION STATEMENT (of the abstract entered in Block 20, if different from Report)

18. SUPPLEMENTARY NOTES

A paper on Pressure and Heat Transfer Measurements on Large Indented Nosetips was presented at the 1979 International Instrumentation Symposium.

19. KEY WORDS (Continue on reverse side if necessary and identify by block number)

Aerodynamic Heating	Tunnel Blockage
Re-entry Bodies	Thin-Skin Model
Pressure Distribution	Cone Buckling
Ablated Nosetip	

20. ABSTRACT (Continue on reverse side if necessary and identify by block number)

This report presents pressure and heat transfer data for 4 indented nosetip shapes. The tests were conducted in the NSWC Hypersonic Tunnel at Mach numbers 5 and 6. The report also presents an instrumentation technique developed as a result of a structural failure of one of the indented nosetip models.

DD FORM 1473 EDITION OF 1 NOV 68 IS OBSOLETE
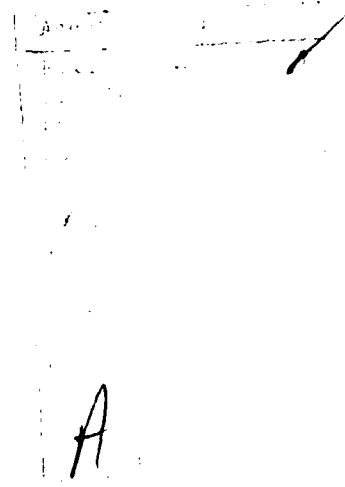1 JAN 73
S/N 0102-LF-014-6601

FOREWORD

During reentry, nosetip configurations often undergo shape changes due to ablation of the nosetip material. It is desirable to quantify pressure distributions and heat transfer rate changes for the purpose of nosetip shape change modeling and software validation.

Significant results obtained from the test program were (1) verification of heat transfer rate augmentation due to a roughened surface, (2) correlation between sharp pressure and temperature differences occurring at boundary layer attachment and separation points, and (3) observance of bimodal flow field.

R. T. RYLAND, JR.
By direction

CONTENTS

ILLUSTRATIONS

TABLES

SYMBOLS

a	Radius of plate (in.)
A	Area
A_S	Shear area (in.^{2})
A_M	Area model (in.^{2})
A_T	Area nozzle throat (in.)
C	Heat capacity of model material
C_D	Drag coefficient
C_p	Pressure coefficient
C_{pa}	Heat capacity of air in Equation (3)
D	Bending stiffness of a cylinder, $\dfrac{E t^3}{12(1 - \nu^2)}$
E	Young's modulus (psi)
F	Force (lb.)
h	Thickness of plate (in.) or cone
H	Heat transfer coefficient
L_e	Equivalent length used in cylinder analogy (in.)
M	Mach number
M_∞	Wind tunnel free stream mach number
P	Pressure (psi)
P_∞	Wind tunnel free stream static pressure
P_{CR}	Critical buckling pressure (psi)

SYMBOLS (Cont.)

P_o	Stagnation pressure
ΔP	Horizontal or vertical pressure difference
q	Load/area of plate (psi)
Q	Aerodynamic heating rate (BTU/Ft^2 sec)
Q_∞	Wind tunnel free stream dynamic pressure $= \frac{1}{2} \rho_\infty U^2_\infty$
R_1	Small radius of truncated cone (in.)
R_2	Large radius of truncated cone (in.)
R_e	Equivalent radius used in cylinder analogy (in.)
R_L	Radius of loading (in.)
Re_∞, RE/L	Wind tunnel free stream Reynolds number per foot
R_N	Radius of hemispherical nosetip
S	Distance along model surface measured from stagnation point
t	Time
T	Model wall temperature
To	Stagnation temperature
V_∞	Wind tunnel free stream velocity
X	Distance along model axis from stagnation point
Y	Radial distance from model axis
α	Angle of attack
α_c	Cone angle
δ	Model wall thickness
σ_{CR}	Critical buckling stress
σ_R	Radial Stress

SYMBOLS (Cont.)

θ	Circumferential position on model: 0° = top, 180° = bottom
ρ	Density of model material
ρ_{∞}	Wind tunnel free stream density
τ	Shear stress
ν	Poisson's ratio

PRESSURE AND HEAT TRANSFER MEASUREMENTS
ON LARGE INDENTED NOSETIPS

INTRODUCTION

This report summarizes the results of a series of heat transfer and pressure tests run in the Naval Surface Weapons Center/White Oak (NSWC/WO) Hypersonic Wind Tunnel as part of the Reentry Aerodynamics Program. The tests described here involved measurements of heating rate and static pressure at various points on the surface of five axisymmetric nosetip configurations having concave or "indented" shapes. The objective of the test program was to obtain heat transfer and pressure distributions on indented nosetip shapes for the purpose of nosetip shape change modeling and software validation.

In addition, one of the test models was destroyed during a tunnel run. Subsequent investigation of the model led to the development of an improved instrumentation technique which allowed for completion of the test series. This report also includes the results of the model analysis, rework and a description of the new instrumentation technique.

PART 1 - TEST SERIES DATA

TEST HARDWARE AND INSTRUMENTATION

The five nosetip shapes included in the test program were designated configurations A through E, and sketches illustrating these shapes are given in Figure 1. Configurations A through D are a family of related shapes which represent the effects of boundary layer transition moving forward on the nosetip, producing higher heating and ablation rates. Configuration E is based on a configuration tested in a previous program. The thin-wall transient technique was employed for measuring heating rates, and five wind tunnel models with a nominal wall thickness of 0.025 inch were machined from billets of 17-4PH stainless steel, following specifications regarding the outer contour of the models. Surface pressure taps were drilled through the model shells at 13 locations along each of two rays spaced 90 degrees apart ($\theta = 45°$, $135°$). The pressure taps were spaced 0.2 inch apart along the model surface, except toward the back of the model, where the spacing was increased to as much as 1 inch. Additional taps were located on the top and bottom rays ($\theta = 0°$, $180°$) near the rear of the model, and two taps were similarly located on the sides of the model ($\theta = 90°$, $270°$). These last two sets of pressure taps were provided for the purpose of measuring pressure differences in the horizontal and vertical planes in order to check the alignment of the model with the wind tunnel flow. Stainless steel tubing with an inside diameter of 0.046 inch was brazed to the model shell at the pressure tap locations, and was smoothed after brazing to match the model contour.

Strain gage pressure transducers were used to measure the model surface pressures. The transducers were mounted in a transducer bank outside the wind tunnel and connected to the model pressure taps via roughly 15 feet of tubing. Pressure response calculations indicated this arrangement would be adequate for measuring steady or average pressures. Such an arrangement is, of course, not suitable for measuring the pressure fluctuations that occur on some concave nosetip shapes.

Thermocouples were welded to the inner surface of the models at locations corresponding to the pressure tap locations. The thermocouples were located along two rays 90 degrees apart, opposite the two rows of pressure taps ($\theta = 225°$, $315°$), and one additional thermocouple was located at the stagnation point. All thermocouples were 36-gage fiber glass insulated Chromel-Alumel and were connected to a $150°F$ reference junction box.

The outer contour of each model was checked after the models were finished by measuring the axial and radial coordinates at the center of each pressure tap, using the stagnation point as a reference point. The thickness of the model shell was measured at each thermocouple location.

Prior to testing, all five models were roughened over the indented region between the edge of the hemispherical nosecap and the start of the 7-degree conical aft section by grit blasting. A nominal roughness height of 3 mils was desired on this part of the model, and some experimentation with grit size and air pressure led to the use of No. 12 chilled iron grit with an air pressure of 60 psi to obtain approximately this roughness. With the exception of model D, the models were roughened over the entire indented region. Model D was roughened only over the bottom half of the indented region. Photographs of models B through E after roughening are shown in Figures 2 through 5, respectively. Roughened samples of 17-4PH stainless steel were sectioned and photomicrographs were made of the sections at a magnification of 100. Traces of the roughened surface, taken from these photomicrographs, are shown in Figure 6. Using these traces, the mean roughness height was determined to be in the range of 2 to 2-1/2 mils.

Nosetip model A was destroyed in a wind tunnel accident which occurred during the first attempt to test this configuration. Breakdown of supersonic flow in the wind tunnel and structural failure of the model shell both occurred during the accident. The accident and subsequent investigation will be covered in a later section.

TEST CONDITIONS AND TEST PROCEDURE

Nosetip model D was tested successfully at the following nominal test conditions:

Mach Number = 5
Angle of Attack = 0 deg.
Supply Temperature = 500°F
Supply Pressure = 1000, 1400 psia
Free-Stream Reynolds No. = 23.31 million per ft

The original plan was to test the remaining four configurations at these nominal conditions. However, model A was not rebuilt following the tunnel accident and, hence, was never tested. Prior to testing configurations B, C, and E, blockage tests were run at Mach 5 with the dummy model of configuration B. Supersonic flow could not be maintained at Mach 5 with this model due to blockage effects and, consequently, the remaining tests could not be run at the desired test conditions.

Following the Mach 5 blockage tests, the Mach 5 Hypersonic Tunnel nozzle was replaced with the Mach 6 nozzle, which has a larger cross sectional area, and the blockage tests were repeated. Satisfactory flow was maintained at Mach 6, indicating the remaining tests could be run at this Mach number. The nominal test conditions for models B, C, and E were as follows:

Mach Number = 6
Angle of Attack = 0 deg.
Supply Temperature = 450-500°F
Supply Pressure = 600, 1000, 1700 psia
Free-Stream Reynolds No. = 10, 20, 26 million per ft

The same procedure was used for all tests. During tunnel startup, the model was kept in a retracted position in the tunnel test cell and was semi-enclosed in a cooling box and blanketed by compressed air to avoid any heating by currents of tunnel air circulating inside the test cell. When the desired test conditions were achieved, the model was injected into the open jet test rhombus at the end of the wind tunnel nozzle and was exposed to the tunnel free stream for a period of 5 to 10 seconds. The model was then retracted into the cooling box and the tunnel shut down. Between runs, the model was cooled to approximately room temperature. The wind tunnel data recording system was turned on just before model injection and data were recorded at a rate of 25 samples per second until the model was retracted from the flow. The test time of 5 to 10 seconds was more than sufficient to obtain both pressure and aerodynamic heating data. Two to four Schlieren photographs were taken during each run while the model was in the wind tunnel flow.

DATA REDUCTION

PRESSURE DATA. For each test, plots of pressure versus time were generated on the computer for all of the measured surface pressures. These plots were examined to determine which portion of the data record to use for calculating the average values of pressure which have been reported. In the data reduction program, pressure ratios (P/P_∞) and pressure coefficients (C_p) were computed for each line of data, based on the wind tunnel supply pressure for that particular line, and were averaged over the portion of the data record used to obtain the average pressures. The wind tunnel supply pressure and temperature reported with the pressure data are average values over the same portion of the data record.

The vertical and horizontal pressure differences reported along with the pressure data were arrived at by examining plots of these pressure differences versus time. It was necessary to use some judgment to obtain a final value, since the pressure differences did not stabilize as well as the other measured surface pressures. An experimental calibration of pressure difference versus angle of attack was not obtained. An approximate relationship for estimating the pitch and yaw angles from the pressure differences is as follows:

$$\frac{\Delta P}{Q_\infty} = 0.016 \text{ per degree of pitch or yaw} \qquad (1)$$

where,

   ΔP = horizontal or vertical pressure difference
   $Q\infty$ = wind tunnel free-stream dynamic pressure

This was obtained from tables of pressure ratios for sharp and blunt cones at angle of attack. The signal conventions used in the pressure difference data are as follows:

   1. Positive vertical pressure difference indicates model nose <u>up</u>.

   2. Positive horizontal pressure difference indicates model nose <u>right</u>, looking upstream.

   HEATING RATE DATA. Heating rates and heat transfer coefficients were computed from the usual heat balance equation used with the thin-wall model transient technique:

$$\rho\ C\ \delta\ \frac{dT}{dt} = Q = H\ (To-T) \tag{2}$$

where,

   ρ = density of model material
   C = heat capacity of model material
   δ = wall thickness
   t = time
   T = wall temperature measured by backface thermocouple
   Q = aerodynamic heating rate
   H = heat transfer coefficient, based on $\Delta T=(To-T)$
   To = stagnation temperature = wind tunnel supply temperature

   The wall thicknesses used in the data reduction should be accurate to +0.001 inch. The density of 17-4PH stainless steel is known accurately and heat capacity measurements have been made on a number of samples of this material in prior investigations. A table of heat capacity versus temperature has been compiled from these measurements for use in the data reduction for heat transfer tests.

   Values of the temperature-time derivative were determined by curve fitting the recorded wall temperature versus time data, in most cases with second-degree polynomials. In some cases, exponential curve fits gave better results, and they were used in the final data reduction. Past experience has shown that a range of values for the temperature-time derivative at a given point in time in the data record can be obtained, depending on how many data points are included in the curve fit and where the particular point in question lies within the set of points included in the curve fit. The current practice in data reduction is to generate a number of values of the derivative at each point in time by varying the number of points included in the curve fits and the point in time where the curve fit starts. The first curve fit in a set of fits is started at the point where the temperature begins to increase during model injection. The next curve fit is started one point later in the record, and so on for a specified number of fits. In the data reduction reported here, 13 25-point fits, 10 20-point fits

and 7 15-point fits were generally used. A value of the heat transfer coefficient is calculated at each point along each of the curve fits and from the resulting set of values a "best" value is selected at each point in time. Usually, a number of the curve fits will give close to the same value of h at a given point in time, and the "best" value of h is obtained by averaging these results.

An accurate value of H at the point of initial heating cannot be obtained directly from curve fits which start at that point. This is due to the fact that the model is not exposed instantaneously to the wind tunnel free stream, but takes some finite time to traverse the tunnel boundary layer, and also due to the initial effects of conduction across the model wall and along the thermocouple wires. The data reduction procedure attempts to circumvent these errors by fitting curves through the "best" H values, starting at various points in time, and extrapolating these curves to obtain a final value of H at the point of initial heating. A procedure for doing this is included in the computer program, but in some cases, a final value selected by "eyeball" judgment from a plot of all computed H values versus time has been used rather than the computer-selected value. Plots of H values versus time and "best" H values versus time are illustrated in Figure 7. The results shown cannot be considered typical - in some cases the H values were less scattered than in this record and in other cases the scatter was worse.

The trend of H values with time, which is apparent in Figure 7, is thought to be due to lateral conduction along the model wall. In areas of low heating rate, H usually increased with time, indicating heat conduction into these areas. In areas of high heating rate, H usually decreased with time, indicating heat conduction out of these areas--although in some cases an initial increase of H with time was noted, as in Figure 7. The technique of data reduction used here is intended to minimize the effects of initial errors, which decrease with time, as well as the effect of lateral heat conduction, which increases with time. This method was originally developed by Fitzsimmons, et.al.[1] and has been used at NSWC for a number of years.

The final H values selected were used to compute final values of the initial heating rate, Q, and a dimensionless Stanton number, defined as follows:

$$St = \frac{H}{\rho_\infty U_\infty Cpa} \tag{3}$$

where:

ρ_∞ = wind tunnel free-stream density
U_∞ = wind tunnel free-stream velocity
Cpa = heat capacity of air = .24 Btu/lb°F

---

1. Nagel, A. L., Fitzsimmons, H. D. and Doyle, L. B., "Analysis and Hypersonic Pressure and Heat Transfer Tests on Delta Wings with Laminar and Turbulent Boundary Layers," NASA CR-535, Appendix A, Aug 1966.

The wind tunnel supply pressure and temperature used in the heat transfer data reduction were averaged over the short period of time (less then 1 second) during which the model was injected. These values may differ slightly from those reported with the pressure results which were obtained by averaging over a different part of the data record.

DATA AND RESULTS

A log of test conditions for all the heat transfer and pressure tests is given in Table 1. The test conditions reported here are those used in the heat transfer data reduction.

Plots of pressure coefficient versus distance, S, measured along the model surface from the stagnation point (wetted length) are given in Figures 8(a) through 8(n). The locations of the first and second corners on the models have been indicated on these plots.

Plots of the dimensionless Stanton number versus distance along the model surface, S, are given in Figures 9(a) through 9(1).

Schlieren photographs taken during the tests are shown in Figures 10(a) through 10(1). The Schlieren photographs taken during run 4 were of poor quality and have not been included in Figure 10.

During run 10 with nosetip model C and run 12 with nosetip model E an abrupt change occurred in the flow field on the model after about 1 to 2 seconds of exposure. Consequently, 2 sets of pressure data have been included in Figure 8 for each of these runs. Two Schlieren photographs for run 10 are included in Figure 10. Only one set of aerodynamic heating data are reported for these tests, since the technique used here gives the heating rate only at the start of heating.

DISCUSSION

PRESSURE DATA. The accuracy of the pressure transducers used in the test program is considered to be $\pm 1/10$ percent of their rated pressure range when carefully calibrated. Transducers having a range of 100 psia were used for measuring all pressures except at the three most aft locations on the models. The last two pressure taps were on the 7-degree conical section and the next tap was close to the end of the shoulder and beginning of the 7-degree conical section. Pressures at these three locations were relatively low and, consequently 25 psia transducers were used.

The variations in the measured pressure coefficients from run to run on the hemispherical part of the models near the stagnation point were examined and it was concluded that a figure of $\pm 1/2$ percent of the rated range of the transducers would be a more reasonable estimate of the accuracy of the test data. Sources of experimental error other than transducer calibration errors are obviously significant. The experimental pressure coefficients on the hemispherical part of model B are plotted in Figure 11 to illustrate the run to run variation in Cp values. These variations are about the same for the model E data, but somewhat larger for the model C and model D data. A Newtonian pressure distribution

15

has also been shown to illustrate that the measured pressures on the hemispherical part of the models decreased much more rapidly than corresponding Newtonian values.

The readings of ΔP in the horizontal and vertical directions taken during the tests were somewhat erratic and tended to drift or shift during some of the tests. Values of flow angularity computed from the ΔP values should be regarded as very approximate with uncertainties as high as ± 100 percent. The ΔP values could have been affected by nonuniformities in the flow fields other than those due to angle-of-attack.

The instrumentation for pressure measurements was not intended for measuring oscillating pressures. Nevertheless, oscillations were detected in the pressures on model C between $S = 1.8$ inches and $S = 4.2$ inches, and on model D between $S = 2.2$ inches and $S = 4.6$ inches. No oscillations were detected on models B and E. Due to the damping effect of the long tubes between the models and transducers and the limited data sampling rate, the pressure data obtained here are not suitable for determining the amplitude or frequency of these pressure oscillations.

The plotted pressure data shown in Figure 8 indicate that flow separation occurred at the first corner on models D and E. In the Schlieren photographs from the tests made with these models, the density gradients in the separated free shear layers are clearly visible. The pressure data and Schlieren photographs indicate that on models B and C the boundary layer remained attached around the first corner, but separated a short distance behind the corner. In the zone of recompression between the first and second corners, peak pressures occurred somewhat ahead of the second corner, except in the case of model E where the pressure was nearly constant along most of the conical portion of the model ahead of the second corner. This plateau value of the pressure coefficient on model E was very close to the value for a sharp cone with the same vortex angle ($47°$).

As mentioned previously, an abrupt change in the flow field occurred during run 10 with model C and during run 12 with model E. The 2 Schlieren photographs included in Figure 10 for run 12 indicate that the flow field was initially axisymmetric with boundary layer separation occurring downstream of the first corner (Fig. 10(f)). During the run, however, separation moved upstream to the corner on the upper portion of the model, producing a non-symmetrical flow field which persisted until the end of the run (Fig. 10(g)). This non-symmetrical separation affected the pressures along the upper row of pressure taps as shown in the two sets of pressure data included for this run (Figs. 8(g), (h)). In run 12 with model E, the boundary layer remained attached around the first corner initially, and then separation moved to the corner during the run. In both cases the flow field was axisymmetric as indicated by the Schlieren photograph (Fig. 10(k)) and pressure data (Figs. 8(l), (m)). A good Schlieren photograph of the final flow field was not obtained in this run, but the pressure data indicate the final flow field was identical to that obtained in runs 11 and 13.

Drag coefficients were computed for nosetips B, C, D, and E using the pressure data from runs 5, 8, 1, and 11, respectively. These results are given in the table below:

Configuration	Pressure Drag Coefficient
B	1.01
C	1.04
D	1.06
E	0.90

AERODYNAMIC HEATING DATA. Since aerodynamic heating rates are obtained by evaluating slopes from experimental data, as discussed in the previous section, accuracies comparable to those obtained in force or pressure measurements are not expected. Past experience indicates that with the technique used here for measuring heating rates accuracies of roughly ±10 to 15 percent can be obtained as a general rule. A comparison of some measurements of laminar heating on a hemispherically blunted cone with theoretical values is shown in Figure 12. These data were obtained with hardware and data reduction methods similar to those used in this test program.

An effort was made to compare the stagnation point heating rates measured in the tests reported here with predictions obtained from the Fay and Riddell equation. In general, agreement within ±25 percent was found, but the comparisons were not considered satisfactory because an accurate determination of the velocity gradient at the stagnation point could not be obtained directly from the experimental pressure data. A better approach would be to first correlate the pressure data for the hemispherical portion of the models, perhaps with the method of Stallings and Campbell[2], and then use the correlation to obtain the stagnation point velocity gradient.

The plotted heat transfer results shown in Figure 9 indicate that the heating rate increased substantially just downstream of the first corner on models B and C, where the boundary layer remained attached. This increase in heating must have been due to boundary layer transition since the roughened area of the model started at the first corner and should have been sufficient to trip the boundary layer. A drop in the heating rate is noted near the point where boundary layer separation can be seen in the Schlieren photographs for models B and C. The heating rates rise again in the recompression zone reaching a peak value at the start of the second corner.

The heating rate data for models D and E show a sharp decrease at the first corner, where boundary layer separation occurred, followed by a rapid rise in the recompression zone. The heating rate on model E reaches a plateau on the conical part of the model ahead of the second corner, similar to the surface pressure.

---

2. Stallings, R. L. Jr. and Campbell, J. F., "An Approximate Method for Predicting Pressure Distributions on Blunt Bodies at Angle of Attack," AIAA Paper No. 70-208, Jan 1970.

In all cases, peak heating rates were attained just ahead of the second corner. It is interesting to note that heating rates on model D were about the same on the smooth side as on the rough side. This indicates that turbulent conditions were achieved over the entire indented region even without the tripping effect of the roughened part of the model.

COMPARISON OF PRESSURE AND HEATING DATA WITH PREDICTION METHODS USED IN SHAPE CHANGE CODES

A comparison is shown in Figures 13(a)-(d) and 14(a)-(d) of the aerodynamic heating and pressure data, respectively, from the wind-tunnel tests with predictions from two of the shape change computer codes used at NSWC. The data shown are from the highest Reynolds number test condition for each of the four configurations tested: B, C, D and E. Predicted values of aerodynamic heating and surface pressure were obtained from the NOHARE computer code developed by PDA, Inc.[3] and the ASCC code developed by Aerotherm/Accurex Corporation[4]. The aerodynamic heating comparisons are made on the basis of the dimensionless Stanton number, St, based on the freestream density and velocity and the stagnation enthalpy.

The prediction methods used in the two computer codes are nearly identical. Pressures are predicted by modifications of Newtonian theory. On the hemispherical nosecap a method developed by Love[5] and improved by Dahm and Anderson[6] is used. Both codes employ integral boundary layer methods to compute aerodynamic parameters and both use empirical methods to predict the effect of surface roughness on heating. The NOHARE code incorporates a procedure for predicting the effect of flow separation ahead of forward facing steps, which was not applicable in this case. Consequently, neither code could predict the effect of the flow separations which occurred on all of the configurations tested. In the comparison of Stanton numbers both rough wall and smooth wall predictions from the ASCC code are shown, whereas only the smooth wall values from the NOHARE code are shown.

The following observations are made regarding these comparisons:

1. Both pressure and heating predictions are in good agreement with the data in the hemispherical nosecap region.

---

3. Smoth, D. H., et. al., "Computer Codes for Nosetip Recession and In-depth Thermal Analysis: NOHARE, NOSEC, NODGEN," PDA, Inc., TR 5002-00-01, Jan 1976.

4. Abdett, M. J., et. al., "PassiveNosetip Technology (PANT II) Program, Vol. II Computer User's Manual: ABRES Shape Change Code (ASCC)," Acurex Corporation/Aerotherm Division, Final Report 76-224, Oct 1976.

5. Love, E. S., et. al., "Some Topics in Hypersonic Body Shaping," AIAA Paper No. 69-181, 1969.

6. Moyer, C. B., et. al., "A Coupled Computer Code for the Transient Thermal Response and Ablation of Non-Charring Heat Shields and Nosetips," Aerotherm Corporation, NSAS CR-1630, Oct 1970.

2. Predicted pressures are in poor agreement with the data over the entire indented portion of the nosetip. The effect of boundary layer separation and reattachment must be estimated in order to get reasonable predictions of surface pressure. However it is noted that on at least part of the aft conical portion of nosetips B and E, the surface pressure is quite close to that on a sharp cone.

3. Except for model C, the ASCC predictions of heating rates near the aft shoulder, taking into account the effect of roughness, are in surprisingly good agreement with the data. This is also true in the case of the smooth wall data and predictions for model D.

4. Agreement between the heating data and predictions over most of the indented portion of the nosetips is quite poor.

5. Comparison of the pressure and heating data in the indented region indicates that a simple correlation between the heating rate and pressure cannot be obtained for all of these configurations.

PART 2 - MODEL FAILURE - ANALYSIS AND MODIFICATION

BACKGROUND

The configuration designated D was installed in the wind tunnel and checked out for testing. As mentioned previously, this model was grit blasted over the bottom half of the concave section.

Configuration D was tested using the axisymmetric Mach 5 nozzle in the Hypersonic Tunnel. A preliminary wind tunnel run was made to check out the operation of the wind tunnel with a recently installed particle separator and to obtain Mach number calibration data from Pitot pressure measurements. Tunnel operation was satisfactory and indicated a maximum operating pressure of 1400 psia with the particle separator. Mach number calibration data were obtained and agreed closely with previous calibrations.

Two tests were run with configuration D on 14 April. The first test was run at 1400 psia supply pressure and 500°F supply temperature. The model was injected into the flow at 0 degrees angle of attack after these running conditions had been obtained and was retracted from the flow after about 10 seconds of exposure, during which time the heat transfer and pressure data were recorded. During this run, 4 of the 27 thermocouples failed, but all of the failures occurred after the heat transfer data were obtained. A second test was run at 1000 psia supply pressure and 500°F supply temperature. Again, the model was injected into the flow after these conditions were obtained, and pressure and heat transfer data were recorded for approximately ten seconds. During the period of data acquisition, five pressure tubes and three thermocouples failed.

Following the period of data acquisition for the second wind tunnel run, the model was left in the tunnel flow while the tunnel pressure was lowered to 500 psia; at this pressure it was intended to record some additional pressure data concerned with the alignment of the model with respect to the wind tunnel flow. At a pressure close to 500 psia, a breakdown of the supersonic flow in the wind tunnel test section occurred. The high pressures acting on the model as a result of this flow breakdown buckled the model shell slightly, but the model remained intact. The model was withdrawn from the tunnel flow, and the tunnel shut down immediately following the flow breakdown, but the rise of pressure and resulting damage to the model were practically instantaneous. All pressure tubes and all but four of the thermocouples were broken during the run. Most of this damage occurred toward the end or after the period of data acquisition; however, good pressure data were obtained from all tubes. Good heating data were obtained from all but 5 thermocouples, 4 of which had failed during the first wind tunnel run.

21

Schlieren photographs taken during the wind tunnel tests at 1400 and 1000 psia revealed a compressed test rhombus, but the entire model was within the rhombus. The model nosetip was located 3-1/2 inches aft of the nozzle exit plane during these two tests. Sample Schlieren photographs are presented in Figures 10(h) and 10(i).

The pressure data taken during the tests with configuration D indicated oscillating pressures over the concave portion of the model. However, the test data do not indicate the true amplitude of the oscillations. It seems likely that the oscillating pressures were resulting in a severe vibration which led to the failure of most of the thermocouples and pressure tubes during the second wind tunnel run. Photographs of the damage to configuration D are presented in Figures 15 and 16. Broken heat transfer gage leads and broken pressure lines can be seen through the rear opening of the model.

An attempt was made to test configuration A at 1400 psia supply pressure and 500°F supply temperature. After studying the Schlieren photographs for the configuration D tests, it was decided to move the nosetip of model A to a point 2 inches aft of the nozzle exit plane in order to move the model base further from the edge of the test rhombus. The model was injected into the tunnel flow after the run conditions had been obtained, and a breakdown of supersonic flow in the test section occurred immediately. The glass window on the west side of the tunnel was broken and debris blown out through the window did extensive damage to the Schlieren bench and mirror on that side of the tunnel. Two fragments of the model were found outside the tunnel and the remainder in the bottom of the test cell. The model support and sting support remained intact in the tunnel.

Pressure and heat transfer data were recorded during the attempt to run configuration A. The pressure data indicate pressures between 100 and 200 psia, but the readings are beyond the rated range of the 100 psia pressure transducers, and are probably not accurate. No Schlieren photographs were taken during this run.

INCIDENT INVOLVING CONFIGURATION D MODEL

Model D was successfully tested at P_0 = 1400 psia and again at P_0 = 1000 psia. After the second test the supply pressure was reduced while the model remained in the flow. The supersonic flow field broke down at $P_0 \approx 500$ psia. Tunnel exhaust during these series was directly to the atmosphere.

Schlieren photographs taken at P_0 = 1400 and 1000 psia indicate that the flow was normal and that no excessive blockage existed for Model D. The test rhombus shocks indicate the ratio of the test cell pressure to the test jet static pressure to be approximately 2. This is well below the value required to break down the flow (approximately 3.5 for a Mach 5, turbulent boundary-layer nozzle), Figures 17 and 18.

The most likely cause of the supersonic flow field breakdown at P_O = 500 psia was an excessive diffuser back pressure. This pressure is controlled by the tunnel exhaust system. At Mach 5 at P_O > 500 psia adequate diffuser back pressure can be maintained by exhausting directly to the atmosphere. At lower P_O values the exhaust is normally redirected to the BBC pumps and the vacuum spheres by opening a 3-foot-diameter valve. Operation of the tunnel at decreasing supply pressures at values near 500 psia is difficult and occasionally results in a breakdown of the supersonic flow field since the BBC pumps cannot handle air mass flows at P_O > 500 and the vacuum valve cannot be opened at pressures much above 500 psia. During this run the vacuum valve was still closed and the exhaust ran to the atmosphere.

In order to determine what loads would be required to cause a buckling failure of the model the following approximate calculation was made:
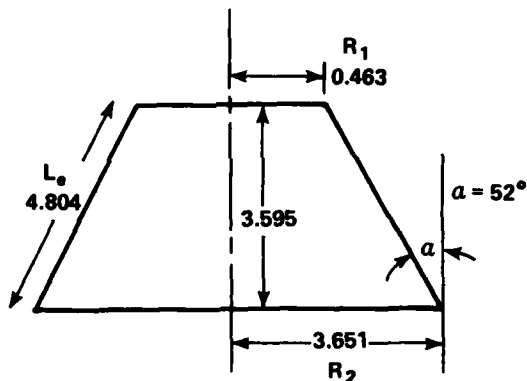
First represent the test nose configuration as a cone-cone model. Consider the fore-cone:

$$R_e = \frac{R_1 + R_2}{2 \cos \alpha}$$

$$= \frac{.463 + 3.651}{2 \cos(52°)} = 3.341$$

$$Z = \frac{L_e^2}{R_e h} (1 - \nu^2)^{1/2}$$

$$= \frac{(4.804)^2}{(3.341)} \frac{(.91)^{1/2}}{.025} = 264$$

The critical buckling stress for this section is;

$$\sigma_{CR} = K_p \ D \left(\frac{h}{Le} \right) \frac{R_2}{R_e \cos \alpha} \tag{4}$$

and the critical buckling pressure,

$$P_{CR} = \frac{\sigma_{CR} \ h \cos \alpha}{R_2} \tag{5}$$

Substitution of σ_{CR} from equation (4) into equation (5) yields,

$$P_{CR} = K_p D \left(\frac{h}{Le} \right)^2 \left(\frac{R_2}{R_e \cos \alpha} \right) \left(\frac{h \cos \alpha}{R_2} \right) \tag{5a}$$

$$= K_p \ D \ \frac{h^3}{L_e^2 R_e}$$

From Reference 7; (Figure 8.28) for

$$Z = 264, \ K_p = 18$$

$$P_{CR} = 18 \left[\frac{\pi^2 (25 \times 10^6)}{12(.91)} \right] \frac{(.025)^3}{(4.804)^2 (3.341)} = 82 \ psi$$

where (25×10^6) represents a modulus of elasticity degraded to account for temperature effects.

7. Bruhn, E. F., <u>Analysis and Design of Flight Vehicle Structures</u> (Tri-State Offset Company, Jan 1965).

The critical buckling pressure for the fore-cone section is 82 psi. Next, consider the aft-cone:
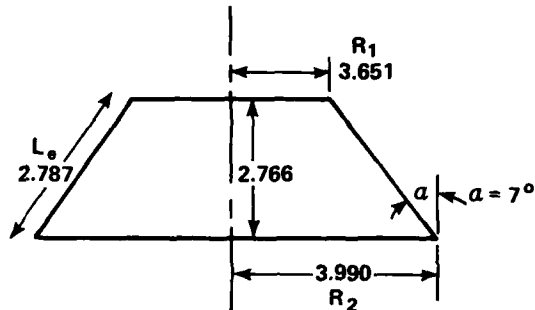
Assume axial compressive loading on aft-cone

$$R_e = \frac{3.651 + 3.99}{2 \cos(7^\circ)}$$

$$= 3.849$$

$$\frac{L}{R_e} = \frac{2.787}{3.849} = .724$$

$$\frac{R_e}{h} = \frac{3.849}{.025} = 154$$

Again from reference 7, for $\frac{R_e}{h} = 154$ and $\frac{L}{R_e} = .724$, Figure C8.25 yields,

$$\frac{\sigma_{CR}}{E} \times 10^3 = 2.3$$

$$\sigma_{CR} = \frac{(25 \times 10^6)(2.3)}{10^3}$$

$$= 57,500 \text{ psi}$$

Using equation (5) results in the following;

$$P_{CR} = \frac{\sigma_{CR} h \cos\alpha}{R_2} = \frac{57,500(.025)(.993)}{3.99} = 358 \text{ psi}$$

25

During the high Reynolds number run, the model was subjected to oscillating pressures with a mean value of 80 psi. The curvature of the fore-cone of configuration D would have increased the buckling strength of the fore-cone over the 82 psi critical buckling strength calculated for the cone-cone approximation. However, it must also be remembered that half the surface of configuration D was grit blasted. This process removed 10-20 percent of the .025-inch-thick surface which would weaken the fore-cone in buckling. Therefore, it is concluded that, at best, the model was marginal in buckling in the high Reynolds number flow field, and that the high loads imposed on the model when the supersonic flow field broke down caused the model to buckle.

The calculations performed above for model D indicate that a loading of 82 psi would cause a cone-cone approximation of the models to buckle. Model A would have been weaker than model D due to its forebody shape. However, as model D survived a run at the high Reynolds number condition, it seems likely that model A should also have survived.

A comparison was made of the wall thickness measurements for models A and D. These measurements which were made before grit blasting, indicated that Model D's wall thickness was always .025 inch or greater. Model A was found to be less thick than .025 inch in several locations, in fact, a minimum thickness of .0205 was recorded. The minimum thickness area is critical from a structural standpoint. When the entire surface of model A was grit blasted the wall thickness was decreased by 10-20 percent. It is felt that after sand blasting the weak section could have failed upon injection into the supersonic flow field. This failure would have caused asymmetries in the model shape which would induce asymmetric forces and moments. Calculations were made to determine if such forces and moments could have caused the model to shear off its supporting bolts as was indicated by the recovered model parts.

NOTE: When supersonic flow is established in a wind tunnel, a starting shock moves down the tunnel nozzle, through the working section, and into the diffuser section. The flow behind the shock is supersonic. The flow ahead of the shock is subsonic. There are large changes in pressure, temperature, and density across the shock. In order to avoid the high loads that would be imparted to the model if the starting shock were to hit it, the tunnel is started with the model out of the flow. The model is then injected into the flow after supersonic flow is established. When supersonic flow breaks down, the starting shock moves from the diffuser through the working section and into the tunnel nozzle in an uncontrolled manner. When the shock impacts the wind tunnel model, large loads are experienced by the model.

Screw Types: N02-S6NC-2, stress area = .00370 in.^{2}

                      SOC HD CAP N05-40NC-2X .31126

                      8 REQ'D - stress area = .00796 in.^{2}

Screws are stainless steel with an ultimate strength = 100,000 psi.

NOTE: Screws were soft material, inner core hardened to a Rockwell
        coefficient of 15-18.

Ultimate strength = 100,000 psi

Shear = .57 ultimate strength = 57,000 psi

Force to exceed shear strength is obtained as:

$$F = \tau \times A_S$$

$$A_S = 8(.00796) + 8(.00370) = .09328 \text{ in.}^2$$

$$F = (57,000)(.09328) = 5320 \text{ lb}.$$

If pressures measured during the configuration D model tests are assumed to act
over half of the model A fore-cone, forces can be generated of sufficient
magnitude to cause the mounting bolts to fail.

INCIDENT INVOLVING CONFIGURATION A MODEL

The configuration A model has a higher bluntness and a sharper conical
forward section than the configuration D model. This implies that the configura-
tion A model would have larger effective tunnel blockage (tunnel blockage depends
on model drag, projected model frontal area, and model position in the test
rhombus), would be weaker in buckling than the configuration D model (a conical
surface is weaker in buckling than a curving indented surface) and the entire
fore-cone was grit blasted. Also, the axial position of the configuration A model
relative to the diffuser inlet was about two inches forward of the configuration
D position. As no Schlieren photographs were taken before the failure, the affect
of the position change cannot be investigated. Pressure and temperature data
were recorded during the model injection. These data do not show the conditions
which should have existed if the flow were normal for any length of time. That
is, if the model had proceeded, intact, into the established supersonic flow field,
the heat-transfer and pressure data should have been approaching a steady-state
condition. The existence of this steady-state condition would have been expected
before the model was far enough into the flow field for its blockage to signifi-
cantly effect the flow. Based on the degree of blockage indicated by the
Schlieren photographs of model D, Figure 10(i) it does not seem likely that the
configuration A model would have caused the supersonic flow field to break down
before the model entered the flow fully, and before some steady-state readings
in pressure and heat-transfer were recorded. It seems more likely that the model
failed structurally when exposed to an asymmetric loading during injection. Both
possibilities were investigated.

BLOCKAGE

Drag coefficients were computed for two of the nosetip models for the purpose of computing blockage parameters for these models.

An experimental pressure distribution was available for computing the forebody pressure drag of configuration D, since this configuration had been tested successfully. Pressure distributions for all the configurations were computed by Mr. Hensel Brown using the Grumman Aircraft inviscid flow field code. The computed pressure distribution was used to determine the forebody drag coefficient for configuration A.

The results of these calculations were as follows:

$$\text{Configuration A} \qquad C_D = 1.04$$

$$\text{Configuration D} \qquad C_D = 1.06$$

The experimental and computed pressure distributions for configuration D were in reasonably good agreement, indicating that the calculated drag coefficient for configuration A should also be a reasonably reliable value.

All indications are that configurations A through E have almost the same drag. As can be seen, the drag coefficients for A and D are almost identical, and these two configurations represent the extremes of model shape. Furthermore, the computed pressure distributions for all the configurations are very similar.

The data used in establishing the method used for determining tunnel blockage was for relatively high Mach number conditions. The incident under consideration was for a lower Mach number than the data base.

$$\text{Blockage Parameter} = C_D \left(\frac{A_{model}}{A_{core}} \right) \qquad (6)$$

Model A

$$\text{Blockage Parameter} = 1.04 \left(\frac{50.3}{227.15*} \right) = .23$$

Model D

$$\text{Blockage Parameter} = 1.06 \left(\frac{50.3}{227.15*} \right) = .23$$

Experience at Mach 17 indicates that a blockage parameter of about .185 is maximum before flow breakdown. However, model D did not break flow at the high Reynolds number condition but did at the low. Based on this analysis one would assume that the models are marginal from the blockage standpoint.

---

*Neglects boundary layer

A second technique for determining blockage effects was obtained from Reference 8. A curve is presented which is described as the upper limit of model area to test section area as a function of Mach number in Figure 19. Any points above the curve will cause flow to break down. It was determined that a diffuser calculation assuming the core area is the actual core area minus the model area was made to determine the curve. The diffuser calculation was made for Mach numbers of 2, 3, and 5 to verify this. The results of these calculations are shown as triangles in Figure 19. A sample calculation is given below:
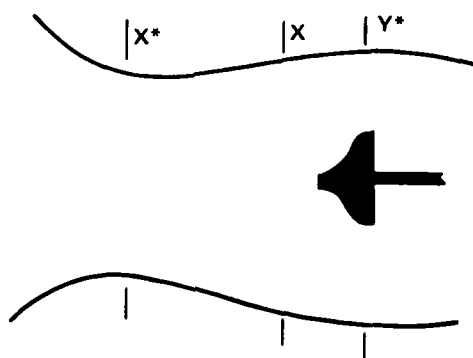
Minimum area calculation (Reference 9) T-8, Mach No. = 5.

$$\frac{A_x}{A_y^*} = \frac{A_x}{A_x^*} \frac{P_{oy}}{P_{ox}} \tag{7}$$

$$= (25)(.06172)(\text{Reference 10})$$

$$\frac{A_x}{A_y^*} = 1.543$$

8. NAVORD Report 1488, Vol. 6, Sec. 20, 1961.

9. Shapiro, A. M., <u>Dynamics and Thermodynamics of Compressible Fluid Flow</u> Vol. I (Tye Ronald Press Company, New York, NY, 1953).

10. NACA Report 1135, Equations, Tables, and Charts for Compressible Flow, 1953.

$$A_y^* = 162.022$$

$$A_m = 87.978$$

$$\frac{A_m}{A_t} = 0.352$$

The Figure 19 curve is then an upper-bound curve as it is for a closed-jet wind tunnel and for ideal conditions. That is, the curve represents the minimum starting area for a tunnel with no model. The presence of the model and its shock structure represent a worse condition. Experimental data are also presented (circular symbols) in Figure 19. These data are for a particular wind tunnel and are representative of the largest disk which could be placed in the tunnel and still allow the tunnel to start. As expected, these data fall below the upper-bound curve. The curve drawn through the points was extrapolated out to the Mach 5 condition. The indented nosetip data point is represented as a square in Figure 19. Compared to other experimental data, the point appears marginal. The fact that Tunnel 8 is an open-jet facility would make blockage leading to flow breakdown appear unlikely.

Reference 11 indicates that while correlations of the types just discussed are useful for planning, the only true test of blockage for marginal cases is to build a blockage model and test it in the nozzle under consideration as every nozzle is different.

As a result of this exercise, it was concluded that model blockage effects probably did not cause the breakdown of the supersonic flowfield during the model A incident. If the model failed upon injection, a flat 8.5-inch-diameter model-supporting disk would have remained in the test position. This would definitely have prevented a normal, fully expanded flow through the nozzle. It is estimated that a test cell pressure of about 1.5 atmospheres would exist in the test cell and the nozzle. The flow in the nozzle then would expand to a Mach number of 3.4 and a jet diameter of about 8.4 inches. Passing through a series of shock and expansion waves, this jet would decelerate to about Mach 2 and impinge on the flat disk where it would spread radially against the walls and the windows of the test cell. It is estimated that a pressure of about 100 psia would be asserted on the door windows, which are about 15 inches from the edge of the jet (Fig. 20).

The impingement jet problem could be avoided in future tests by employing a conical fixture mounted on the support sting, such that if the model were to be torn away, the cone would remain exposed to the flow instead of a flat plate. This would ensure a more orderly progression of the flow by the sting, and greatly reduce the chance for formation of an impingement jet or a breakdown of the supersonic flow field.

---

11. Pope, A. and Goin, K. L., High-Speed Wind Tunnel Testing (John Wiley & Sons, Inc., New York, NY, 1965).

In order to determine if an impingement jet loading could have broken the plate glass window of the wind tunnel, the strength of the window in shear and bending were investigated.
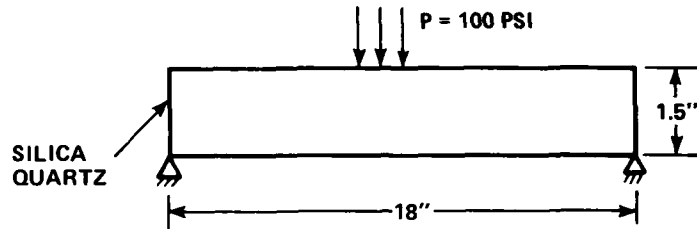
Consider shear:

$$\tau = F/A_S$$

$$F = 100\pi R_L{}^2$$

where R_L - radius of loading

$$A_S = 2\pi R_L h$$

$$\tau = \frac{100\pi R_L{}^2}{2\pi R_L h}$$

$$\tau = \frac{50R_L}{h}$$

$$t = 1.5"$$

$$\tau = \frac{50}{1.5} R_L$$

$$\tau = 33R_L$$

$$\tau_{MAX} = 33(9) = 297 \text{ psi}$$

From conversations with R. Koubek of Corning Glass, max allowable stress is 5000 psi. Examining above, it does not appear that the window would have failed in shear. Consider bending for clamped plate support, worst case, at edge:

$$\sigma_{R_{MAX}} = 3/4 \; \frac{P \, a^2}{h^2} \tag{8}$$

$$= \frac{3}{4} \frac{(100)(9)^2}{(1.5)^2} = 2700 \text{ psi}$$

for simply supported plate, worst case, at center:

$$\sigma_{R_{MAX}} = \frac{3(3 + \gamma)g \, a^2}{8h^2}$$

$$= \frac{3(3.3)100(9)^2}{8(1.5)^2}$$

$$= 4500 \text{ psi}$$

The 5000 psi value required for failure is for a perfect (flawless) window. As small scratches or cracks occur, the bending value required for failure drops off sharply. The window that failed had a number of small flaws; therefore, it seems quite possible that an impingement jet acting on the window could have caused it to fail.

MODEL REWORK

Calculations were made to determine if the remaining models could be beefed up to ensure their survival. The approach taken was to use a high-temperature epoxy to fill the models, thus providing reinforcement. The epoxy could be worked around the heat-transfer gages to prevent interference with these measurements.

EFFECTS OF FILLING A CORE WITH EPOXY. For this analysis, a comparison will be made for cylindrical shapes, as no data are readily available for conical shapes. Consider uniform radial pressure loading only.
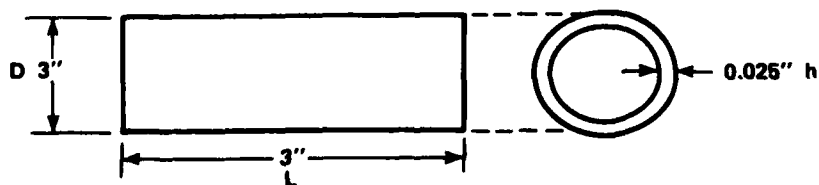
Again from reference 7;

$$z_L = \frac{L^2}{R(h)} \sqrt{1 - \nu^2} \tag{9}$$

$$= \frac{9}{1.5(.025)} \sqrt{.91}$$

$$z_L = 229$$

Figure C8.16 from reference 7 yields,

$$K_y = 15$$

The critical buckling pressure is defined as;

$$P_{CR} = \frac{K_y \pi^2 E}{12(1 - \nu^2)} \left(\frac{h}{L}\right)^2 \frac{h}{R} \tag{10}$$

Substitution yields,

$$= \frac{15 \pi^2 (25 \times 10^6)}{12(.91)} \left(\frac{.025}{3}\right)^2 \left(\frac{.025}{1.5}\right)$$

$$P_{CR} = 390 \text{ psi}$$

Compare the above result with that for a cylinder filled with a soft elastic core. From Reference 12 (subscript c denotes soft elastic core);

$$\nu = .3 \qquad\qquad E = 25 \times 10^6 \qquad\qquad \lambda = \frac{a}{R} = \frac{.5}{1.5} = .33$$

$$\nu_c = .34 \qquad\qquad E_c = 25 \times 10^4$$

12. Seidel, P., "The Stability Under Axial Compression and Lateral Pressure of Circular-Cylindrical Shells with Elastic Core," Journal of Aerospace Sciences, Vol. 29, Jul 1962.

33

$$\phi_2 = \frac{3(1 - \nu^2)}{(1 - \nu_c^2)} \frac{E_c}{E} \left(\frac{R}{h}\right)^3 \tag{11}$$

$$= 3 \frac{(.91)}{(.88)} (.01) \left(\frac{1.5}{.025}\right)^3$$

$$\phi_2 = 6700$$

$$\xi = \left[\frac{1}{1 - \nu_c} \frac{E_c}{E} \left(\frac{R}{h}\right)\right]\left[1 - \lambda^2\right] \bigg/ \left(1 + \frac{1 + \nu_c}{1 - \nu_c} \lambda^2\right) \tag{12}$$

For a solid core, $\lambda = 0$, thus:

$$\xi = \left[\frac{1}{1 - .34} (.01) \left(\frac{1.5}{.025}\right)\right] (1) \bigg/ (1)$$

$$\xi = .909$$

Using ϕ_2 and ξ it is now possible to evaluate critical external pressure P_{CR}.

$$\frac{P_{CR}3}{D} \bigg/ (1 + \xi) = 3\phi_2^{2/3} \tag{13}$$

$$P_{CR} = (1 + \xi) \, 3\phi_2^{2/3} \frac{D}{R^3}$$

$$= (1.909)(3)(6700)^{2/3} \frac{35.77}{(1.5)^3}$$

$$= 21,501 \text{ psi}$$

This result would cause yielding of the metal shell; however, it does confirm the existence of an order of magnitude strengthening effect for the epoxy filled case.

We can also examine the effect of filling the core with epoxy by computing an interface pressure and comparing it with the applied pressure. The stiffness of the core material acts as if it were an applied internal pressure.

CYLINDER   **CORE**

$$\xi_{cylinder} = \frac{(P - P_i)}{Eh} \ R^2 \ (1 - \frac{\nu}{2}) = \Delta P \frac{R^2}{Eh} (1 - \frac{\nu}{2}) \qquad (14a)$$

$$\xi_{core} = \frac{P_i}{E_c} \ (1 - \nu_c)(R_c) \qquad (14b)$$

Equating the deflections of the cylinder and core yields:

$$\Delta P \frac{R^2}{Eh} (1 - \frac{\nu}{2}) = \frac{P_i}{E_c} \ (1 - \nu_c)R_c$$

Substituting known values and assuming a nominal pressure loading of P = 100 psi yields:

$$(100 - P_i) \ \frac{(1.5)^2}{25 \times 10^6 (.025)} \ (1 - .15) = \frac{P_i}{25 \times 10^4} (1 - .34)1.5$$

solving for P_i gives

$$P_i = 61.7 \text{ psi}$$

This result indicates that of the 100 psi applied pressure, 61.7 psi, or 61.7 percent of the load was absorbed by the core.

35

To reach a buckling strength of 82 psi as is required to buckle the cone-cone approximations of model configuration A, a load of $\frac{82(100)}{38.3} = 214$ psi would have to be applied.

SUMMARY

An investigation of the accident indicated that the strength of the 0.025-inch model shells was marginal at the test conditions involved, and that the models should be strengthened. Models B, C and E were strengthened by partly filling the model shell with epoxy resin. Model D was tested successfully prior to the accident with model A, but was damaged by a flow breakdown which occurred during tunnel shut down after the last data run. Since the required data had been obtained, model D was not repaired. Model A was not rebuilt and hence, no data were obtained, for this configuration. A dummy model of configuration B was constructed after the accident to be used for blockage testing before testing the instrumented models B, C, and E. It is highly probable that the breakdown of supersonic flow which occurred in the accident with model A was not due to blockage effects, but it was necessary to determine whether or not this would occur with the remaining configurations to be tested. Of the three remaining configurations, B was the most similar to configuration A; therefore, configuration B was chosen for the blockage testing.

One can never make a positive, 100 percent certain decision as to whether the flow breakdown caused model A to fail or if the failure of model A caused the flow to break down. However, on the basis of the available information it appears most likely that model A failed upon injection into the supersonic flow-field, and that the model was sheared from its supports, exposing a flat plate to the flow. This caused an impingement jet to form and a breakdown of the supersonic flowfield. The force of the impingement jet on the wind tunnel window caused the window to fail, and the window glass to be blown.

CONFIG. A
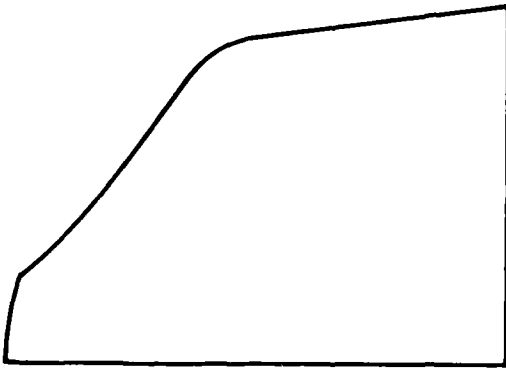
CONFIG. B

CONFIG. C

CONFIG. D
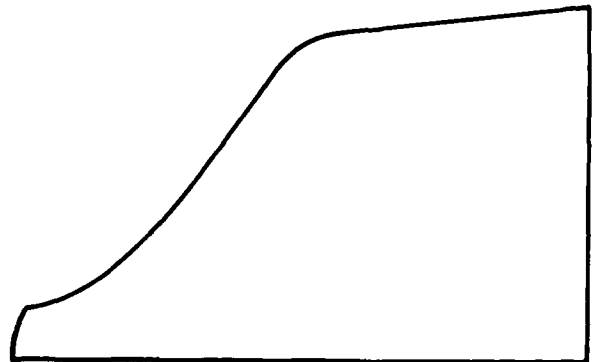
CONFIG. E

FIGURE 1 INDENTED NOSETIP CONFIGURATIONS FOR IAP 202 WIND TUNNEL TEST PROGRAM
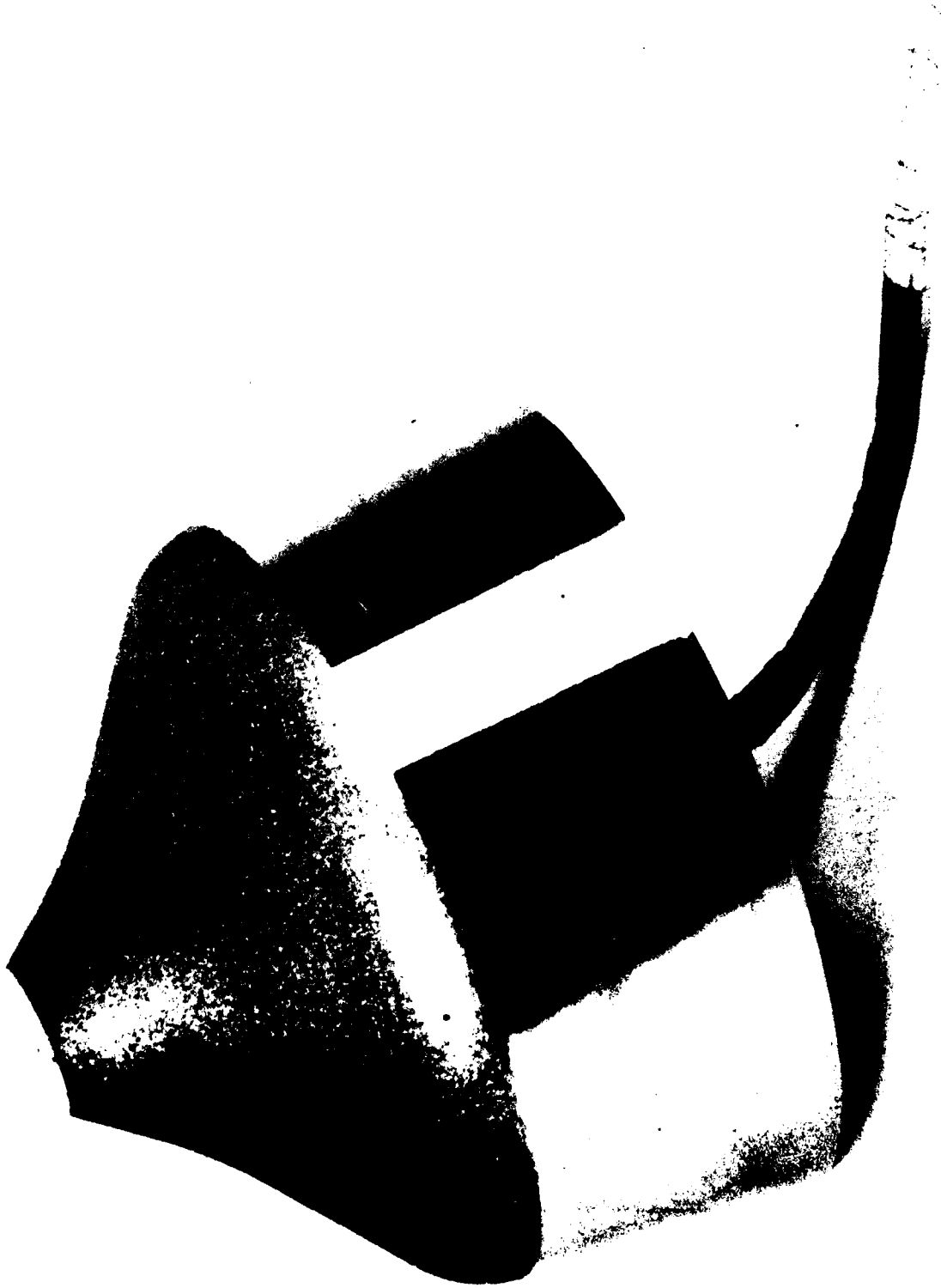
FIGURE 2 MODEL B
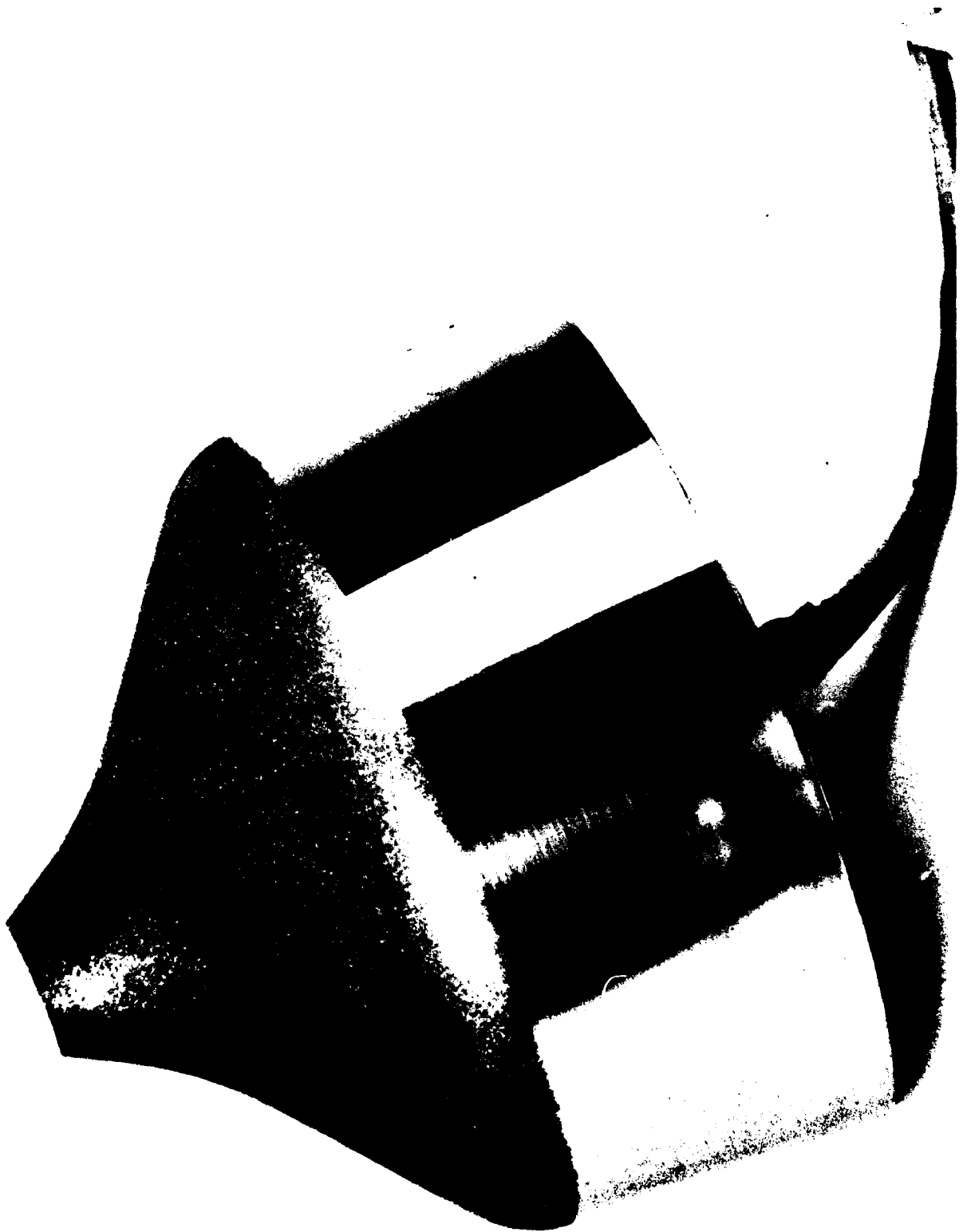
FIGURE 3 MODEL C
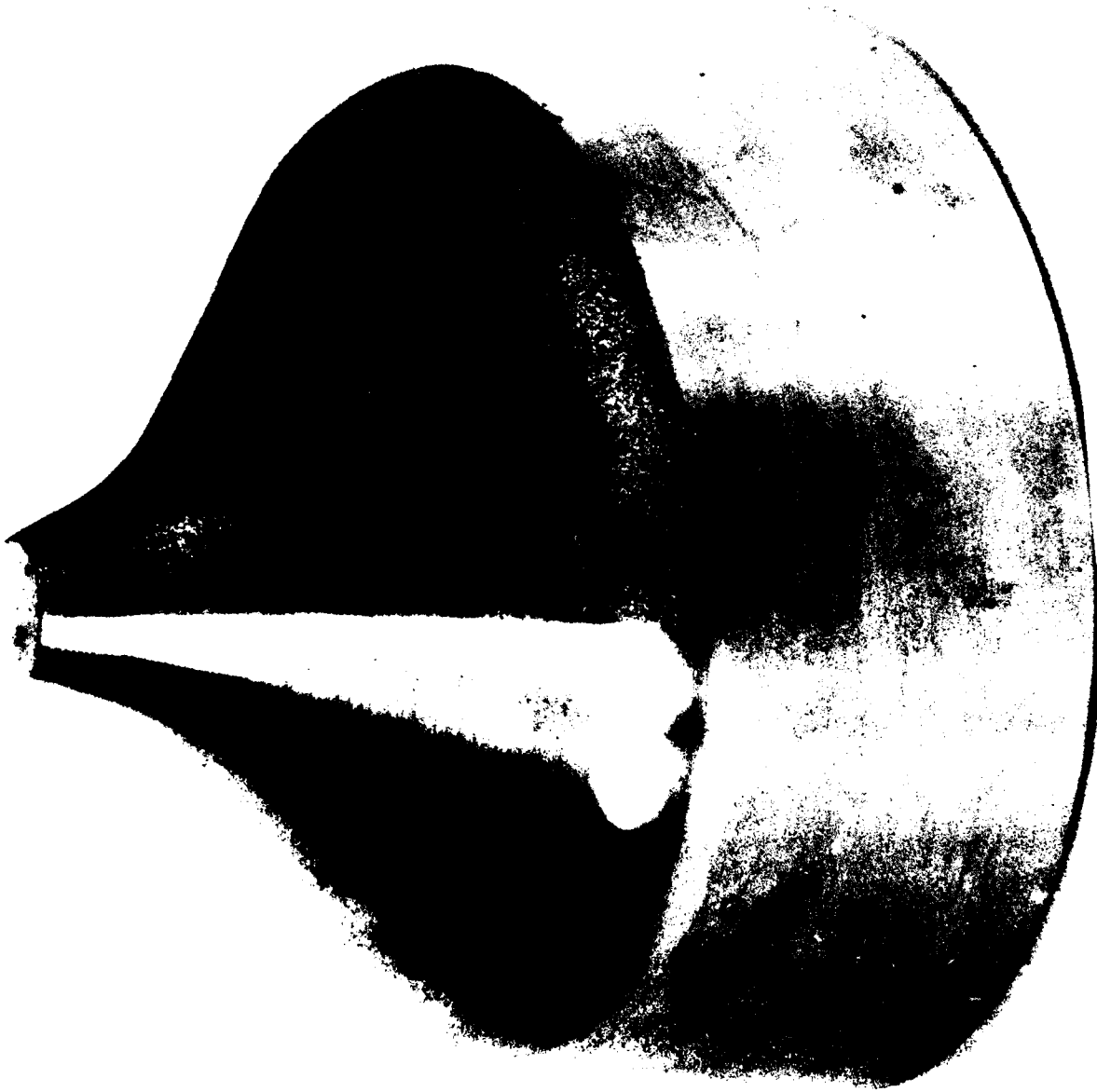
FIGURE 4 MODEL D

FIGURE 5 MODEL E

0.001 INCH
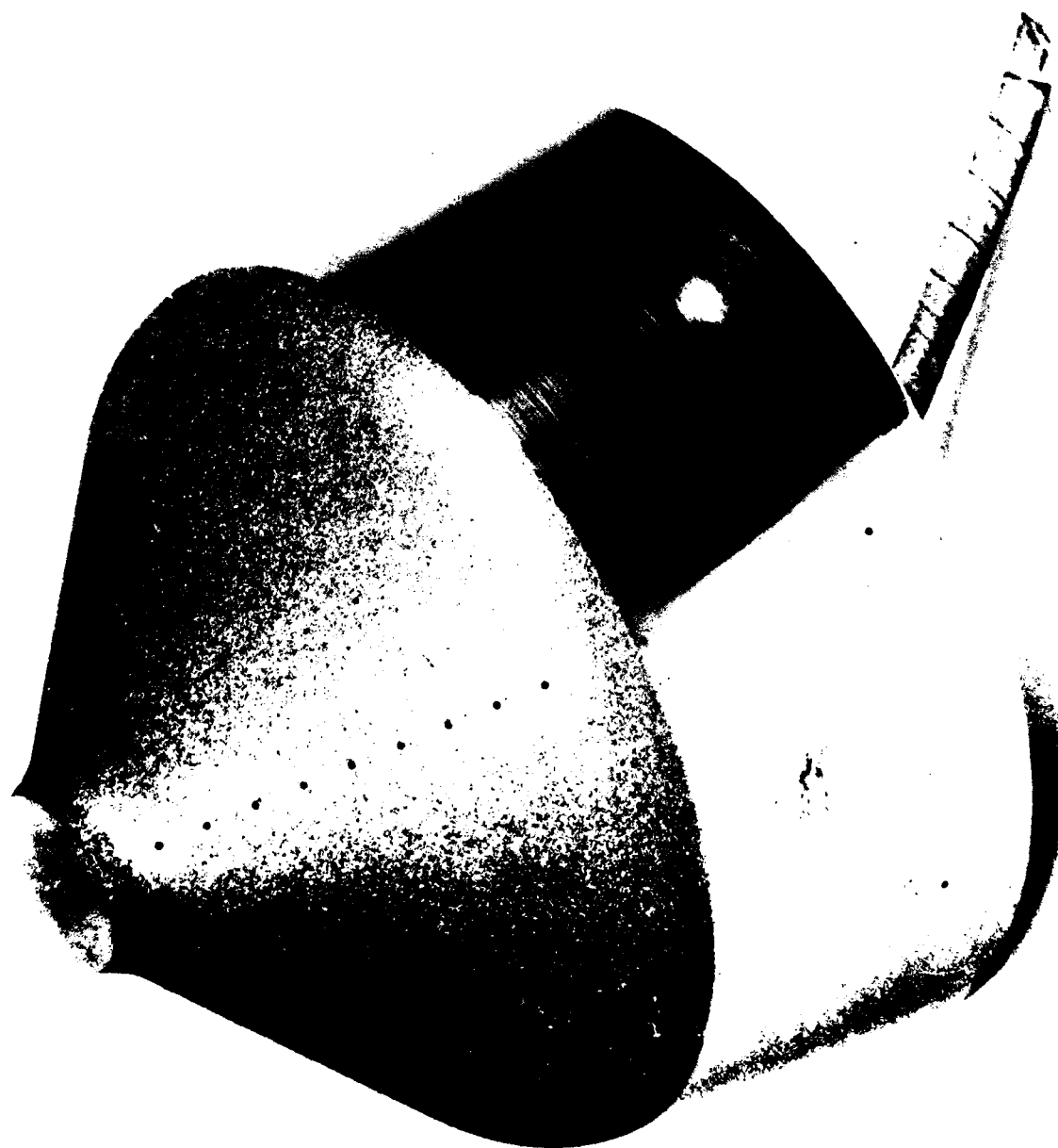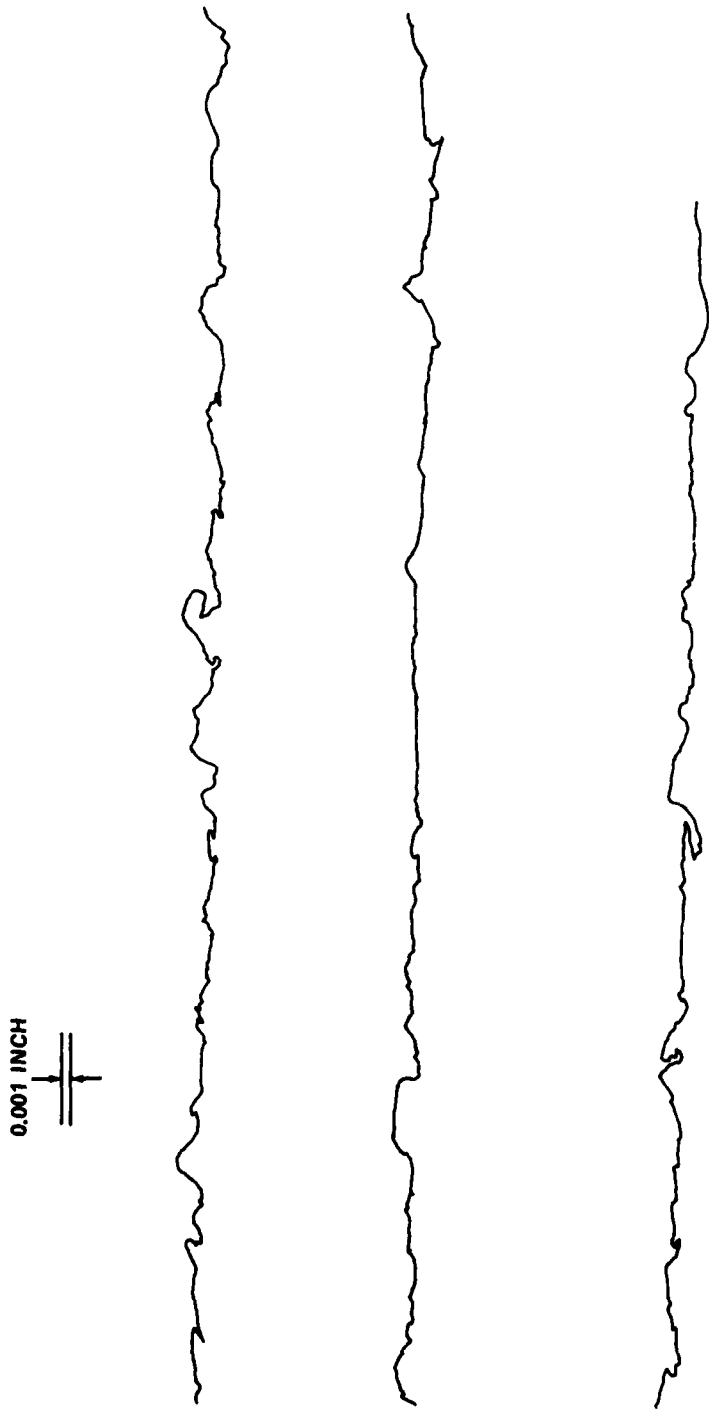
FIGURE 6 PROFILES OF SURFACE ROUGHNESS TRACED FROM PHOTOMICROGRAPHS

(a) SUMMARY OF H VALUES FROM: (b)   SELECTED "BEST" H VALUES
  13   25–POINT CURVE FITS
  10   20–POINT CURVE FITS
  7   15–POINT CURVE FITS
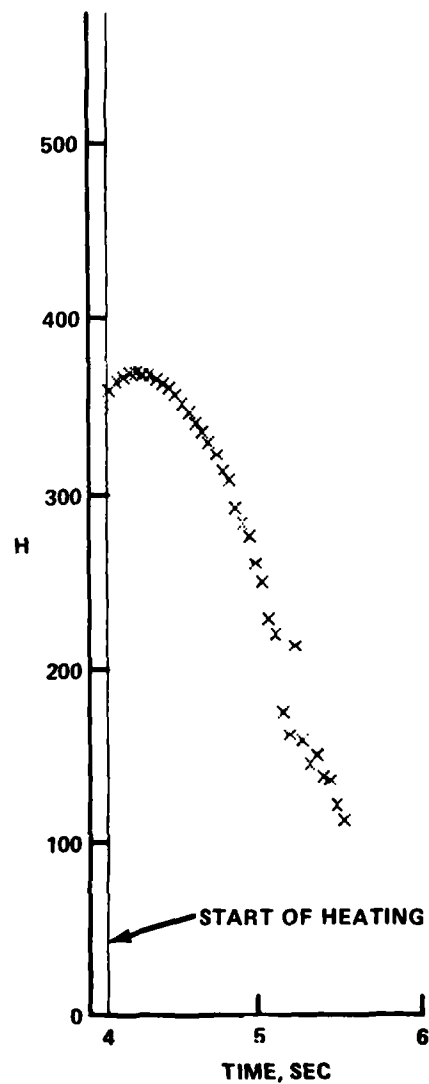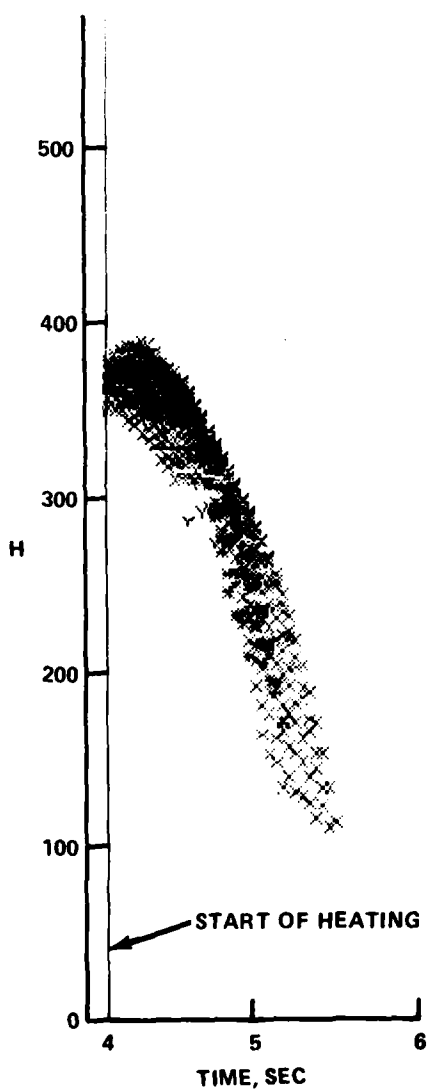
FIGURE 7 EXAMPLE OF HEAT TRANSFER DATA REDUCTION

RUN 4 MODEL B
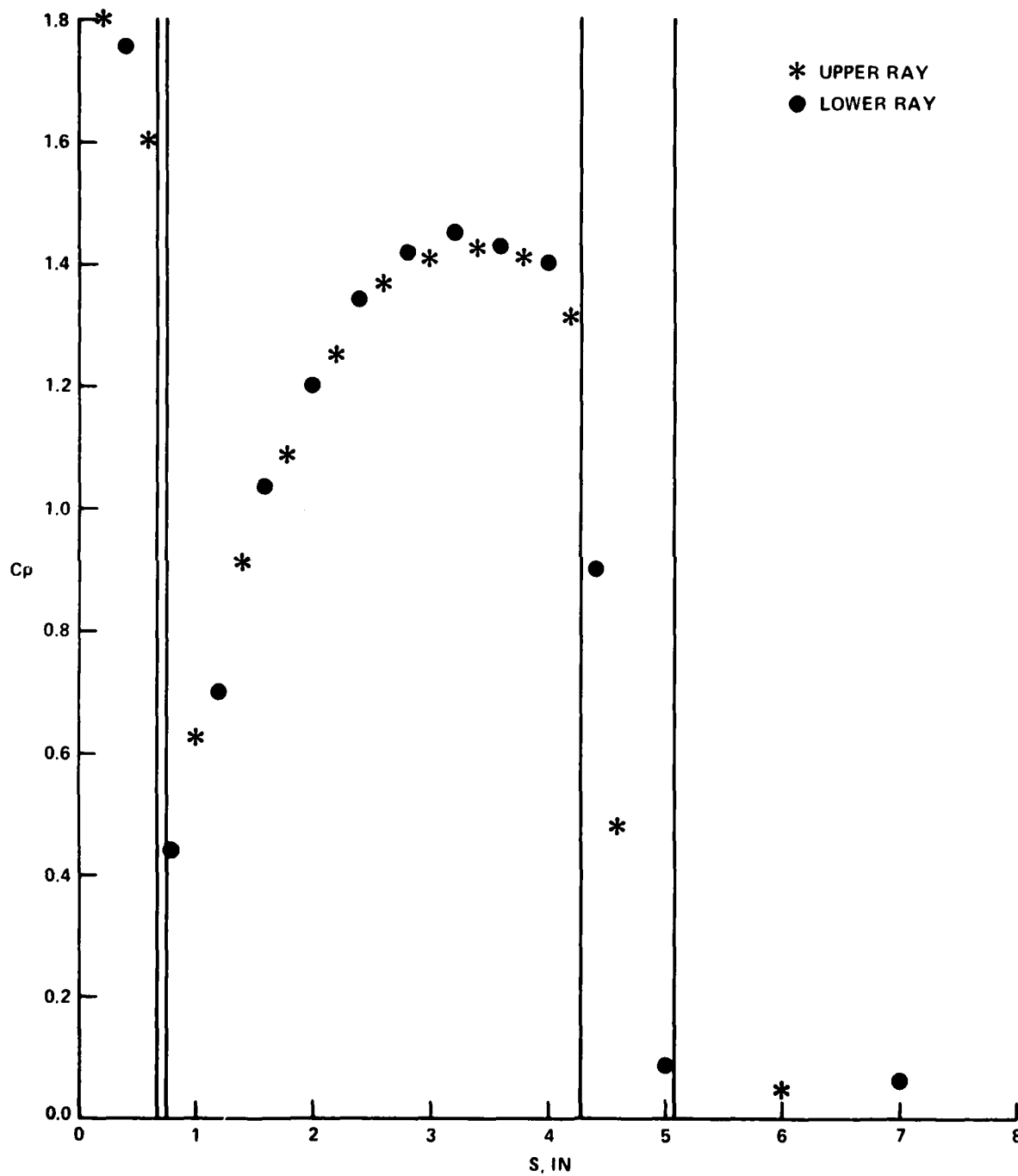
FIGURE 8(a) PLOTTED PRESSURE DATA
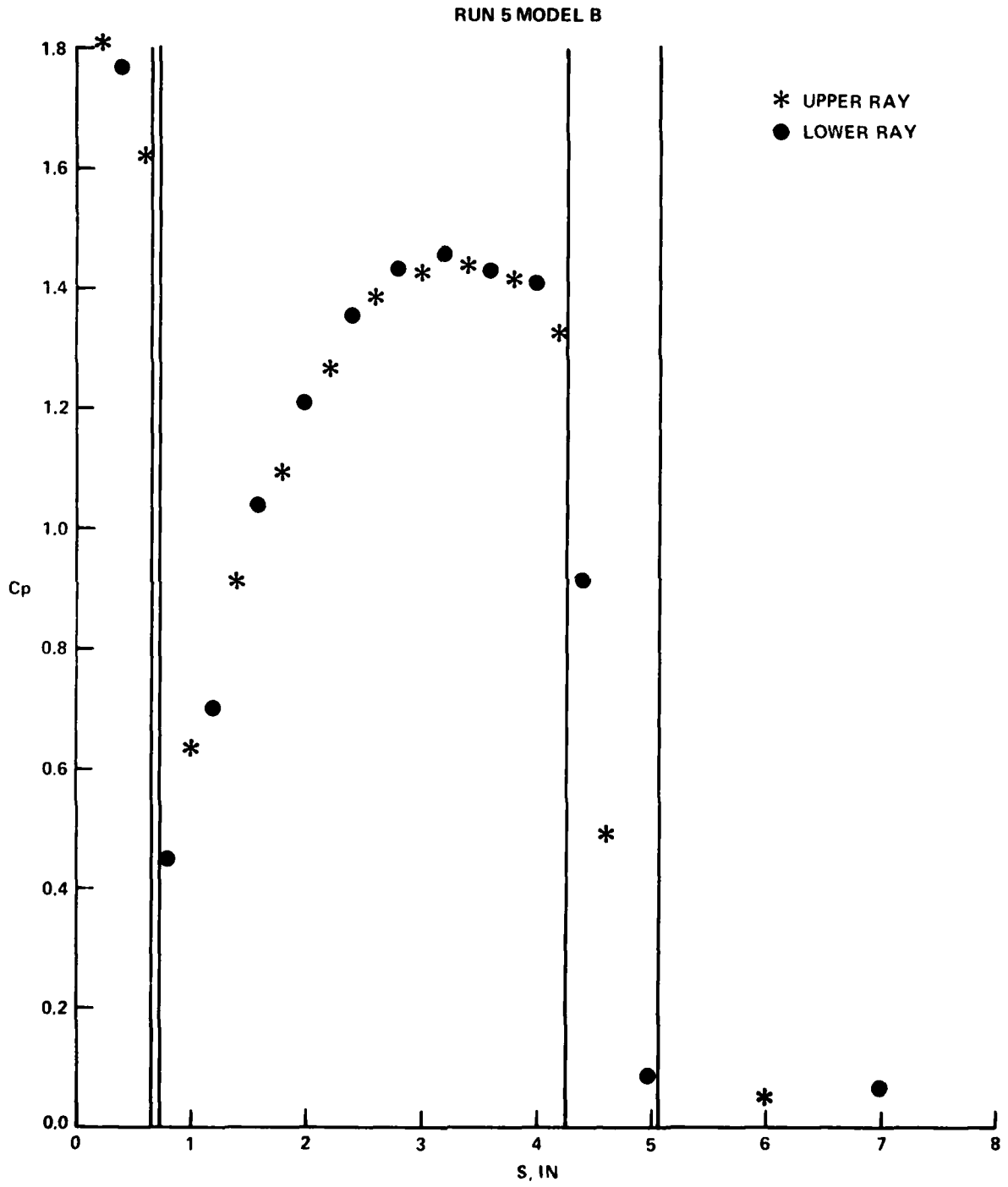
FIGURE 8(b) PLOTTED PRESSURE DATA (CONTINUED)

RUN 6 MODEL B
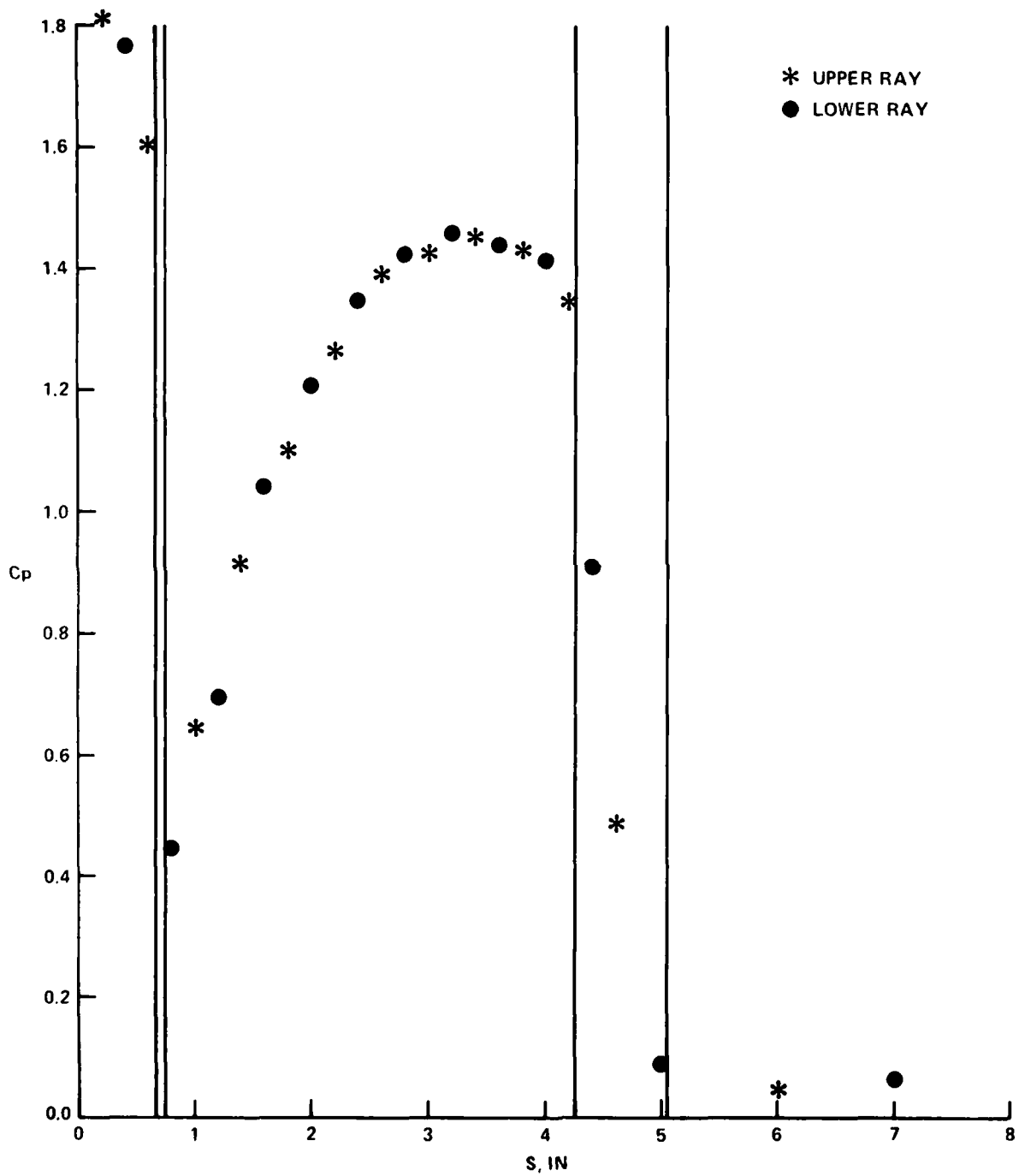
FIGURE 8(c) PLOTTED PRESSURE DATA (CONTINUED)

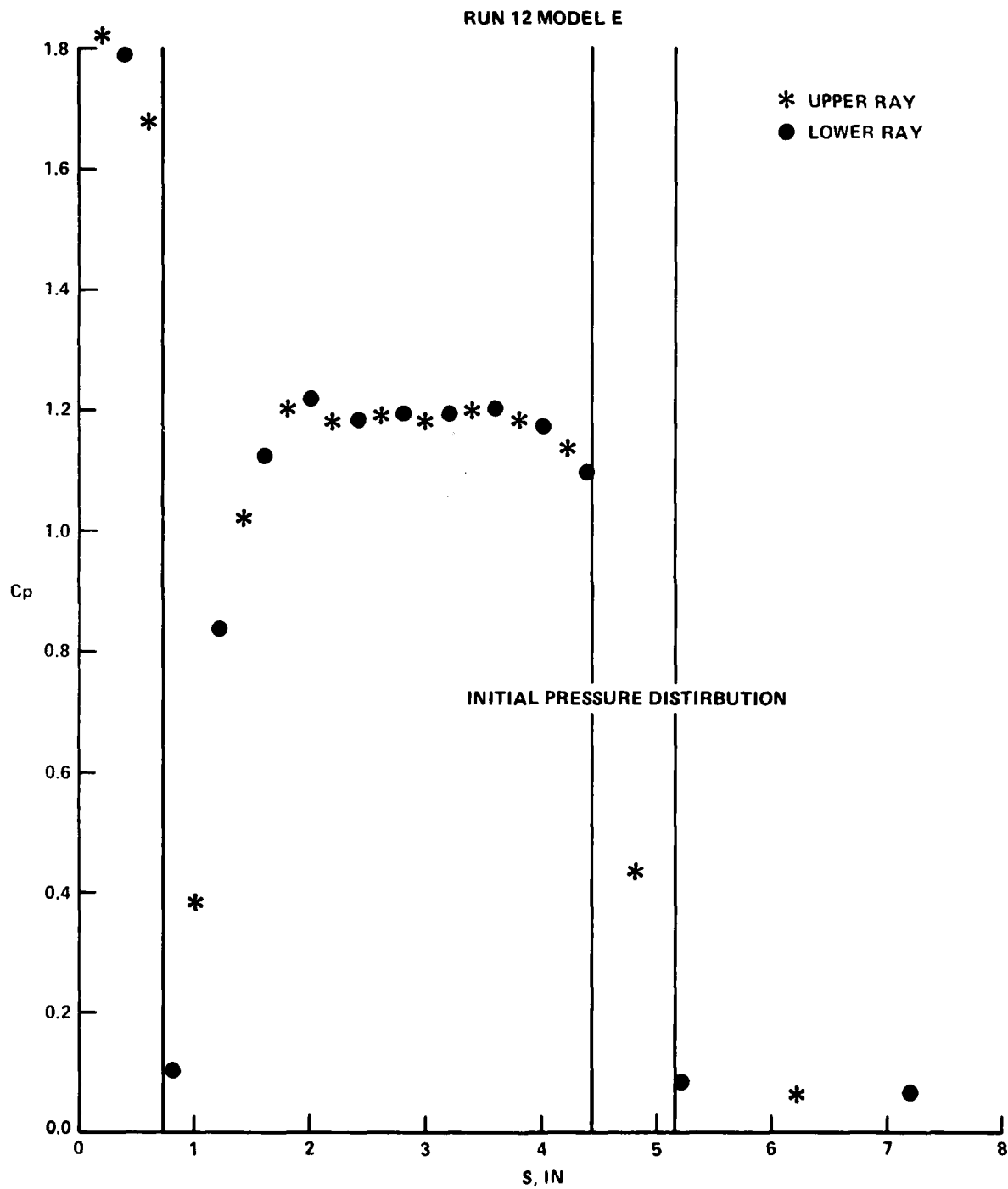FIGURE 8(d) PLOTTED PRESSURE DATA (CONTINUED)

RUN 8 MODEL C
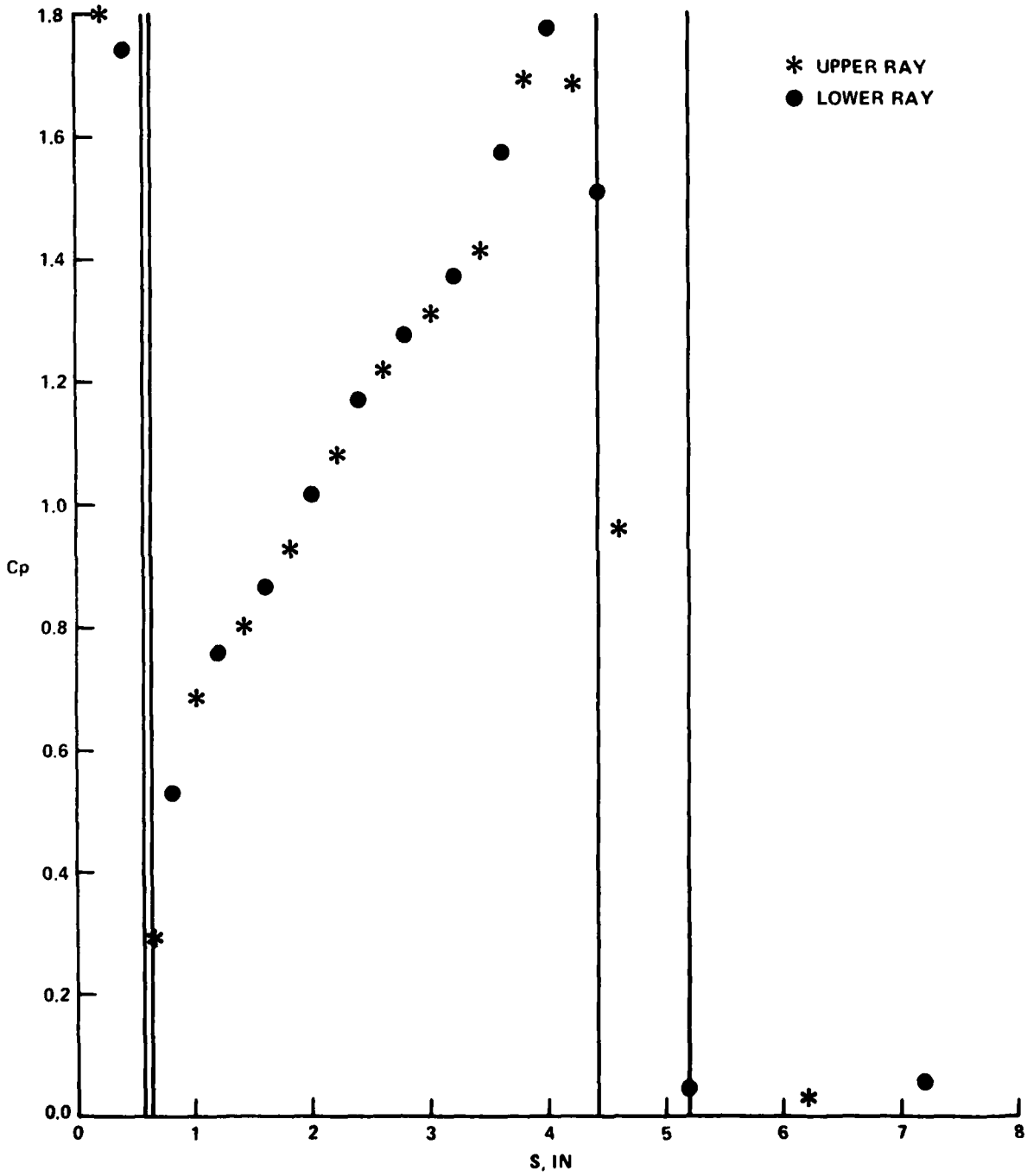
FIGURE 8(e) PLOTTED PRESSURE DATA (CONTINUED)
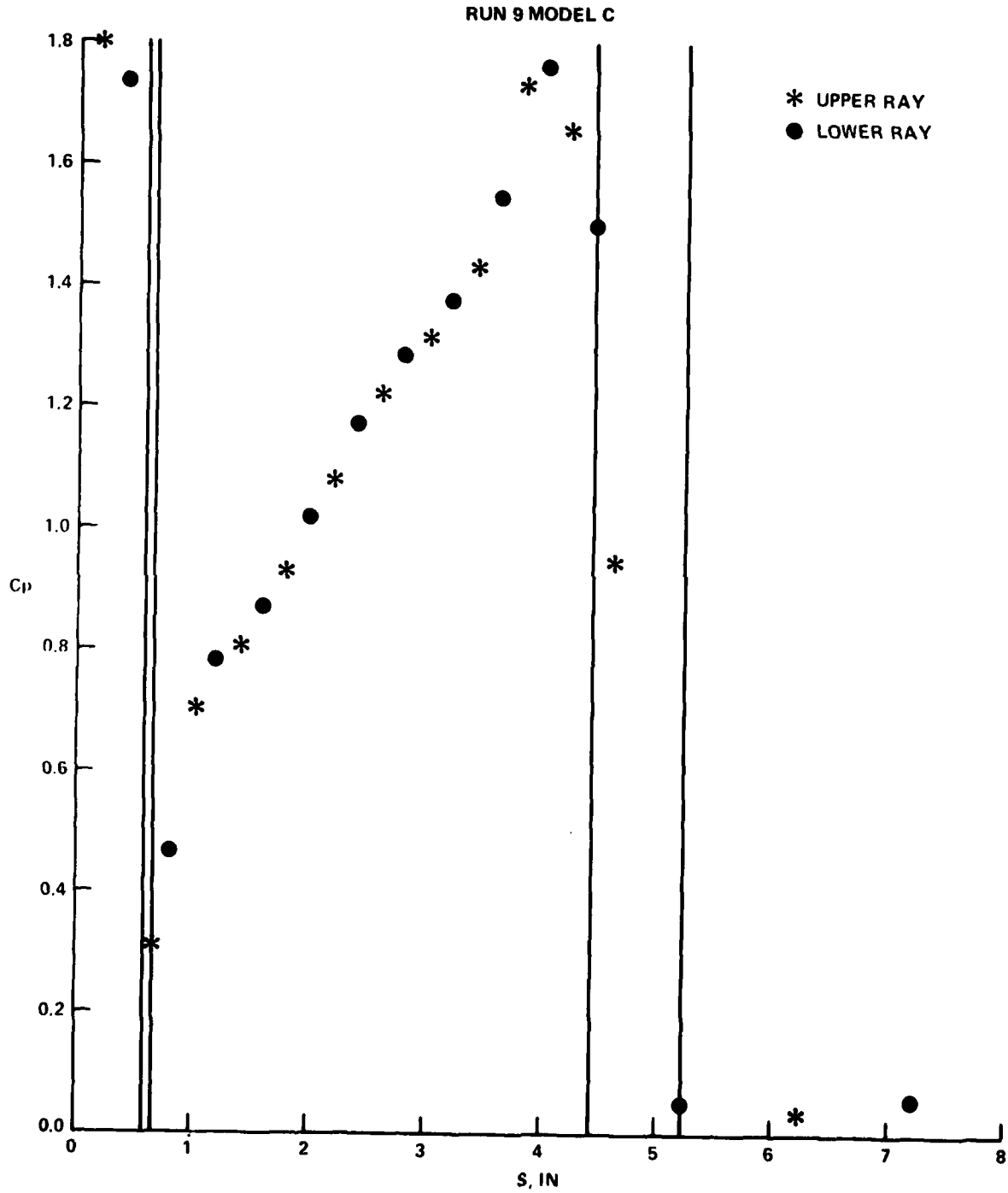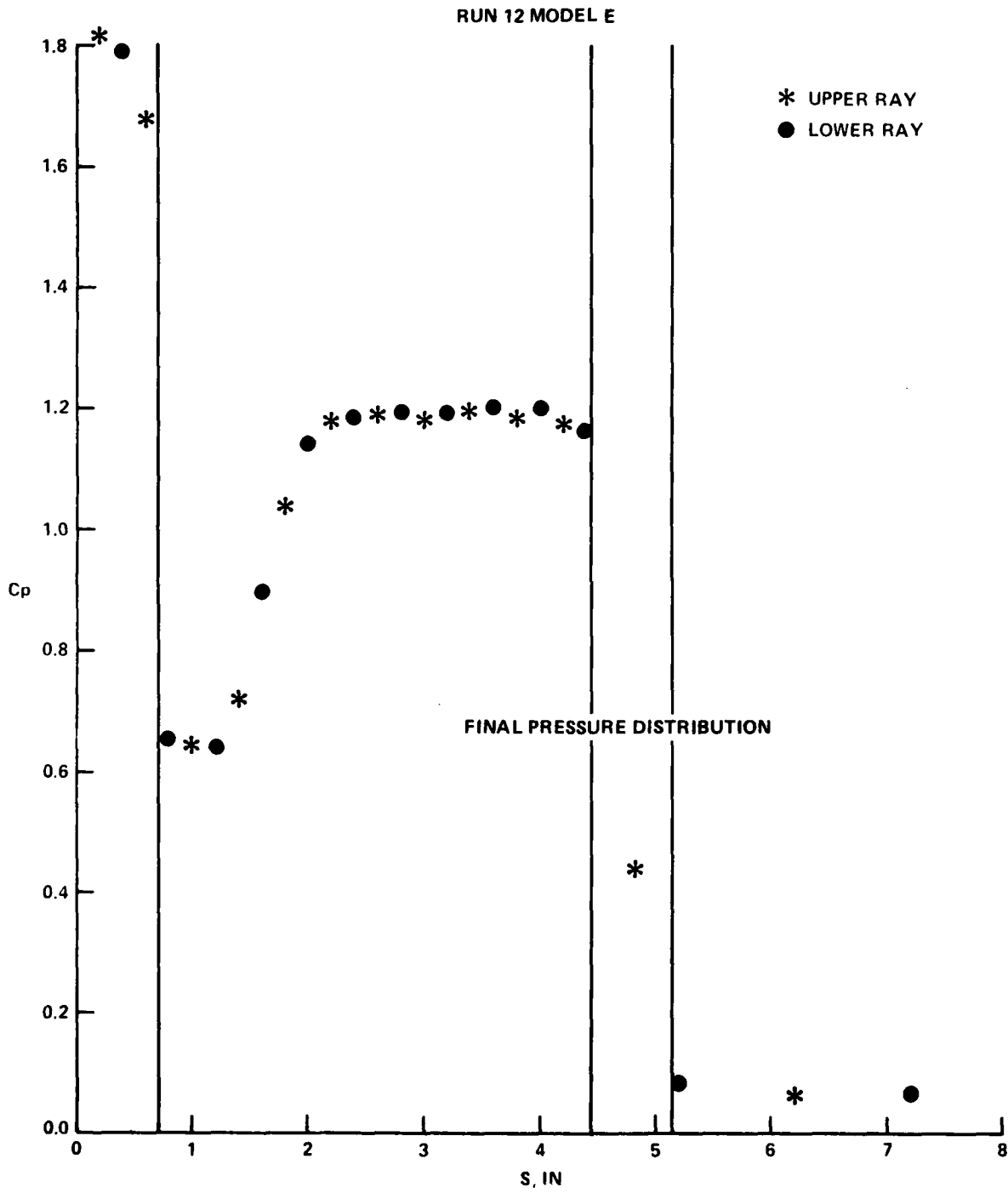
FIGURE 8(f) PLOTTED PRESSURE DATA (CONTINUED)

RUN 10 MODEL C
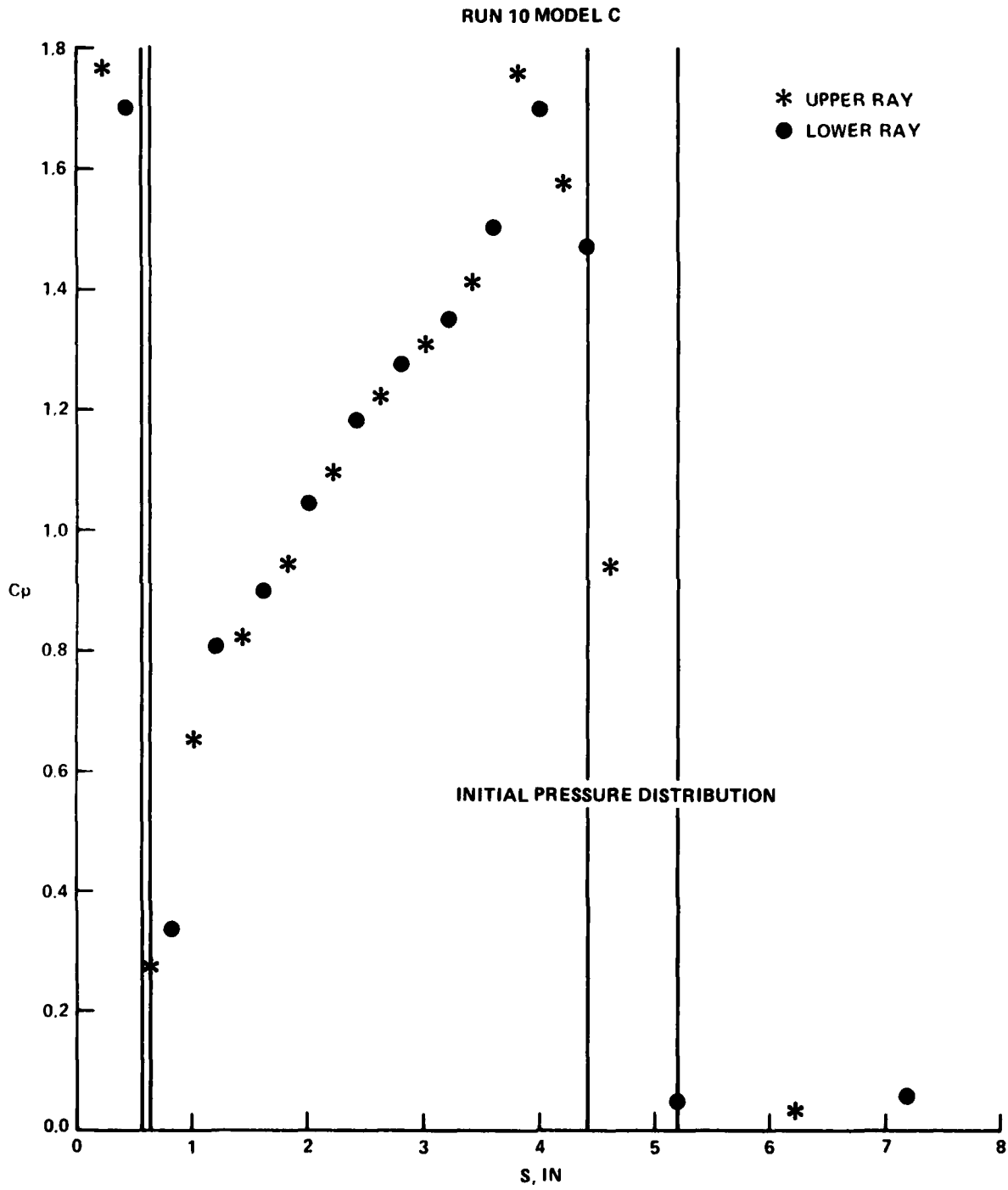
FIGURE 8(g) PLOTTED PRESSURE DATA (CONTINUED)
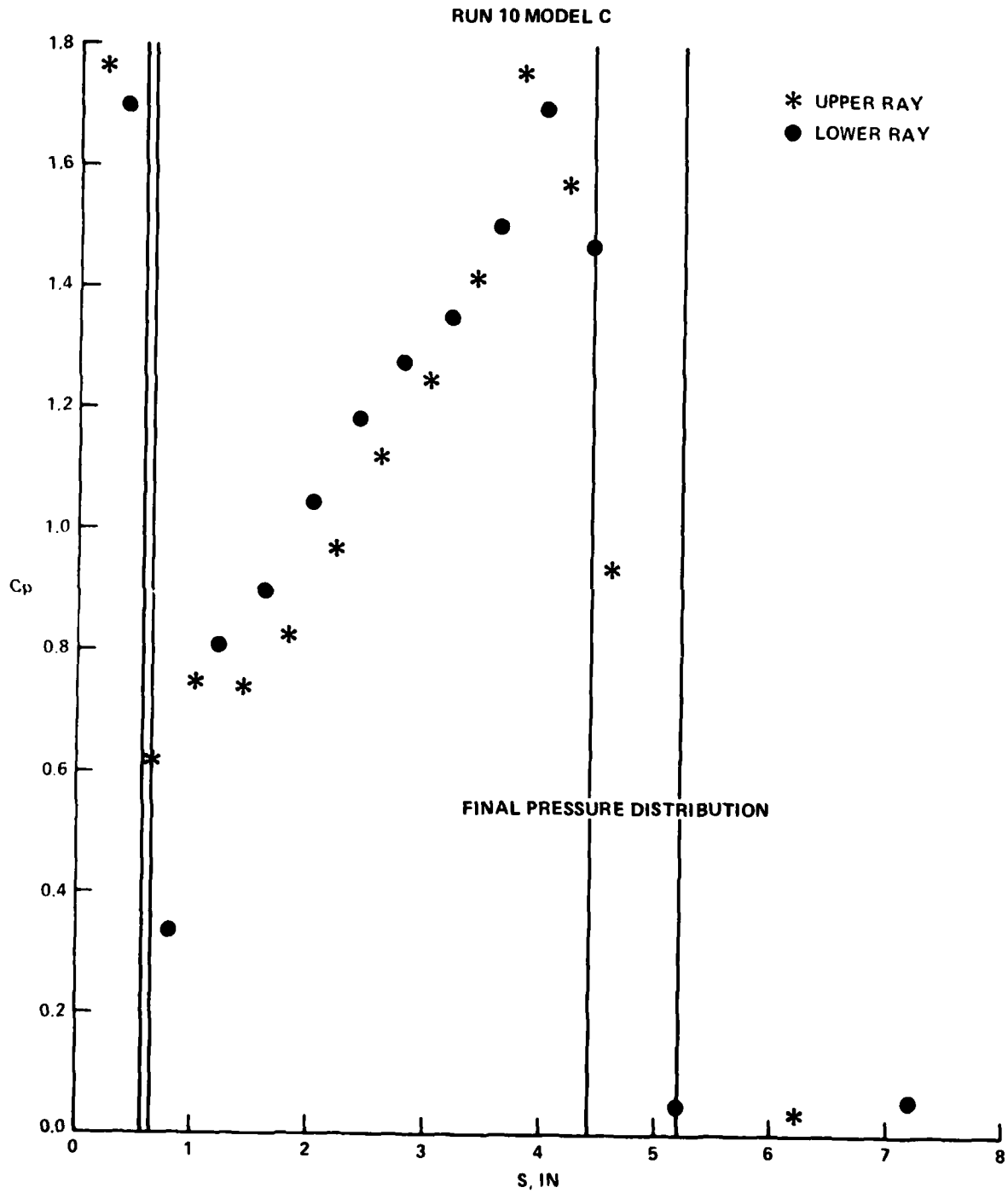
FIGURE 8(h)   PRESSURE DISTRIBUTION ON INDENTED NOSETIP WITH Bi-MODEL FLOW

RUN 1 MODEL D

FIGURE 8(i) PLOTTED PRESSURE DATA (CONTINUED)

FIGURE 8(j) PLOTTED PRESSURE DATA (CONTINUED)

FIGURE 8(k) PLOTTED PRESSURE DATA (CONTINUED)

FIGURE 8(I) PLOTTED PRESSURE DATA (CONTINUED)

RUN 12 MODEL E
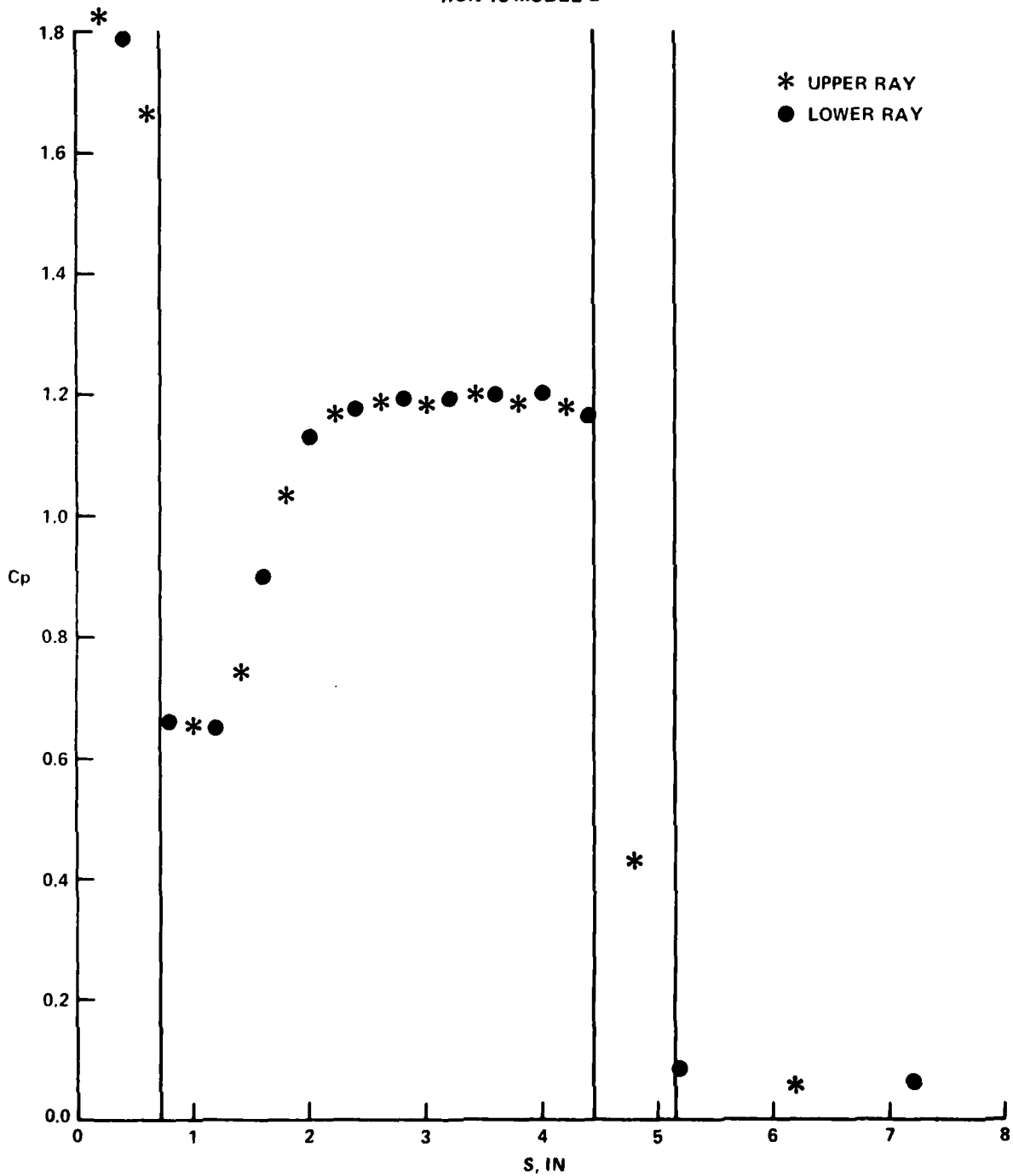

FIGURE 8(m) PLOTTED PRESSURE DATA (CONTINUED)

RUN 13 MODEL E

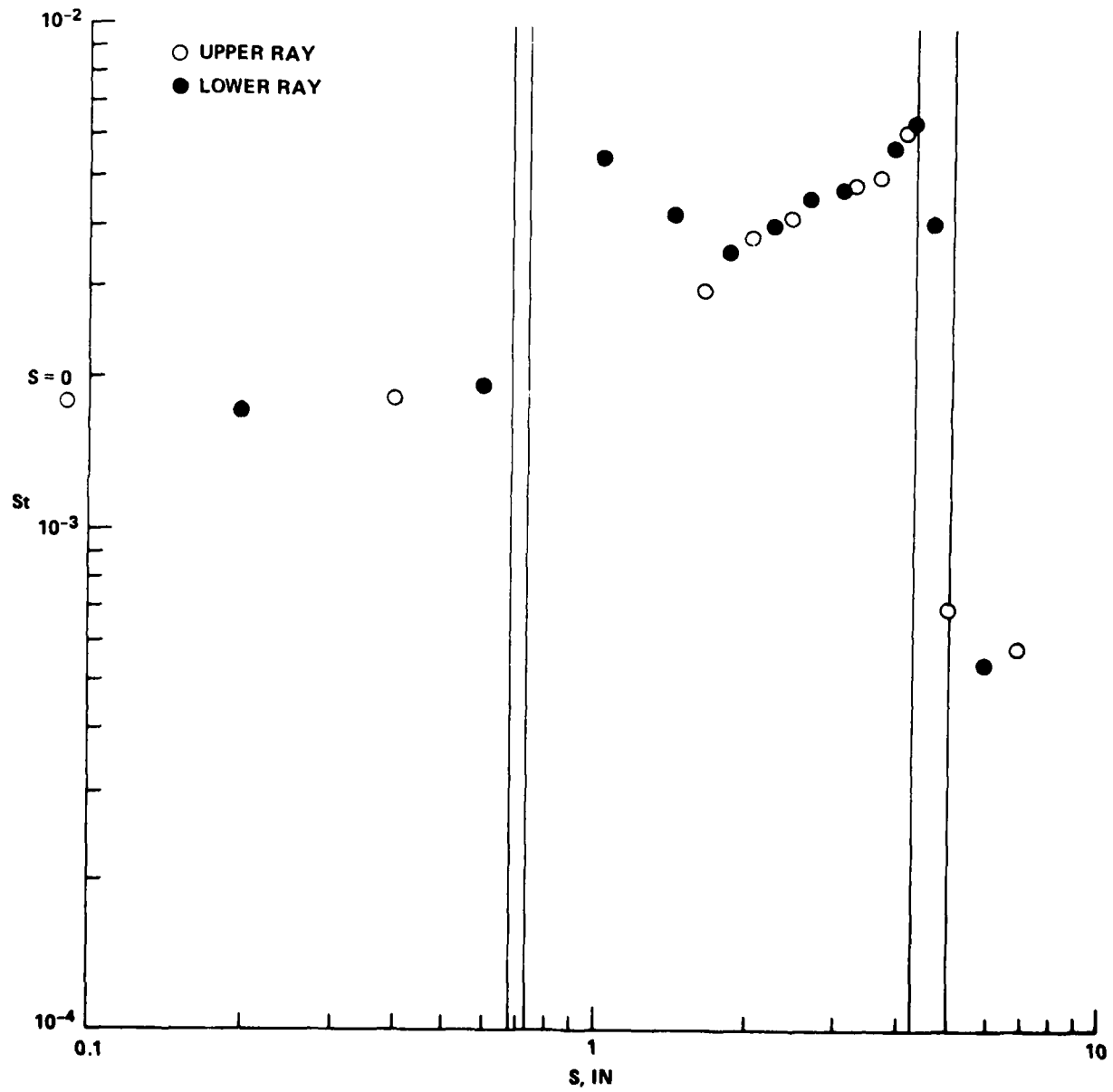FIGURE 8(n) PLOTTED PRESSURE DATA (CONTINUED)

RUN 4 MODEL B

FIGURE 9(a) PLOTTED HEAT TRANSFER DATA
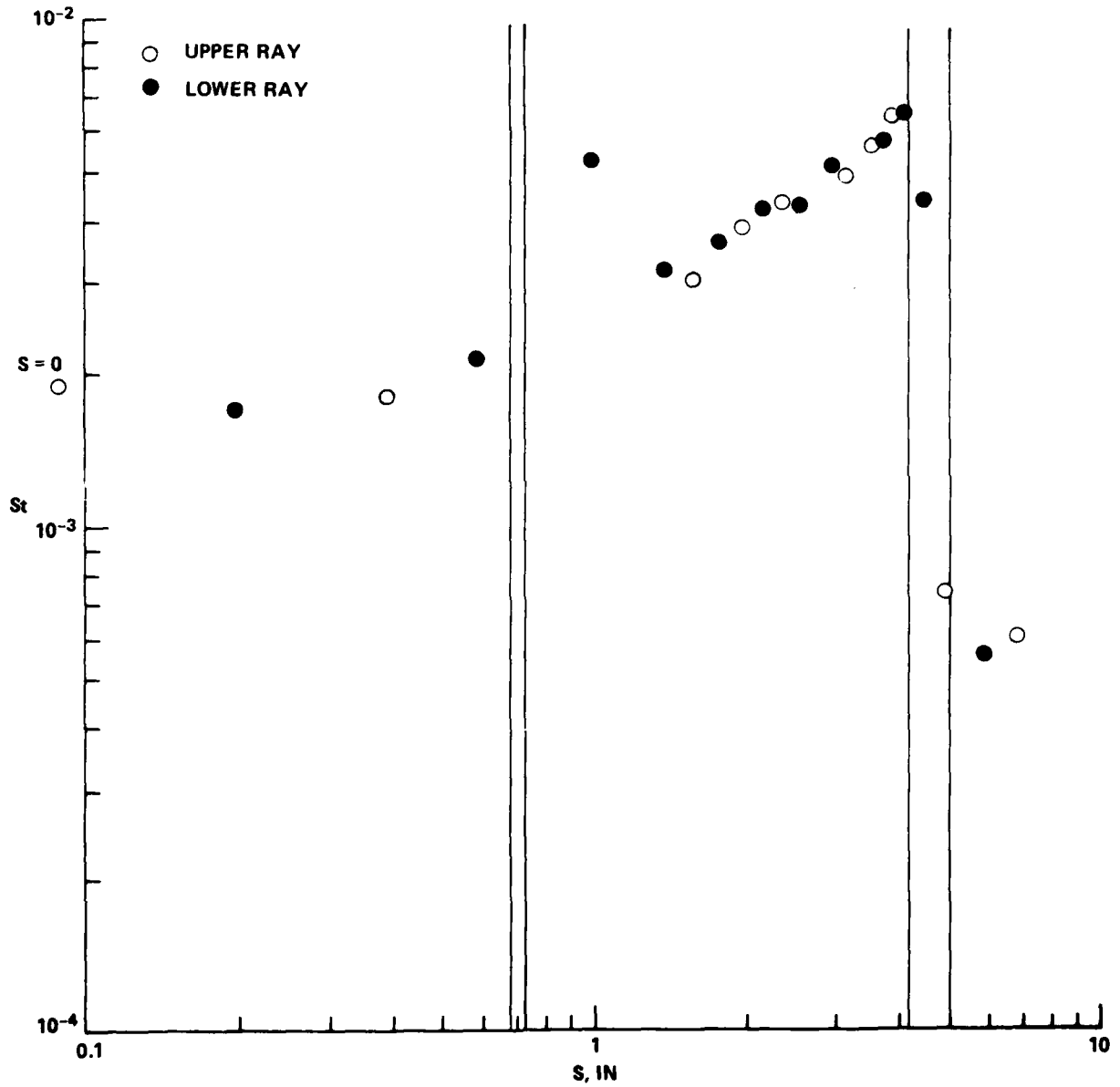
RUN 5 MODEL B

FIGURE 9(b) PLOTTED HEAT TRANSFER DATA (CONTINUED)
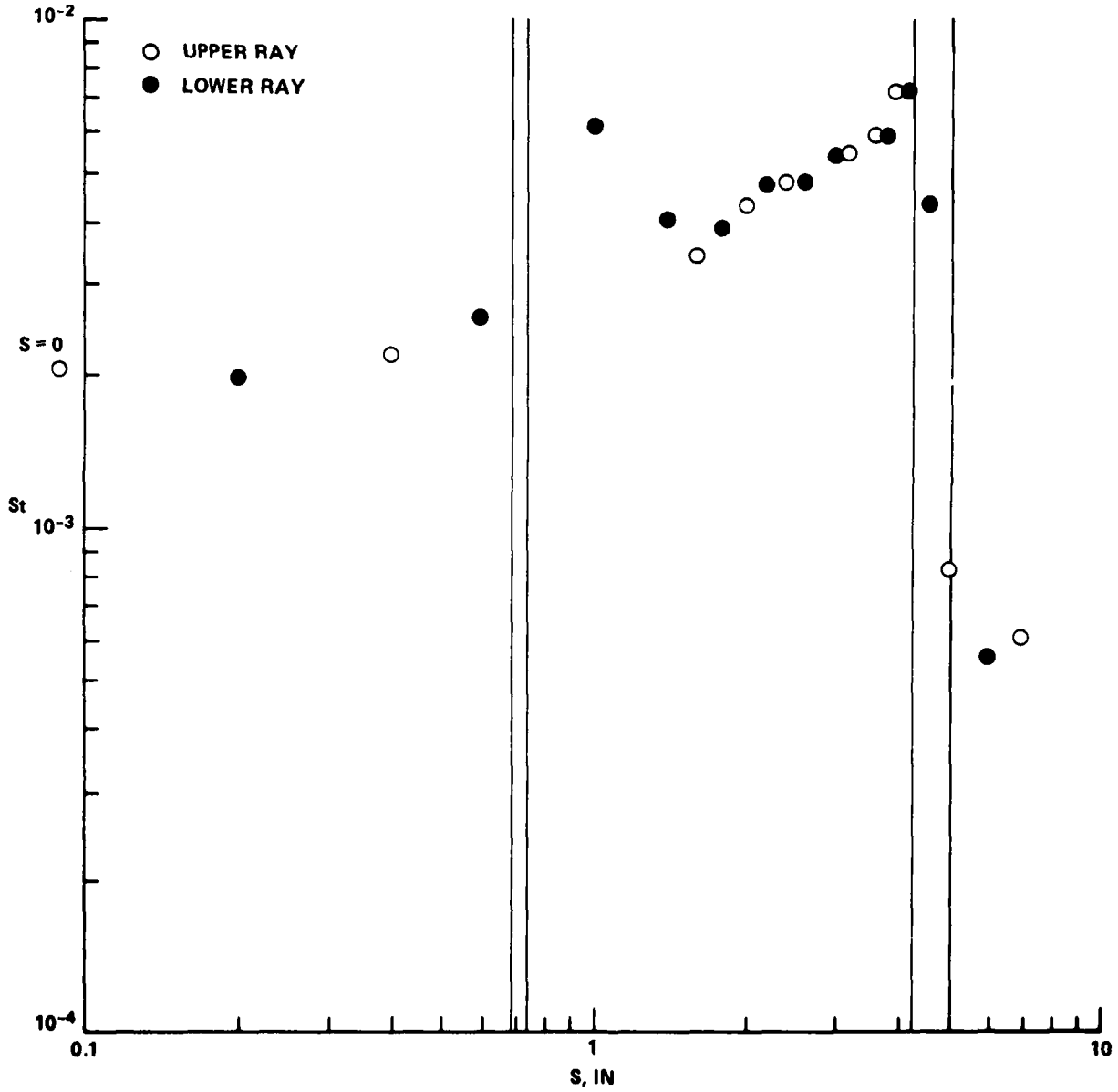
RUN 6 MODEL B

FIGURE 9(c) PLOTTED HEAT TRANSFER DATA (CONTINUED)
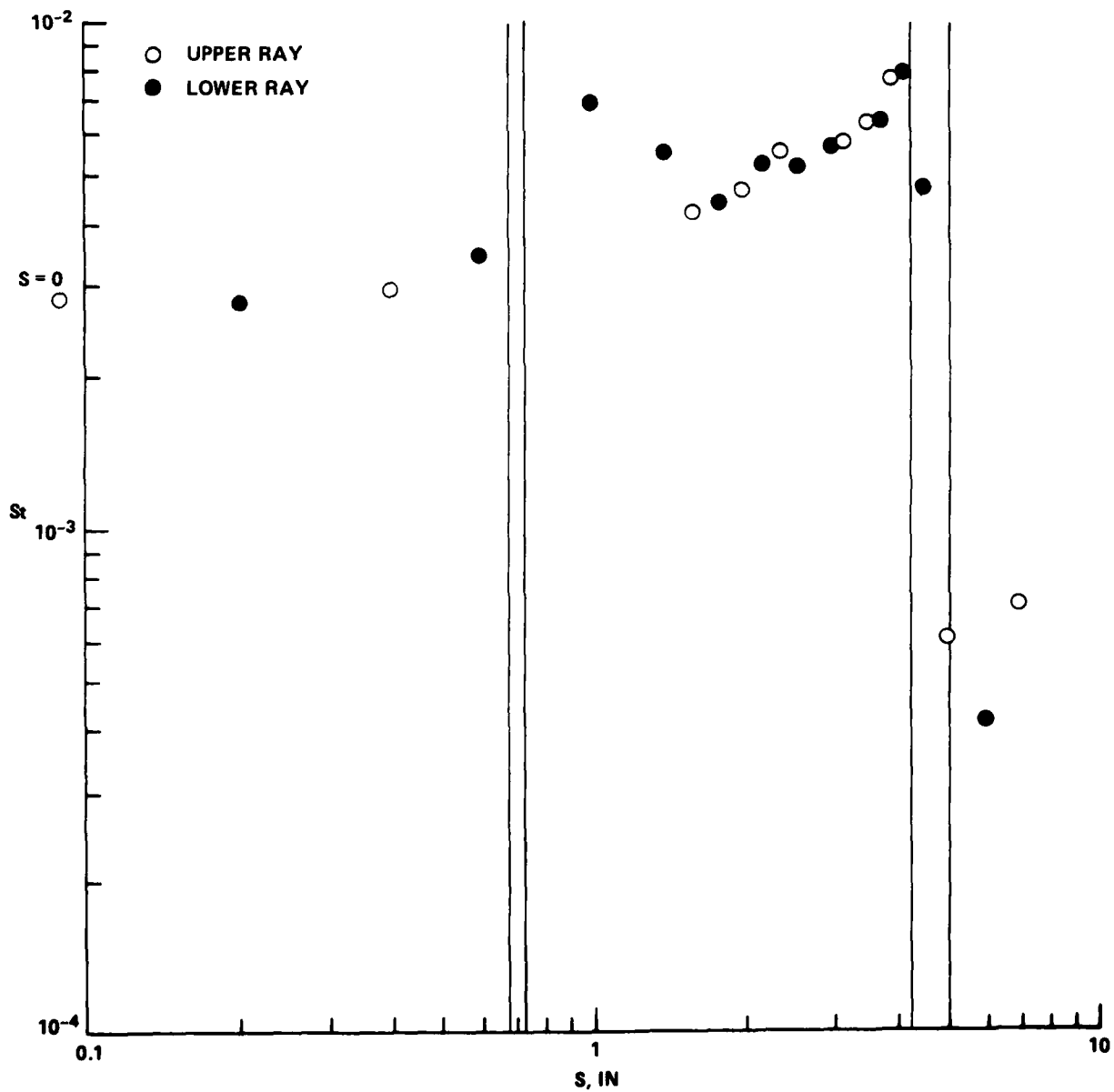
RUN 7 MODEL B

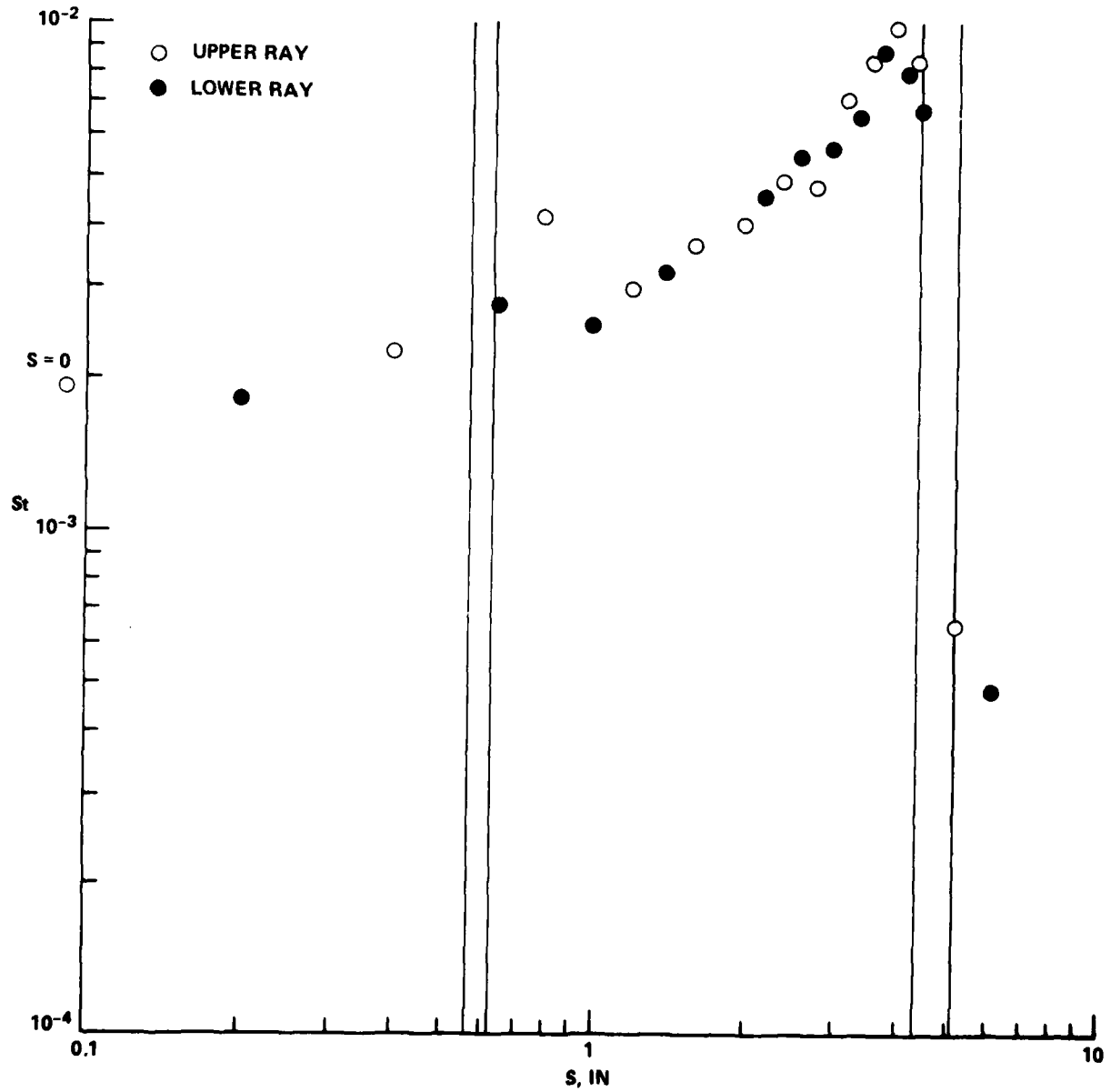FIGURE 9(d) PLOTTED HEAT TRANSFER DATA (CONTINUED)

RUN 8 MODEL C

FIGURE 9(e) PLOTTED HEAT TRANSFER DATA (CONTINUED)

RUN 9 MODEL C

FIGURE 9(f) PLOTTED HEAT TRANSFER DATA (CONTINUED)

RUN 10 MODEL C

FIGURE 9(g) PLOTTED HEAT TRANSFER DATA (CONTINUED)

RUN 1 MODEL D
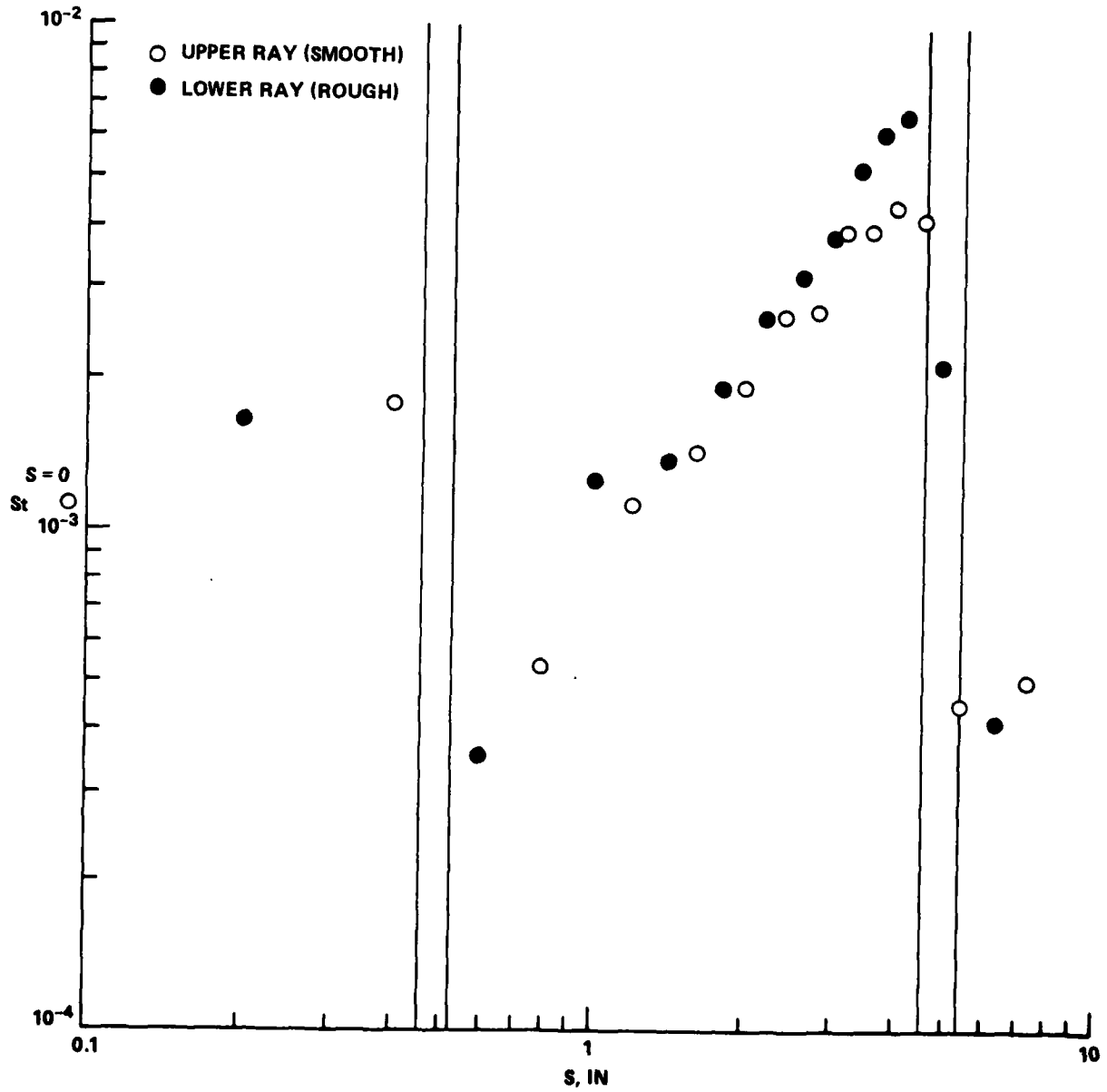
FIGURE 9(h) PLOTTED HEAT TRANSFER DATA (CONTINUED)

RUN 2 MODEL D
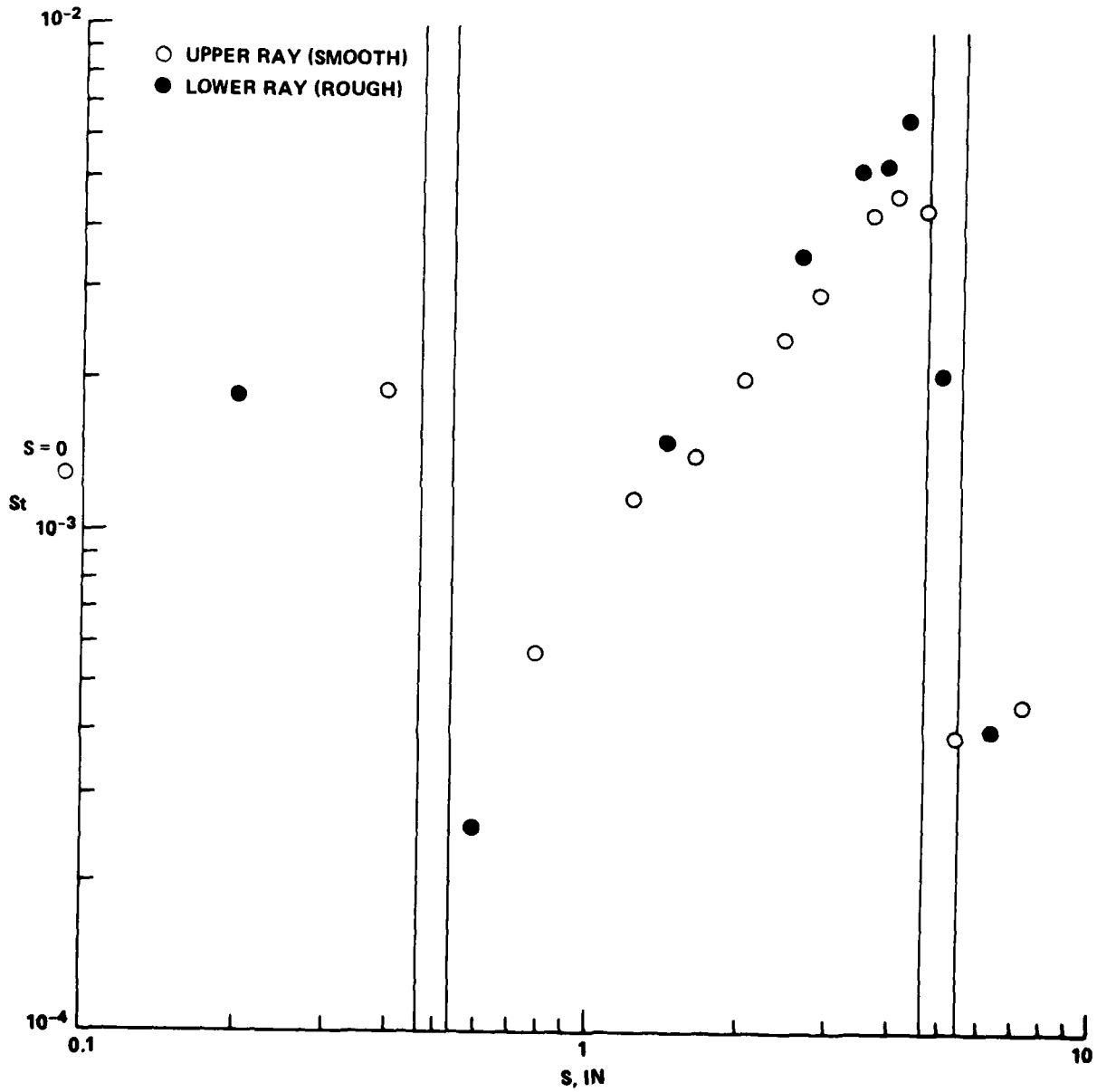
FIGURE 9(i) PLOTTED HEAT TRANSFER DATA (CONTINUED)
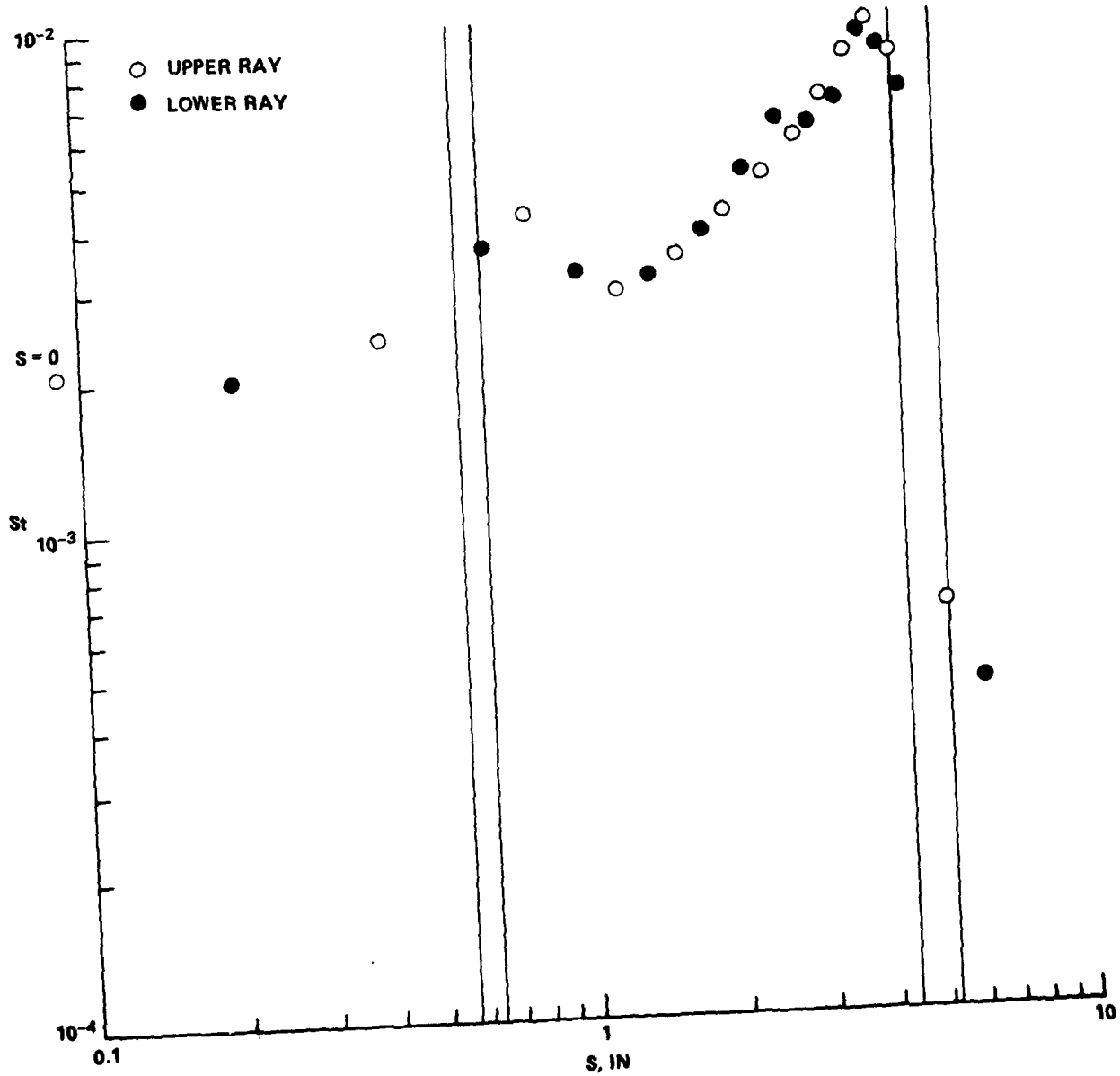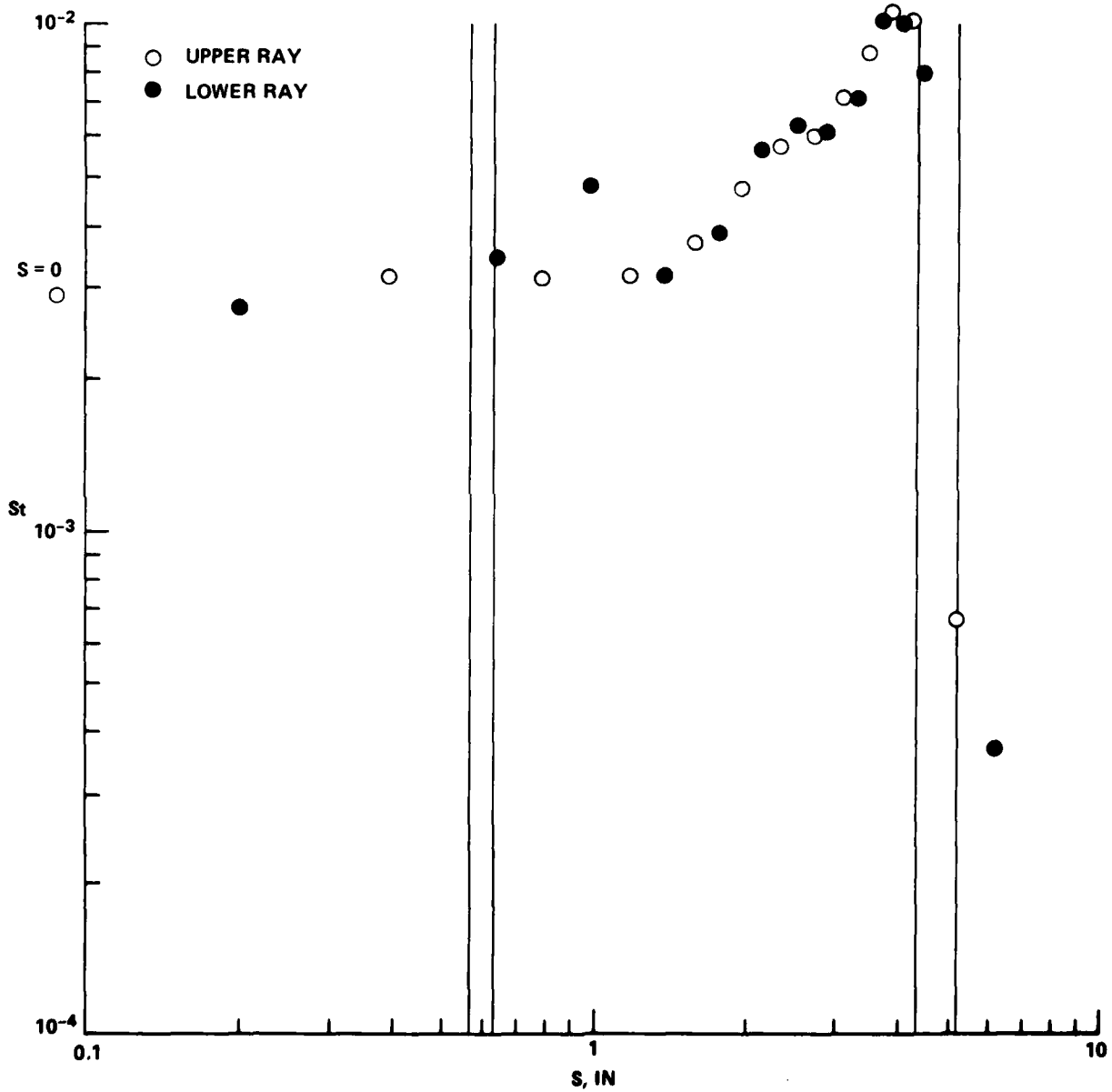
RUN 11 MODEL E
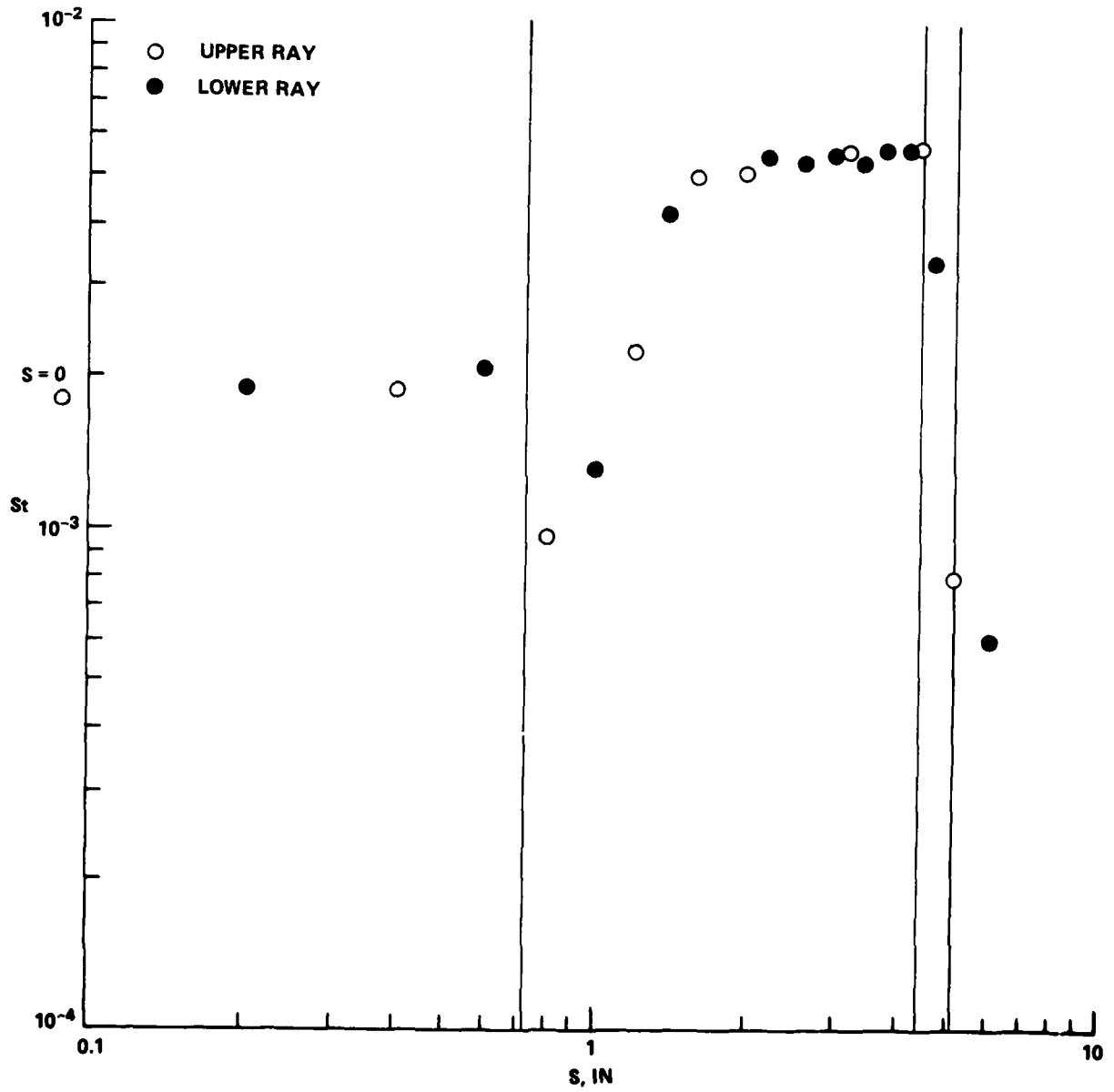
FIGURE 9(j) PLOTTED HEAT TRANSFER DATA (CONTINUED)

RUN 12 MODEL E
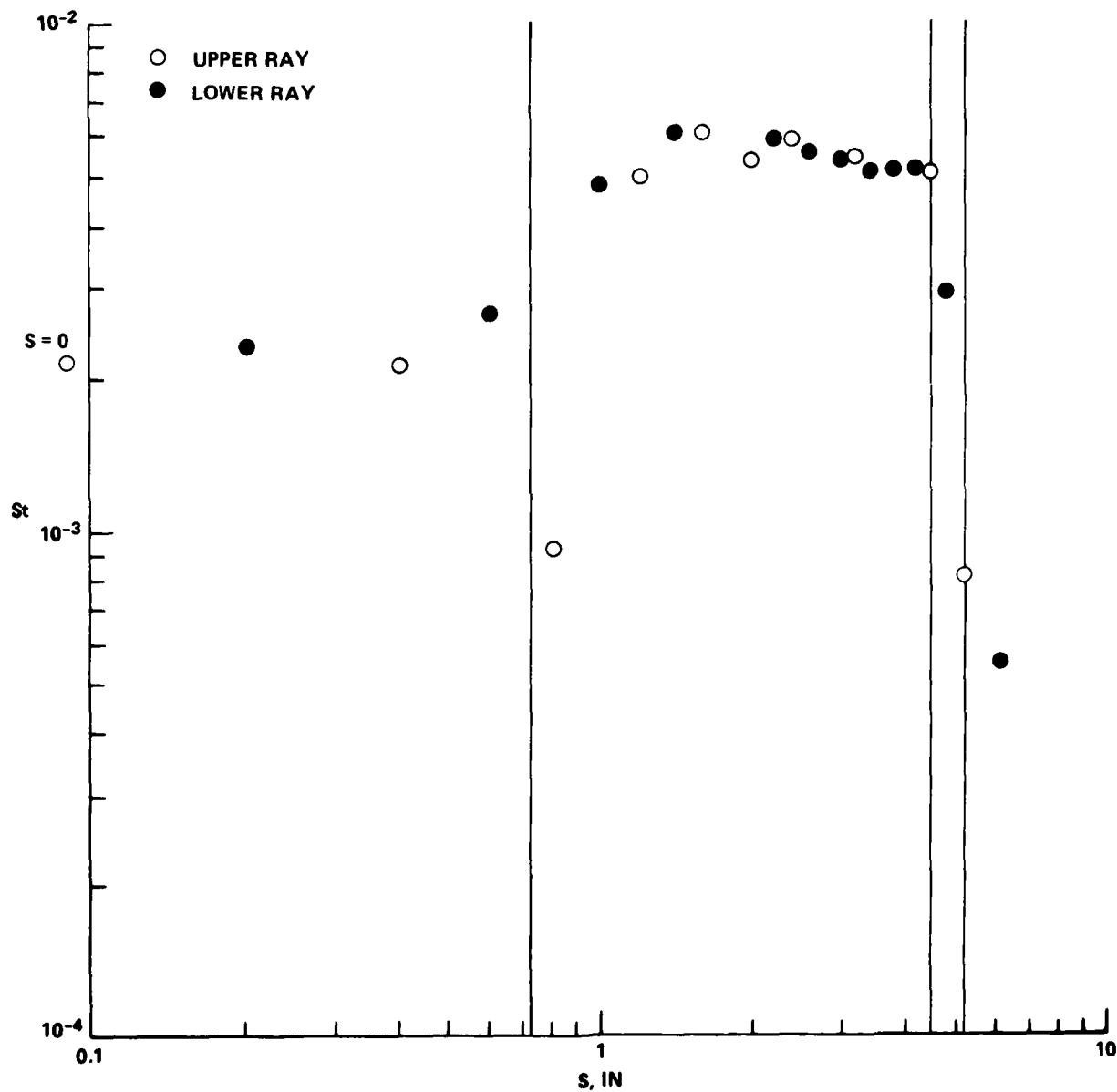
FIGURE 9(k) PLOTTED HEAT TRANSFER DATA (CONTINUED)

RUN 13 MODEL E
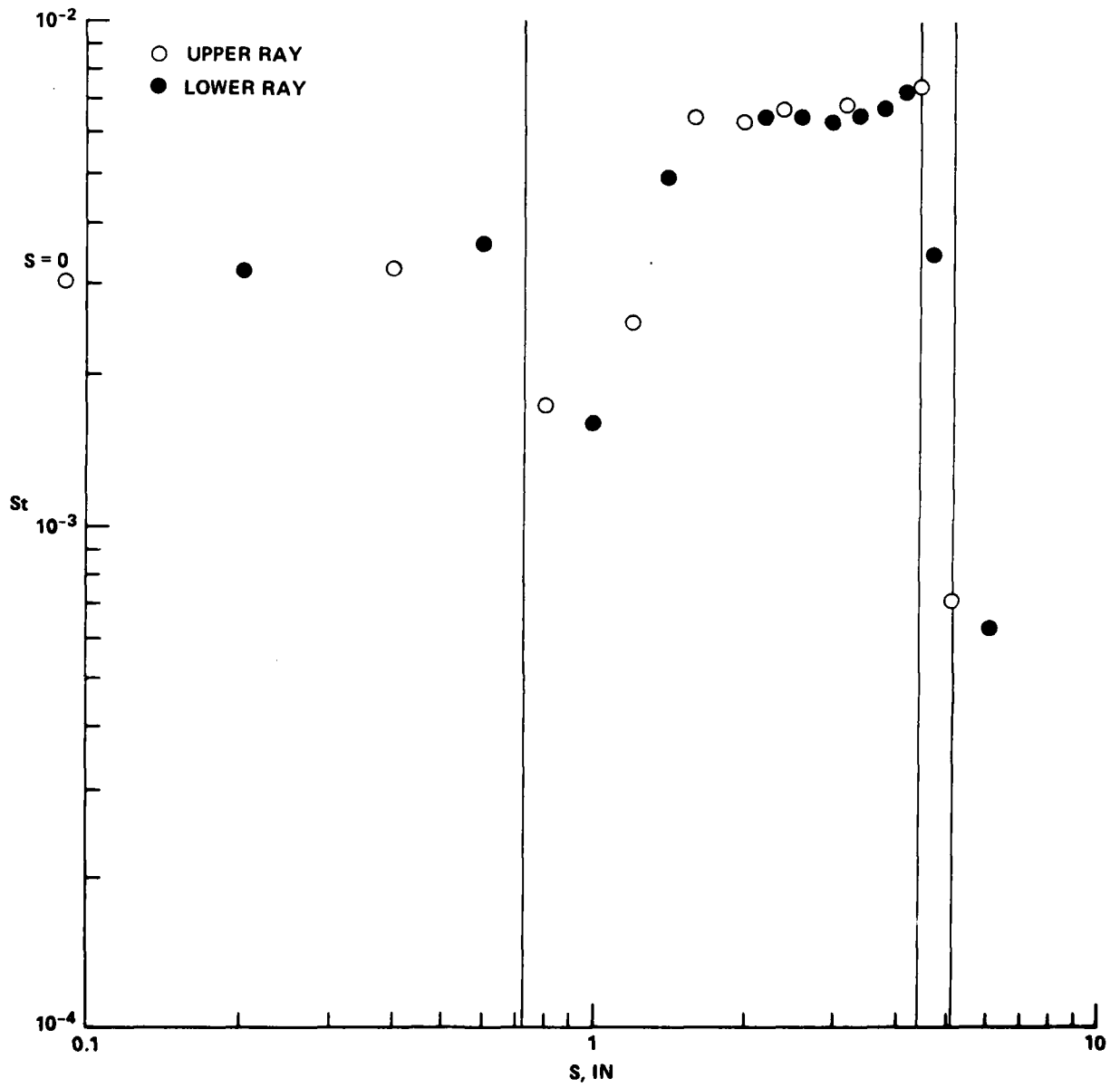
FIGURE 9(I) PLOTTED HEAT TRANSFER DATA (CONTINUED)

FIGURE 10(a) SCHLIEREN PHOTOGRAPH — RUN 5 MODEL B

FIGURE 10(b) SCHLIEREN PHOTOGRAPH — RUN 6 MODEL B

FIGURE 10(c) SCHLIEREN PHOTOGRAPH – RUN 7 MODEL B

FIGURE 10(d) SCHLIEREN PHOTOGRAPH – RUN 8 MODEL C

FIGURE 10(e) SCHLIEREN PHOTOGRAPH – RUN 9 MODEL C

FIGURE 10(f) SCHLIEREN PHOTOGRAPH — RUN 10 MODEL C — INITIAL FLOW FIELD

FIGURE 10(g) SCHLIEREN PHOTOGRAPH – RUN 10 MODEL C – FINAL FLOW FIELD

FIGURE 10(h) SCHLIEREN PHOTOGRAPH — RUN 1 MODEL D

FIGURE 10(i) SCHLIEREN PHOTOGRAPH – RUN 2 MODEL D

FIGURE 10(j) SCHLIEREN PHOTOGRAPH – RUN 11 MODEL E

FIGURE 10(k) SCHLIEREN PHOTOGRAPH – RUN 12 MODEL E – INITIAL FLOW FIELD

FIGURE 10(I) SCHLIEREN PHOTOGRAPH – RUN 13 MODEL E
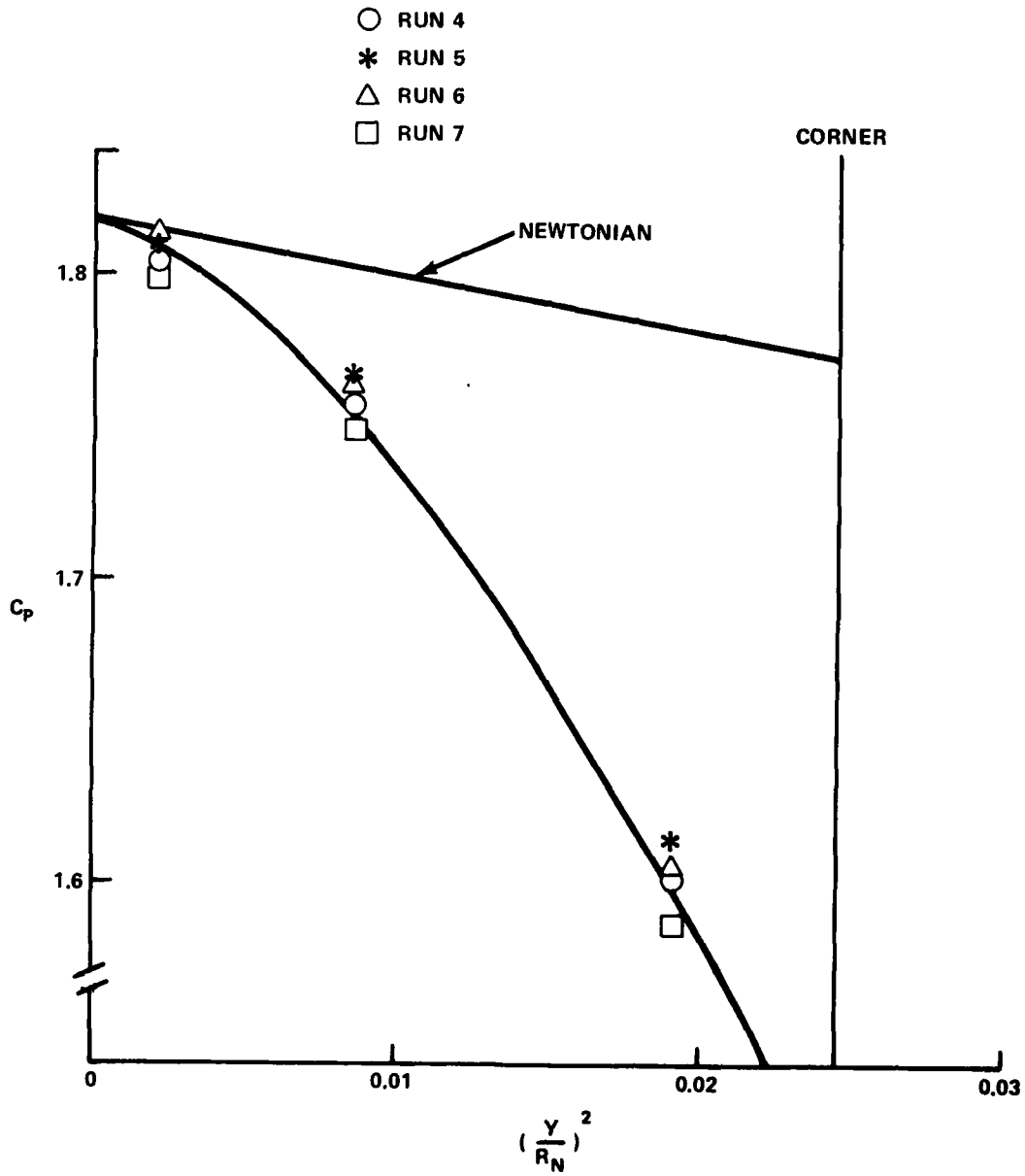
FIGURE 11 PRESSURE DISTRIBUTION ON HEMISPHERICAL NOSE CAP OF MODEL B
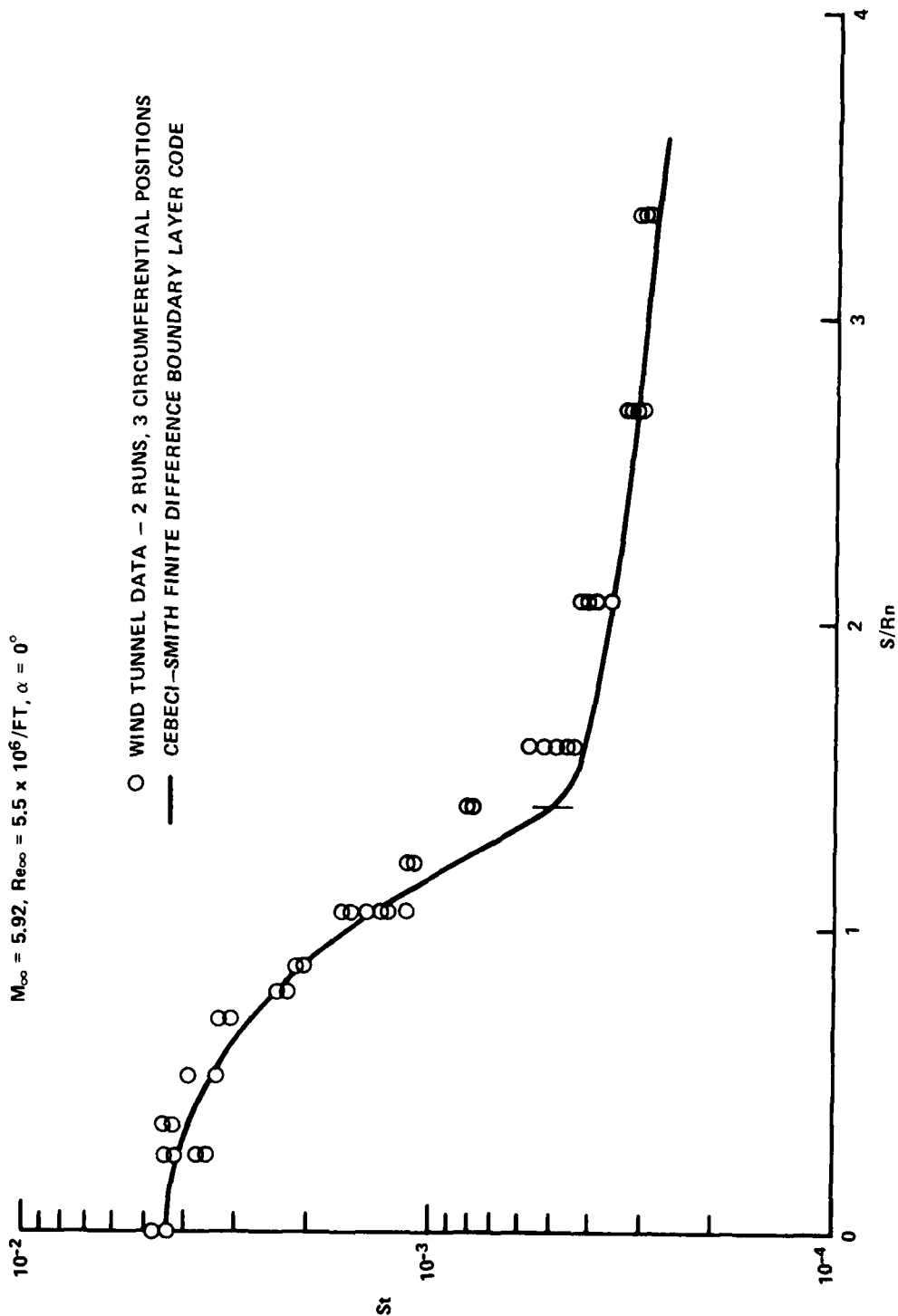
FIGURE 12 COMPARISON OF HEAT TRANSFER MEASUREMENTS ON A HEMISPHERE –
CONE WITH LAMINAR BOUNDARY LAYER THEORY
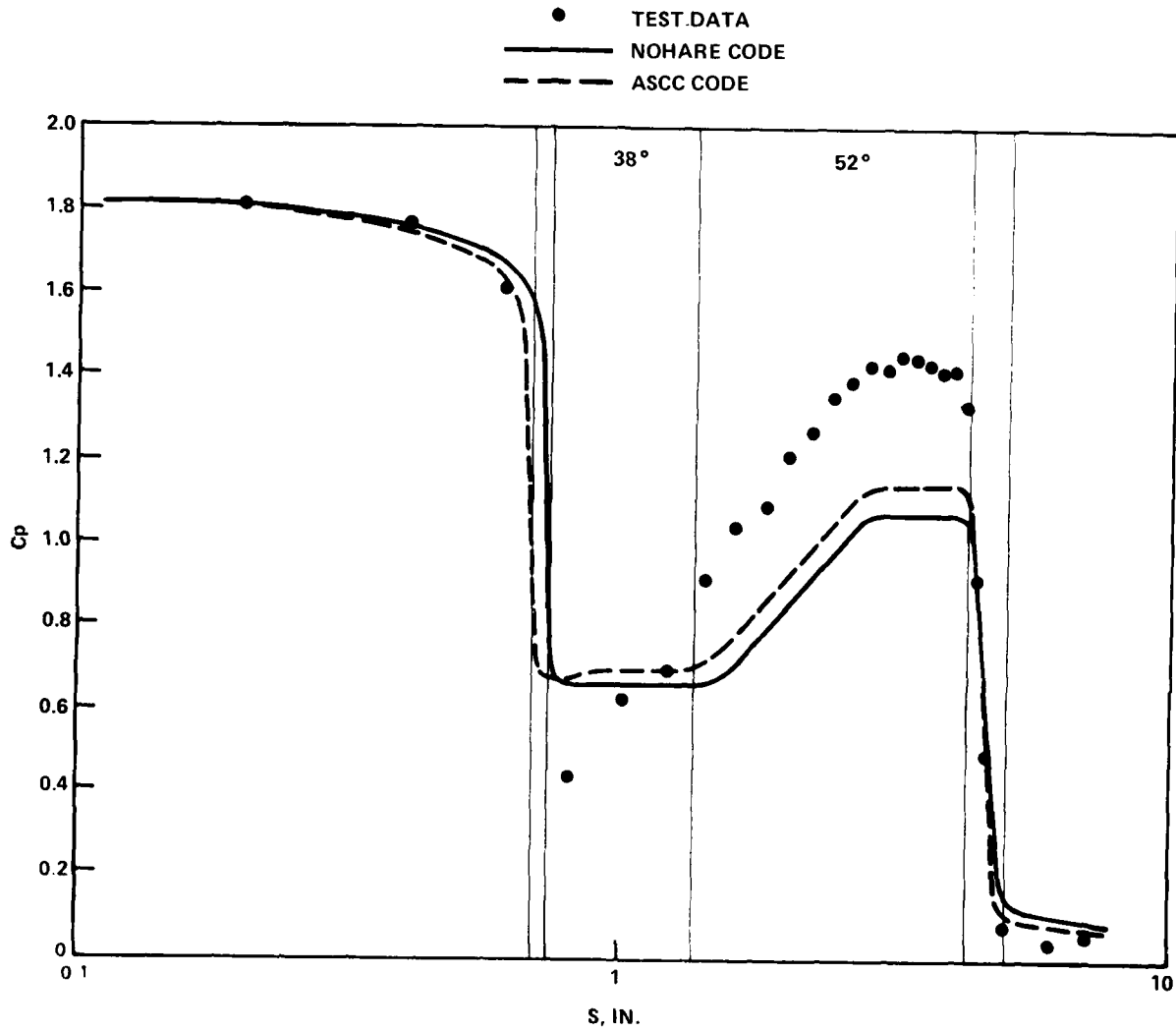
FIGURE 13(a) PRESSURE DATA (MODEL B, RUN 5)
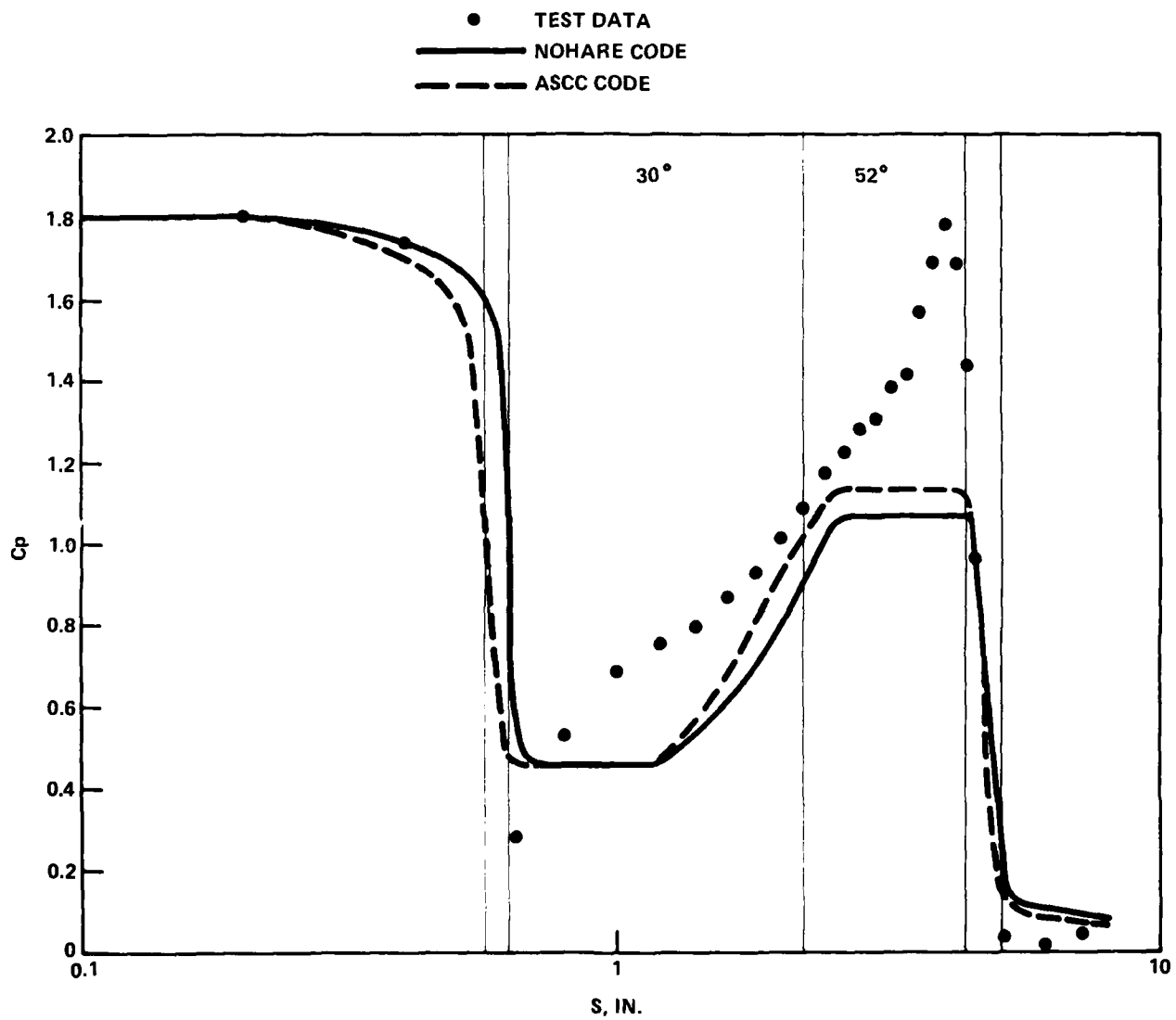
FIGURE 13(b) PRESSURE DATA (MODEL C, RUN 8)
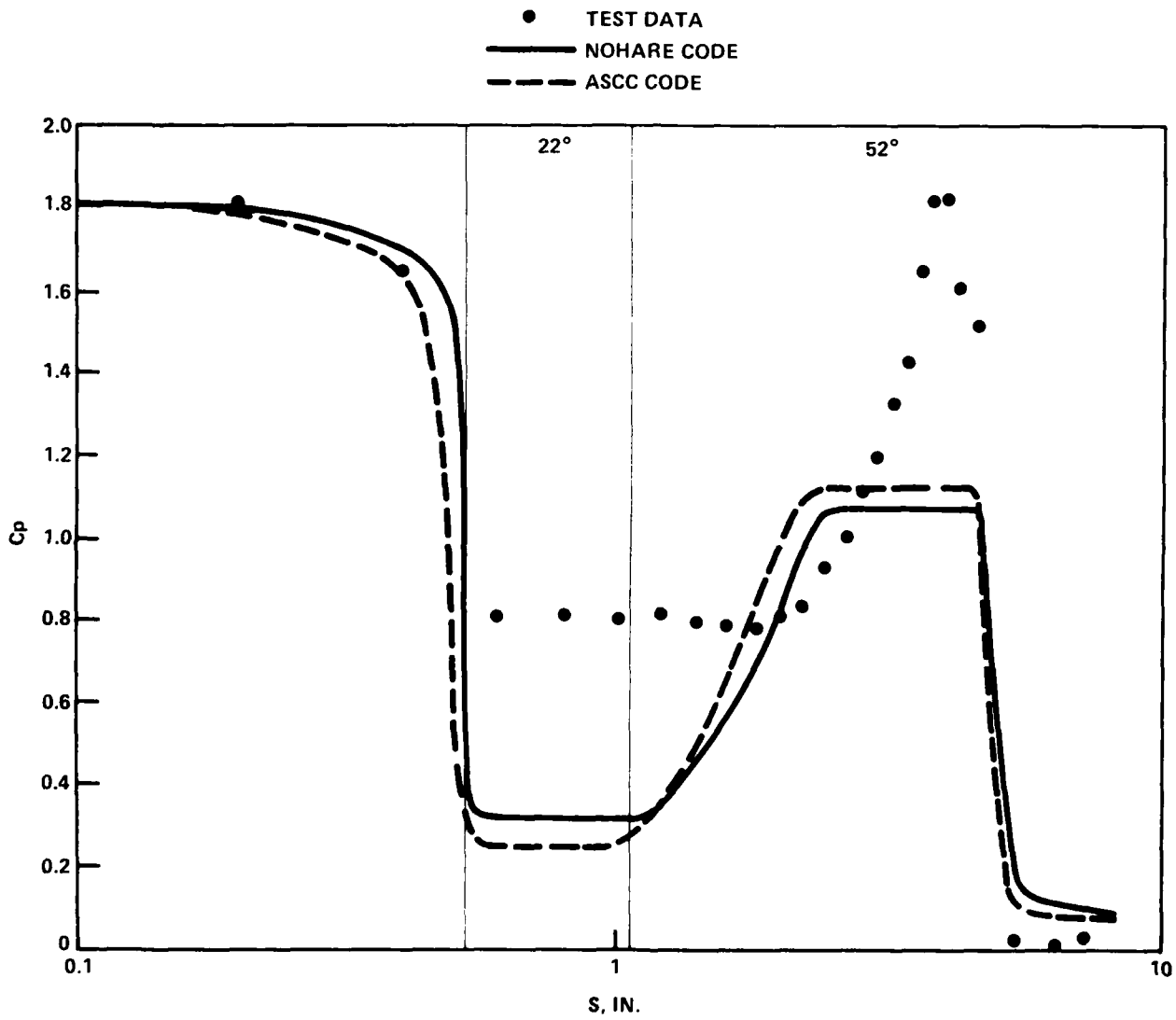
FIGURE 13(c) PRESSURE DATA (MODEL D, RUN 1)
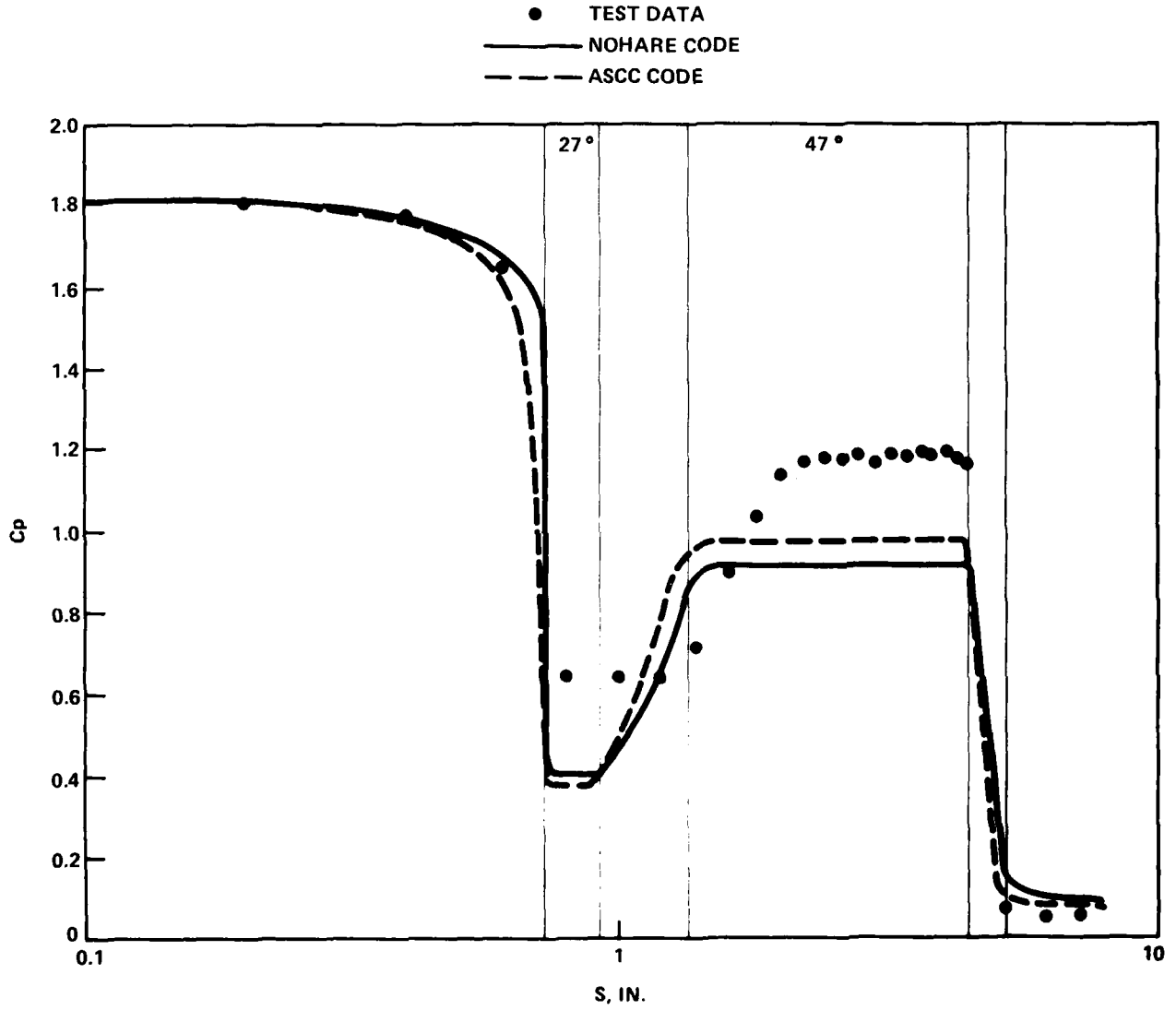
FIGURE 13(d) PRESSURE DATA (MODEL E, RUN 11)
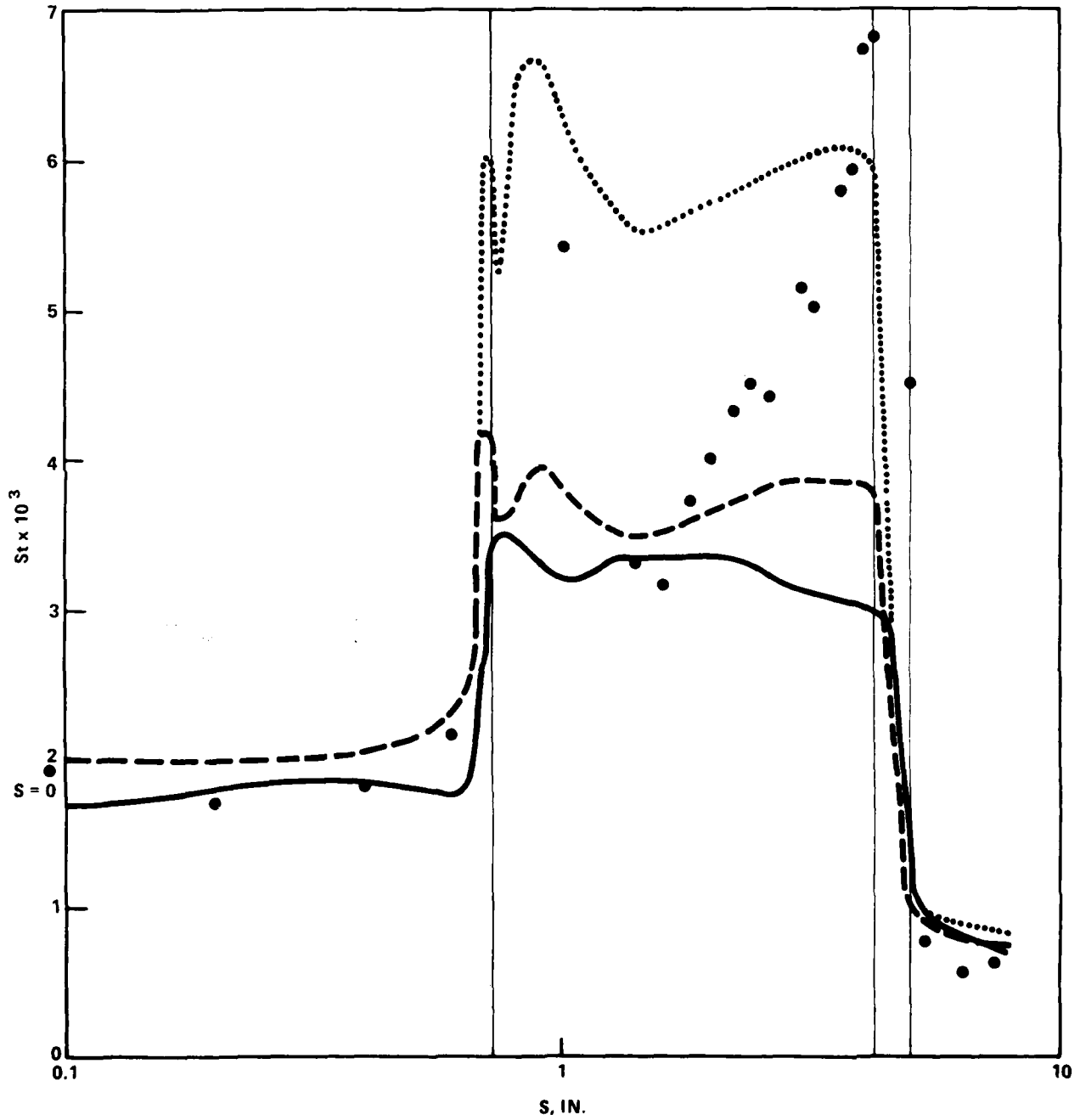
FIGURE 14(a) HEATING DATA (MODEL B, RUN 5)
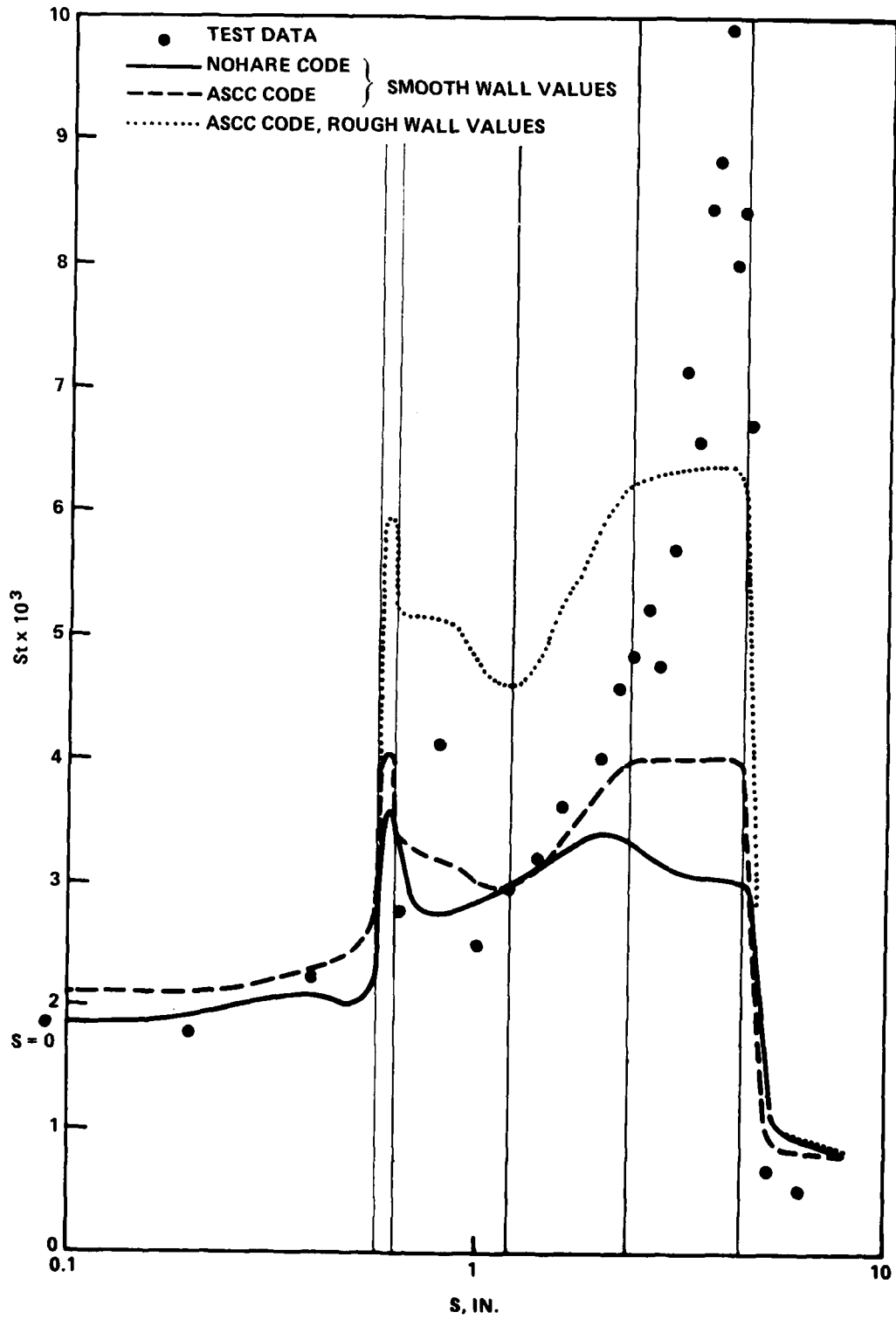
FIGURE 14(b) HEATING DATA (MODEL C, RUN 8)
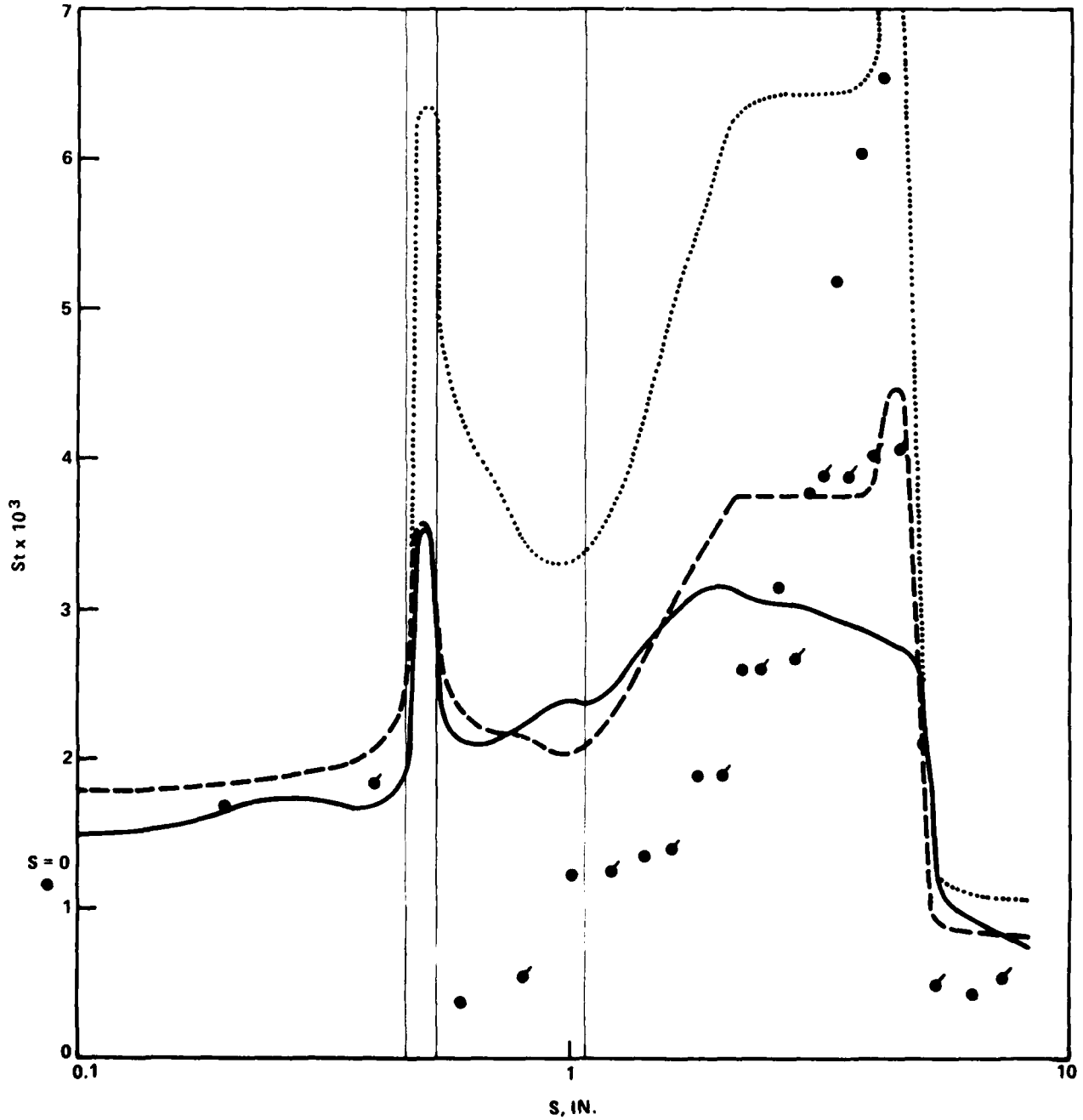
FIGURE 14(c) HEATING DATA (MODEL D, RUN 1)
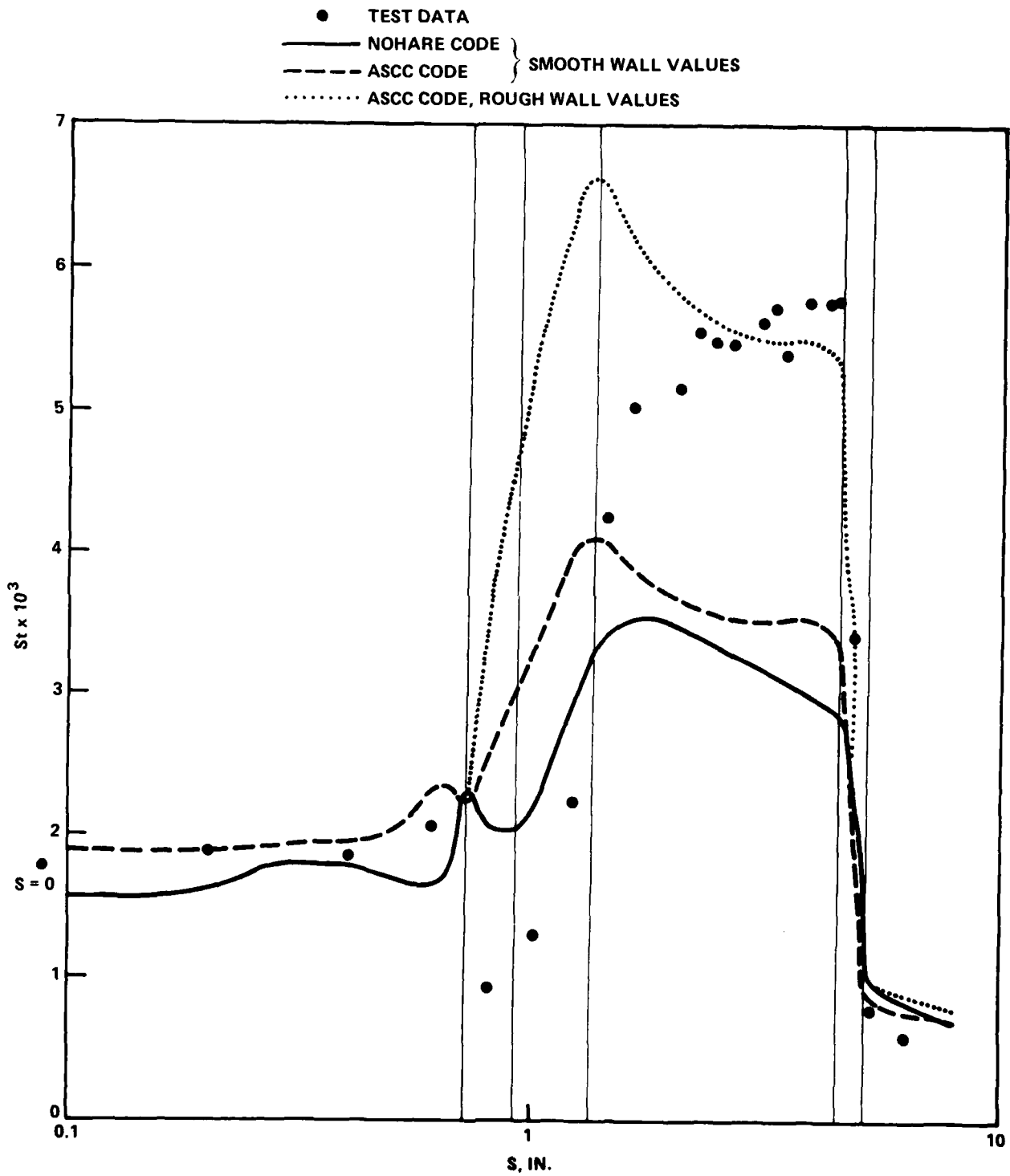
FIGURE 14(d) HEATING DATA (MODEL E, RUN 11)

FIGURE 15 DAMAGE TO CONFIGURATION D MODEL

FIGURE 16 DAMAGE TO CONFIGURATION D MODEL
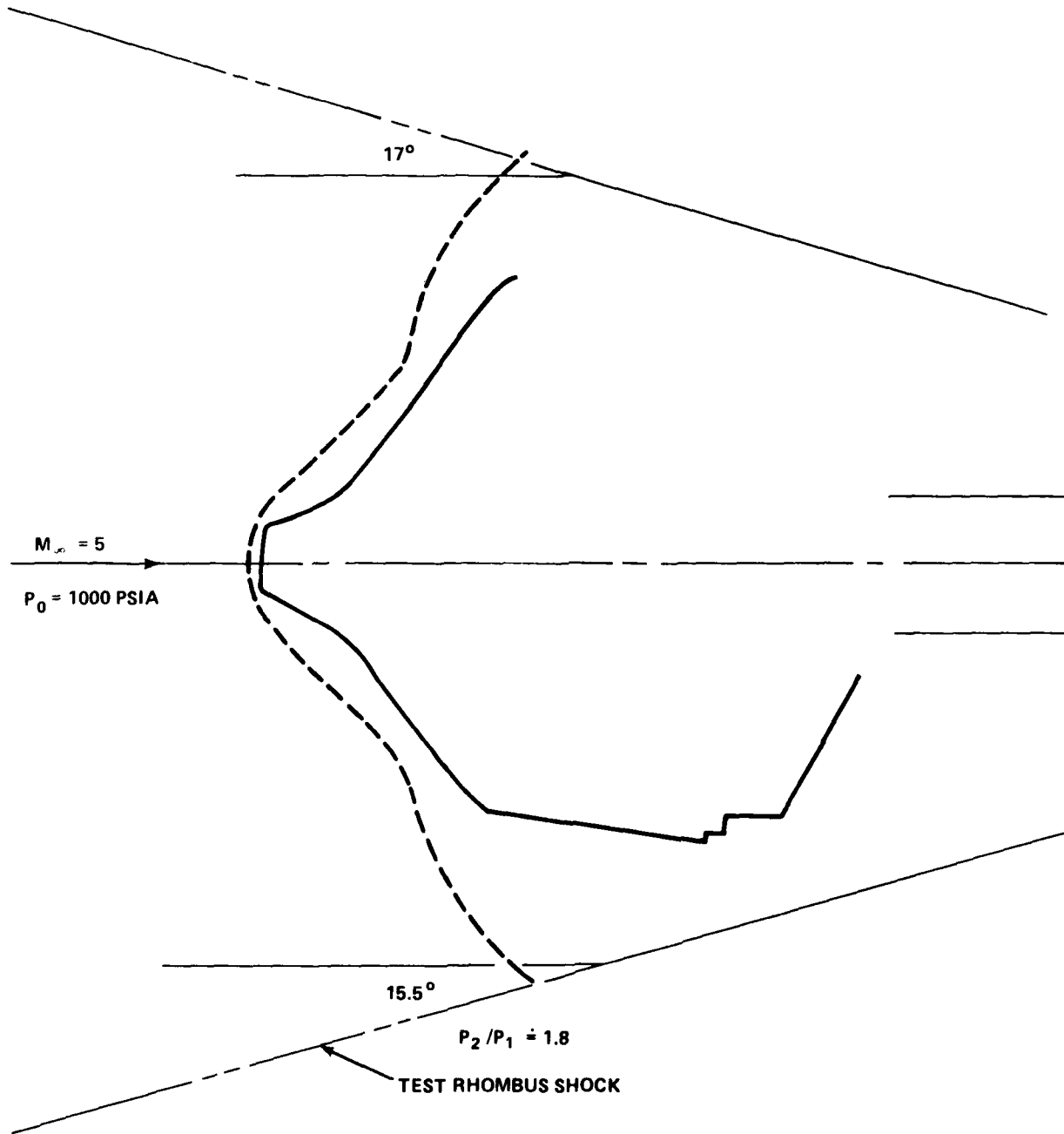
FIGURE 17 PRESSURE RATIO, CONFIGURATION D (P_0 = 1000 PSIA)
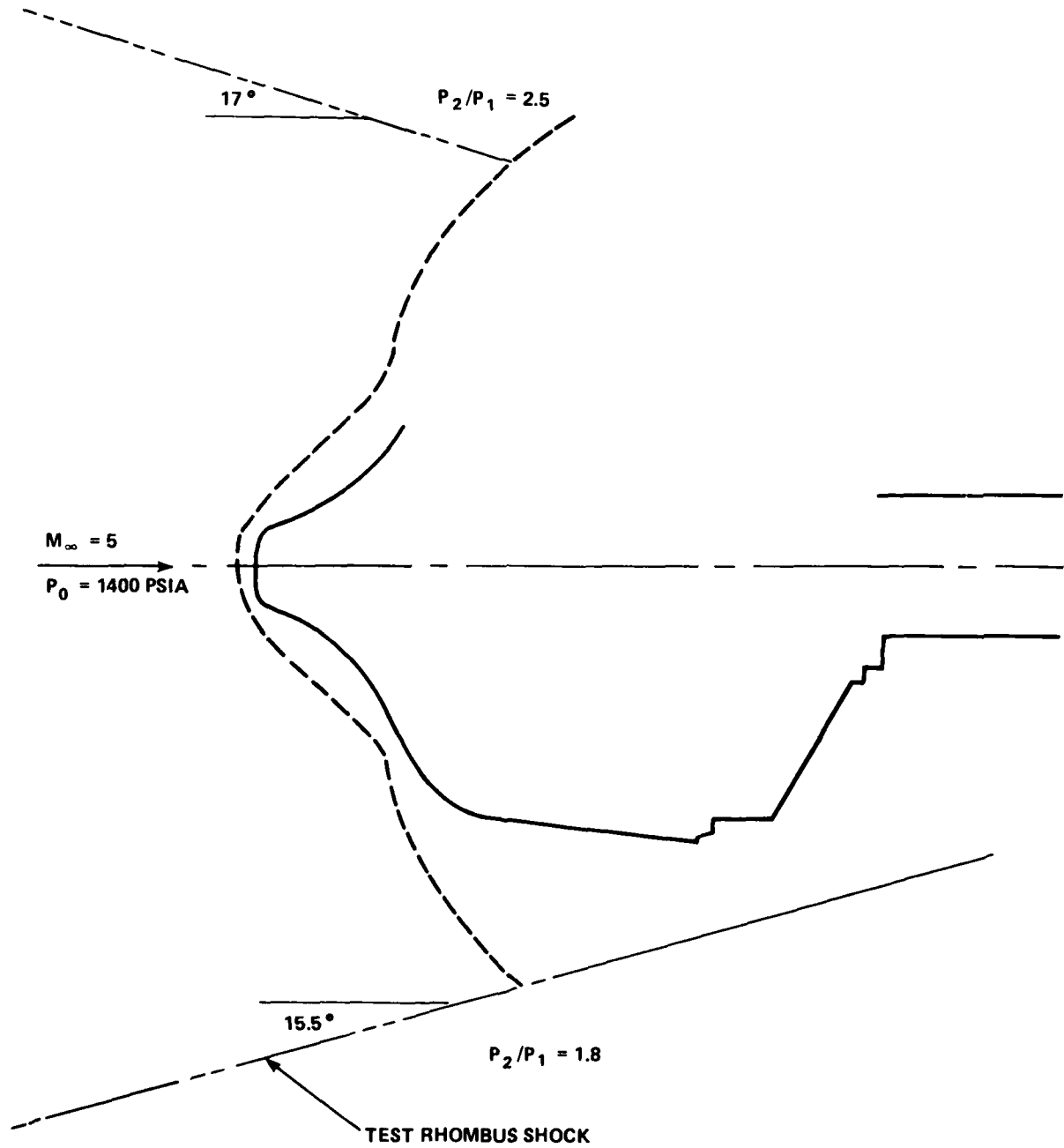
FIGURE 18 PRESSURE RATIO, CONFIGURATION D (P_0 = 1400 PSIA)

▲– SHAPIRO MIN STARTING AREA CALCULATION
○– DISK, NADC, MAX AREA BEFORE BLOCKAGE
■– T NUMBER 8 A_M/A_T IAP TEST 202
A_M– FRONTAL AREA OF MODEL
A_T– AREA OF TEST SECTION

FROM NAVORD REPORT
1488, VOL 6, SEC 20

A_M/A_T
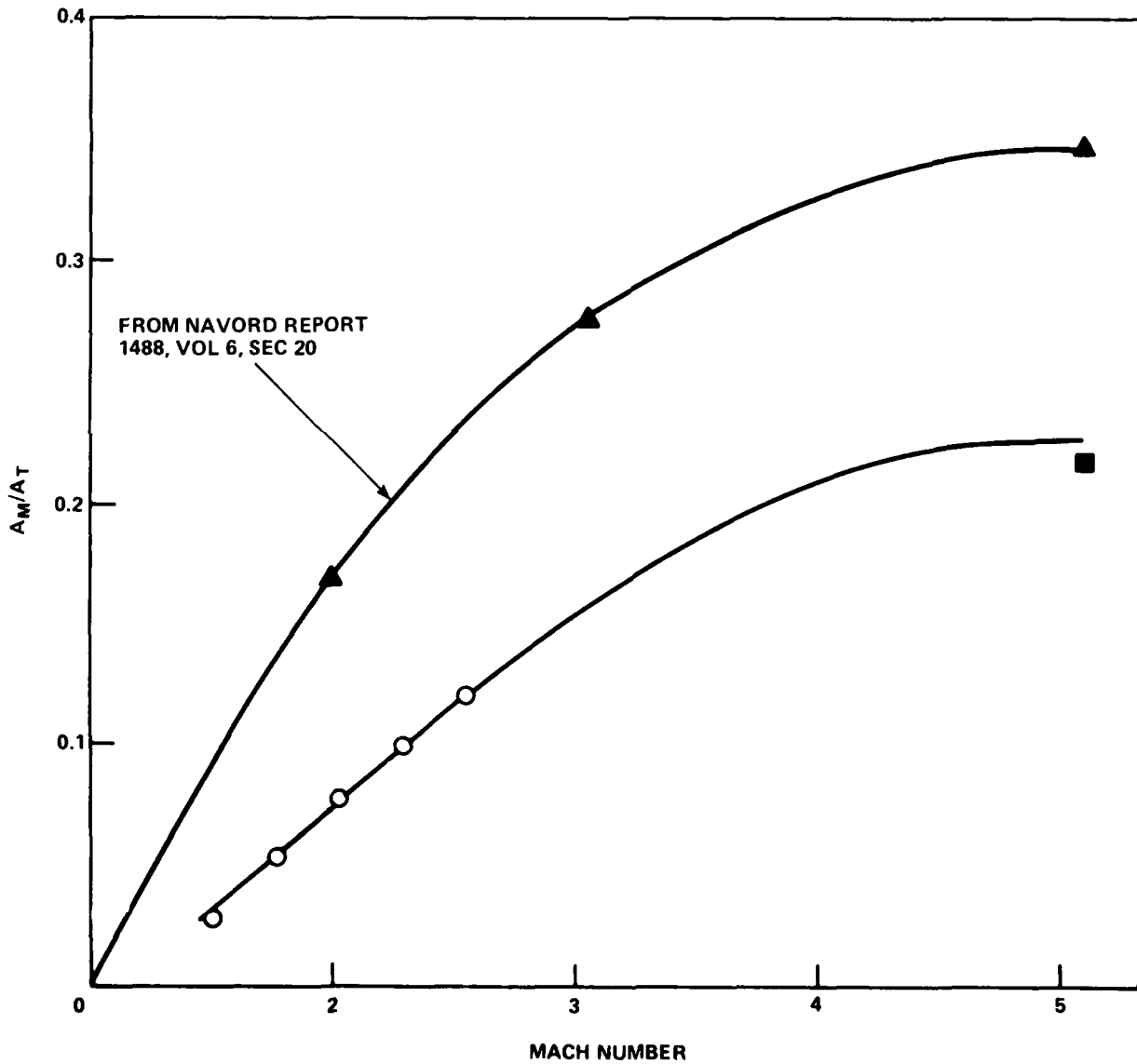
MACH NUMBER

FIGURE 19 UPPER LIMIT OF MODEL AREA TO TEST SECTION AREA AS A FUNCTION OF
MACH NUMBER
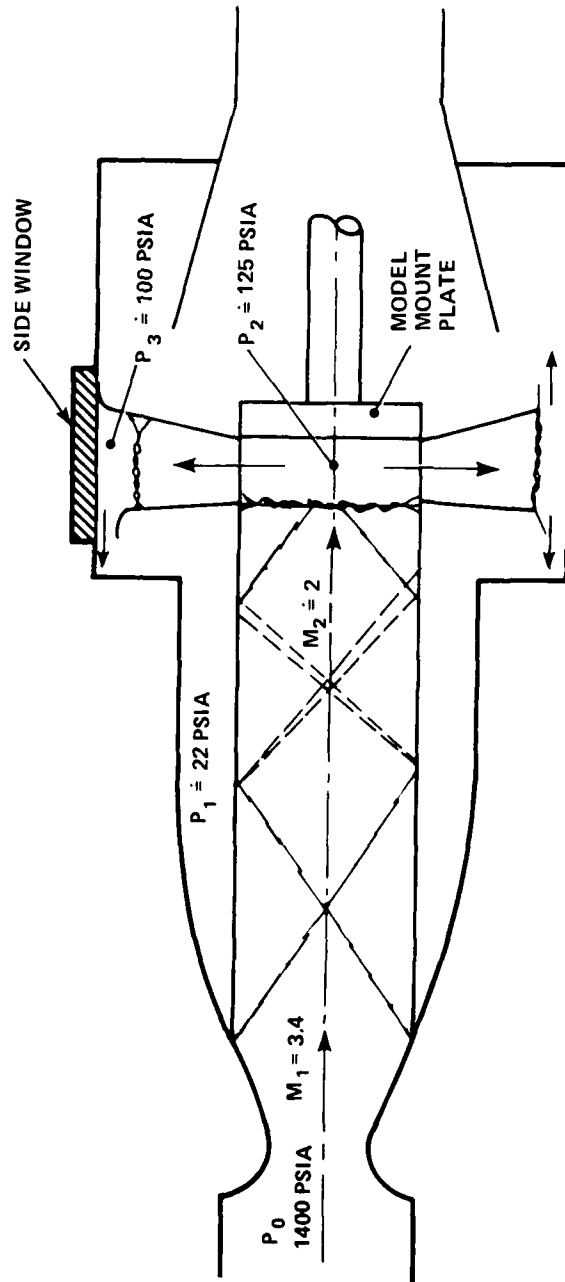
FIGURE 20 IMPINGEMENT JET (P$_0$ = 1400 PSIA)

SIDE WINDOW

P$_3$ $\doteq$ 100 PSIA

P$_2$ $\doteq$ 125 PSIA

MODEL MOUNT PLATE

M$_2$ $\doteq$ 2

P$_1$ $\doteq$ 22 PSIA

M$_1$ = 3.4

P$_0$ 1400 PSIA

1.0

1.1

1.25   1.4   1.6

2.8   2.5
3.2   2.2
3.6
4.0   2.0

1.8
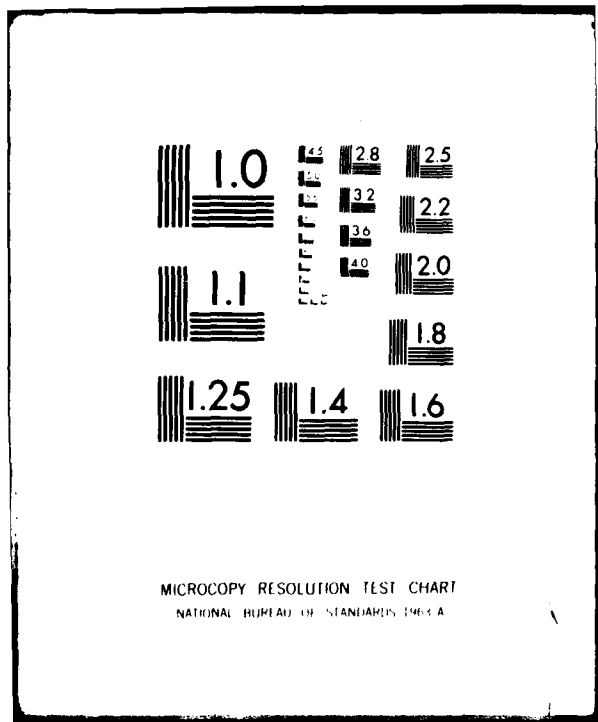
MICROCOPY RESOLUTION TEST CHART
NATIONAL BUREAU OF STANDARDS 1963 A

TABLE 1 LOG OF HEAT TRANSFER AND PRESSURE TESTS

Run No.	Model	Mach No.	Supply Pressure psia	Conditions Temperature ^{o}F	Tunnel Reynolds No. 1/ft x 10^6	Initial Wall Temp. ^{o}F
1	D	5.03	1402	514	31.3	59–67
2	D	5.02	998	494	23.0	43–60
3	A	~5	~1400	~500	no data – see note (d)	
4	B	5.96	1753	488	26.9	88–95
5	B	5.96	1694	505	25.3	84–96
6	B	5.96	1208	488	18.5	94–104
7	B	5.93	592	468	9.5	98–108
8	C	5.96	1706	509	25.3	83–87
9	C	5.96	1228	493	18.7	97–108
10	C	5.93	611	474	9.7	97–108
11	E	5.96	1719	494	26.1	87–94
12	E	5.96	1200	480	18.7	92–102
13	E	5.93	586	453	9.6	105–112

Notes:

a) The test conditions listed are those used in the heat transfer data reduction.

b) All tests were run at 0° angle of attack.

c) Run 2: Model D was damaged when a flow breakdown occurred during tunnel shutdown.

d) Run 3: A flow breakdown occurred immediately after model injection and model A was destroyed.

BIBLIOGRAPHY

Abdett, M. J., et. al., "Passive Nosetip Technology (PANT II) Program, Vol. II Computer User's Manual: ABRES Shape Change Code (ASCC)," Acurex Corporation/ Aerotherm Division, Final Report 76-224, Oct 1976.

Bruhn, E. F., Analysis and Design of Flight Vehicle Structures (Tri-State Offset Company, Jan 1965).

Love, E. S., et. al., "Some Topics in Hypersonic Body Shaping," AIAA Paper No. 69-181, 1969.

Moyer, C. B., et. al., "A Coupled Computer Code for the Transient Thermal Response and Ablation of Non-Charring Heat Shields and Nosetips," Aerotherm Corporation, NASA CR-1630, Oct 1970.

NACA Report 1135, Equations, Tables, and Charts for Compressible Flow, 1953.

Nagel, A. L., Fitzsimmons, H. D. and Doyle, L. B., "Analysis and Hypersonic Pressure and Heat Transfer Tests on Delta Wings with Laminar and Turbulent Boundary Layers," NASA CR-535, Appendix A, Aug 1966.

NAVORD Report 1488, Vol. 6, Sec. 20, 1961.

Pope, A. and Goin, K. L., High-Speed Wind Tunnel Testing (John Wiley & Sons, Inc., New York, NY, 1965).

Seidel, P., "The Stability Under Axial Compression and Lateral Pressure of Circular-Cylindrical Shells with Elastic Core," Journal of Aerospace Sciences, Vol. 29, Jul 1962.

Shapiro, A. M., Dynamics and Thermodynamics of Compressible Fluid Flow Vol. I (Tye Ronald Press Company, New York, NY, 1953).

Smith, D. H., et. al., "Computer Codes for Nosetip Recession and In-Depth Thermal Analysis: NOHARE, NOSEC, NODGEN," PDA, Inc., TR 5002-00-01, Jan 1976.

Stallings, R. L. Jr. and Campbell, J. F., "An Approximate Method for Predicting Pressure Distributions on Blunt Bodies at Angle of Attack," AIAA Paper No. 70-208, Jan 1970.

DISTRIBUTION

Copies

Commander
Naval Sea Systems Command Headquarters
Department of the Navy
Attn: Chief Technical Analyst
        SEA-05121
        SEA-033
        SEA-031
        SEA-09G32   2
        SEA-035
Washington, DC   20360

Commander
Naval Air Systems Command Headquarters
Department of the Navy
Attn: AIR-03B
        AIR-03C
        AIR-320
        AIR-320C
        AIR-310
        AIR-50174   2
Washington, DC   20360

Office of Naval Research
800 N. Quincy St.
Attn: ONR 100
        M. Cooper, 430B   2
Arlington, VA   22217

Commander
Naval Ship Research and Development Center
Attn: Central Library (5641)
        Aerodynamics Lab. (5643)
Bethesda, MD   20034

Commander
Naval Weapons Center
Attn: Technical Library (533)
        Code 406
        R. E. Meeker (4063)
China Lake, CA   93555

DISTRIBUTION (Cont.)

Copies

Director, U. S. Naval Research Laboratory
Attn: Library
        Code 6503
Washington, DC   20390

NASA
Langley Research Center
Langley Station
Attn: MS/185 Technical Library
        Aero & Space Mech Div.
        Dennis Bushnell
        Ivan Beckwith
        R. Trimpi
        Julius Harris
Hampton, VA   23665

NASA
Lewis Research Center
21000 Brookpart Road
Attn: Library 60-3
        Chief, Wind Tunnel & Flight Div.
Cleveland, OH   44135

NASA
George C. Marshall Space Flight Center
Attn: Mr. T. Reed, R-AERO-AU
        Mr. W. K. Dahm, BB31
Huntsville, AL   35812

NASA
600 Independence Avenue, S. W.
Attn: F. C. Schwenk, Director, Research (Code RR)
Washington, DC   20546

NASA
P.O. Box 33
College Park, MD   20740

Technical Library
Director Defense Research and Engineering (DDR&E)
Room 3E-1036, The Pentagon
Attn: Stop 103
Washington, DC   20301

Defense Documentation Center
Cameron Station   12
Alexandria, VA   22314

DISTRIBUTION (Cont.)

Copies

Commander (5632.2)
Naval Missile Center
Attn: Technical Library
Point Mugu, CA 93041

Commanding Officer
USA Aberdeen Research and Development Center
Aberdeen Proving Ground
Attn: STEAP-TL
       AMXRD-XSE
Aberdeen, MD 21005

Director of Intelligence
Headquarters, USAF (AFNINDE)
Attn: AFOIN-3B
Washington, DC 20330

Los Angeles Air Force Station
SAMSO/DYAE
P.O. Box 92960
Worldway Postal Center
Attn: Code RSSE
       Code RSSM
Los Angeles, CA 90009

Headquarters, Arnold Engineering
  Development Center
Arnold Air Force Station
Attn: Library/Documents
       R. W. Henzel, TD
       CAPT C. Tirres/DYR
Tullahoma, TN 37389

von Karman Gas Dynamics Facility
ARO, Inc.
Arnold Air Force Station
Attn: Dr. J. D. Whitfield
       Dr. F. Galanga
Tullahoma, TN 37389

Commanding Officer
Harry Diamond Laboratories
Attn: Library
Washington, DC 20438

DISTRIBUTION (Cont.)

Copies

Commanding General
U. S. Army Missile Command
Redstone Arsenal
Attn: AMSMI-RR
       Chief, Document Section   2
       AMSMI-RDK, R. A. Deep
       AMSMI-RDK, T. R. Street
Redstone Arsenal, AL 35809

Department of the Army
Office of the Chief of Research
  and Development
ABMDA, The Pentagon
Washington, DC 20350

Commanding Officer
Picatinny Arsenal
Attn: SMUPA-VC-3 (A.A. Loeb)
Dover, New Jersey 07801

Commander (ADL)
Naval Air Development Center
Johnsville, PA 18974

Air Froce Weapons Laboratory
Kirtland Air Force Base
Attn: CAPT Tolman/SAS
       Tech. Library (SUL)
Albuquerque, NM 87117

U. S. Army Ballistic Missile Defense Agency
1300 Wilson Boulevard
Arlington, VA 22209

The Johns Hopkins University (C/NOw 7386)
Applied Physics Laboratory
Johns Hopkins Road
Attn: Document Library   2
       Dr. F. Hill
       Dr. L. L. Cronvich
       L. Glover
Laurel, MD 20910

Director, Defense Nuclear Agency
Headquarters, DASA
Attn: STSP (SPAS)
Washington, DC 20305

DISTRIBUTION (Cont.)

Copies

Commanding Officer
Naval Intelligence Support Center
4301 Suitland Road
Washington, DC 20390

Department of Aeronautics
DFAN
USAF Academy
Colorado 80840

Armament Development and Test Center
Attn: Technical Library, DLOSL
Eglin AFB, FL 32542

Headquarters, Edgewood Arsenal
Attn: A. Flatau
Edgewood Arsenal, MD 21010

Commander
U. S. Army Natick Development Center
AMSNM-UBS
Attn: AMXNM-UBS
       G. A. Barnard
Natick, MA 01760

NASA Ames Research Center
Attn: Dr. M. Horstman
Moffett Field, CA 94035

Fluid Dynamics Laboratory
Wright-Patterson Air Force Base
Attn: D. J. Harney
Dayton, OH 45433

AFFDL/FXG
Wright Patterson Air Force Base
Attn: Mr. Melvin Buck
Dayton, OH 45433

Aerospace Engineering Program
University of Alabama
P.O. Box 6307
Attn: Prof. W. K. Rey, Chm.
Tuscaloosa, AL 35486

DISTRIBUTION (Cont.)

Copies

AME Department
University of Arizona
Attn: Dr. L. B. Scott
Tucson, AZ 85721

Polytechnic Institute of New York
Graduate Center Library
Route 110, Farmingdale
Attn: Dr. R. Cresci
Long Island, NY 11735

Polytechnic Institute of New York
Spicer Library
333 Jay Street
Attn: Reference Dept.
Brooklyn, NY 11201

California Institute of Technology
Attn: Graduate Aeronautical Laboratories
       Aero. Librarian
     Dr. A. Roshko
Pasadena, CA 91109

University of California
Dept. of Mechanical Engineering
Attn: Prof. F. Greif
Berkely, CA 94720

GASDYNAMICS
University of California
Richmond Field Station
1301 South 46th Street
Attn: A. K. Oppenheim
Richmond, CA 94804

Dept. of Aerospace Engineering
University of Southern California
University Park
Attn: Dr. John Laufer
Los Angeles, CA 90007

University of California, San Diego
Department of Aerospace and Mechanical Engineering
  Sciences
Attn: Dr. P. A. Libby
LaJolla, CA 92037

DISTRIBUTION (Cont.)

Copies

Case Western Reserve University
Division of Fluid, Thermal and Aerospace
  Engineering
Attn: Dr. Eli Reshotko
Cleveland, OH 44106

The Catholic University
Attn: Dr. C. C. Chang
Washington, DC 20017

University of Cincinnati
Attn: Department of Aerospace Engineering
       Dr. Arnold Polak
Cincinnati, OH 45221

Department of Aerospace Engineering Sciences
University of Colorado
Boulder, CO 80302

Cornell University
Graduate School of Aero. Engineering
Attn: Prof. W. R. Sears
Ithaca, NY 14850

University of Delaware
Mechanical and Aeronautical Engineering Dept.
Attn: Dr. James E. Danberg
Newark, DE 19711

Georgia Institute of Technology
225 North Avenue, N. W.
Attn: Dr. Arnold L. Ducoffe
Atlanta, GA 30332

Technical Reports Collection
Gordon McKay Library
Harvard University
Div. of Eng'g. and Applied Physics
Pierce Hall, Oxford Street
Cambridge, MA 02138

Illinois Institute of Technology
3300 South Federal
Attn: Dr. M. V. Morkovin
Chicago, IL 60616

DISTRIBUTION (Cont.)

Copies

University of Illinois
101 Transportation Bldg.
Attn: Aeronautical and Astronautical
        Engineering Dept.
Urbana, IL   61801

Iowa State University
Attn: Aerospace Engineering Dept.
Ames, IO 50010

The Johns Hopkins University
Attn: Prof. S. Corrsin
Baltimore, MD   21218

University of Kentucky
Wenner-Gren Aero. Lab.
Attn: C. F. Knapp
Lexington, KY   40506

Department of Aero. Engineering, ME 106
Louisiana State University
Attn: Dr. P. H. Miller
Baton Rouge, LA   70803

University of Maryland
Attn: Dr. S. I. Pai, Institute for Fluid Dynamics
        and Applied Mathematics
        Dr. John D. Anderson, Jr., Dept. of
        Aerospace Engineering
College Park, MD   20740

Michigan State University
Attn: Library Documents Dept.
East Lansing, MI   48823

Massachusetts Institute of Technology
Attn: Prof. A. H. Shapiro, Head Mech. Engr. Dept.
        Aero. Engineering Library
        Prof. R. F. Probestein
        Dr. E. E. Covert
        Aerophysics Laboratory
Cambridge, MA   02139

University of Michigan
Attn: Dr. M. Sichel, Dept. of Aero Engineering
        Engineering Library
        Aerospace Engineering Library
        Mr. C. Cousineau, Engin-Trans Lib.
Ann Arbor, MI   48104

DISTRIBUTION (Cont.)

Copies

Serials and Documents Section
General Library
University of Michigan
Ann Arbor, MI 48104

Mississippi State University
Department of Aerophysics and Aerospace Engineering
P.O. Drawer A
Attn: Mr. Charles B. Cliett
State College, MS 39762

U. S. Naval Academy
Attn: Engineering Dept., Aerospace Division
Annapolis, MD 21402

Library, Code 2124
U. S. Naval Postgraduate School
Attn: Technical Reports Section
Monterey, CA 93940

New York University
University Heights
Attn: Dr. Antioni Ferri, Director of Guggenheim
       Aerospace Laboratories
       Prof. V. Zakkay
New York, NY 10453

North Carolina State College
Attn: Dr. F. R. DeJarnette
Raleigh, NC 27607

D. H. Hill Library
North Carolina State University
P.O. Box 5007
Raleigh, NC 27607

University of North Carolina
Attn: Dept. of Aero. Engineering
Chapel Hill, NC 27514

Northwestern University
Technological Institute
Attn: Dept. of Mech. Engineering Library
Evanston, IL 60201

DISTRIBUTION (Cont.)

Copies

Dept. of Aero-Astro Engineering
Ohio State University
2036 Neil Avenue
Attn: Engineering Library
Columbus, OH 43210

The Pennsylvania State University
Attn: Dept. of Aero Engr., Hammond Bldg.
      Library, Documents Section
University Park, PA 18602

Bevier Engr. Library
126 Benedum Hall
University of Pittsburgh
Pittsburgh, PA 15261

Princeton University
Aerospace & Mech. Science Dept.
D-214 Engrg. Quadrangel
Attn: Dr. I. E. Vas
Princeton, NJ 08540

Purdue University
School of Aeronautical and Engineering Sciences
Attn: Dr. B. Reese, Head, Dept. of
         Aero. and Astro.
Lafayette, IN 47907

Rensselaer Polytechnic Institute
Attn: Dept. of Aeronautical Engineering and
         Astronautics
Troy, NY 12181

Department of Mechanical Industrial and
  Aerospace Engrg.
Rutgers - The State University
Attn: Dr. R. H. Page
New Bruswick, NJ 08903

Stanford University
Attn: Librarian, Dept. of Aeronautics and
         Astronautics
Stanford, CA 94305

Stevens Institute of Technology
Attn: Mechanical Engineering Dept., Library
Hoboken, NJ 07030

DISTRIBUTION (Cont.)

Copies

The University of Texas at Austin
Applied Research Laboratories
P.O. Box 8029
Attn: Director
       Engr. S. B. 114B/Dr. Friedrich
Austin, TX 78712

University of Toledo
2801 W. Bancroft
Attn: Dept. of Aero Engineering
Toledo, OH 43606

University of Virginia
School of Engineering and Applied Science
Attn: Dr. I. D. Jacobson
Charlottesville, VA 22901

University of Washington
Attn: Engineering Library Dept. of Aeronautics
          and Astronautics
Seattle, WA 98105

West Virginia University
Attn: Library
Morgantown, WV 26506

Federal Reports Center
University of Wisconsin
Mechanical Engineering Building
Attn: S. Reilly
Madison, WI 53706

Los Alamos Scientific Laboratory
P.O. Box 1663
Attn: Reports Library
Los Alamos, NM 87544

Institute for Defense Analyses
400 Army-Navy Drive
Attn: Classified Library
Arlington, VA 22202

DISTRIBUTION (Cont.)

Copies

Kaman Sciences Corporation
P.O. Box 7463
Attn: Library
        Mr. F. Barbera
        Mr. P. Wells
        Mr. D. Foxwell
Colorado Springs, CO   80933

Kaman Sciences Corporation
Avidyne Division
83 Second Avenue
Attn: Dr. J. R. Ruetenik
Burlington, MA   01803

Rockwell International
B-1 Division
Technical Information Center
(BA08) International Airport
Los Angeles, CA   90009

Rockwell International Corporation
Technical Information Center
4300 E. Fifth Avenue
Columbus, OH   43216

M. I. T. Lincoln Laboratory
P.O. Box 73
Attn: Library A-082
Lexington, MA   02173

The RAND Corporation
1700 Main Street
Attn: Library - D
Santa Monica, CA   90406

Aerojet Electrosystems Co.
1100 W. Hollyvale Avenue
Attn: Engineering Library
Azusa, CA   91702

The Boeing Company
P.O. Box 3999
Attn: 87-67
Seattle, WA   98124

DISTRIBUTION (Cont.)

Copies

United Aircraft
Research Laboratories
Attn: Dr. William M. Foley
East Hartford, CT 05108

United Aircraft Corporation
400 Main Street
Attn: Library
East Hartford, CT 06108

Hughes Aircraft Company
Centinela at Teale
Attn: Company Tech. Doc. Center
       6/Ell, B. W. Campbell
Culver City, CA 90230

Lockheed Missiles and Space Co.
P.O. Box 504
Attn: G. T. Chrusciel
       R. Nelson
       C. Louis
       B. Smith
Sunnyvale, CA 94086

Lockheed Missiles and Space Co.
3251 Hanover Street
Attn: Technical Information Center
Palo Alto, CA 94304

Lockheed-California Co.
Attn: Central Library Dept.
Burbank, CA 91503

Vice President and Chief Scientist
Dep. 03-10
Lockheed Aircraft Corp.
P.O. Box 551
Burbank, CA 91503

Martin Marietta Corporation
P.O. Box 988
Attn: Science-Technology Library
       (Mail No. 398)
Baltimore, MD 21203

DISTRIBUTION (Cont.)

Copies

Martin Company
3211 Trade Winds Trail
Attn: Mr. H. J. Diebolt
Orlando, FL 32805

General Dynamics
P.O. Box 748
Attn: Research Library 2246
       George Kaler, Mail Zone 2880
Fort Worth, TX 76101

Calspan Corporation
4455 Genesee Street
Attn: Library
Buffalo, NY 14221

Air Force University Library
(SE) 63-578
Maxwell Air Force Base
Montgomery, AL 36112

McDonnell Company
P.O. Box 516
Attn: R. D. Detrich, Dept. 209 Bldg. 33
St. Louis, MI 63166

McDonnell Douglas Astronautics Company - West
5301 Bolsa Avenue
Attn: 368, B4A0
       J. S. Murphy, A3
       J. Copper
       J. Xerikos
Huntington Beach, CA 92647

Fairchild Hiller
Republic Aviation Division
Attn: Engineering Library
Farmingdale, NY 11735

General Applied Science Labs. Inc.
Merrick and Stewart Avenues
Westbury
Attn: Dr. F. Lane
       L. M. Nucci
Long Island, NY 11590

DISTRIBUTION (Cont.)

Copies

General Electric Company
R&D Lab. (Comb. Bldg.)
Attn: Dr. H. T. Nagamatsu
Schenectady, NY 12301

The Whitney Library
General Electric Research and Development Center
The Knolls, K-1
P.O. Box 8
Attn: M. F. Orr, Manager
Schenectady, NY 12301

General Electric Company
Missile and Space Division
P.O. Box 8555
Attn: MSD Library
      Dr. J. D. Stewart
Philadelphia, PA 19101

General Electric Company
AEG Technical Information Center, N-32
Cincinnati, OH 45215

General Electric Company
Re-Entry & Environmental Systems Division
3198 Chestnut Street
Attn: W. Daskin
      R. Neff
      B. McGuire
Philadelphia, PA 19101

AVCO-Everett Research Lab.
2385 Revere Beach Parkway
Attn: Library
      Dr. George Sutton
Everett, MA 02149

LTV Aerospace Corporation
Vought Aeronautics Division
P.O. Box 5907
Attn: Unit 2-51131 (Library)
Dallas, TX 75222

LTV Aerospace Corporation
Missiles and Space Division
P.O. Box 6267
Attn: MSD-T-Library
Dallas, TX 75222

DISTRIBUTION (Cont.)

Copies

Northrop Norair
3901 West Broadway
Attn: Tech. Info. 3360-32
Hawthorne, CA   90250

Government Documents
The Foundren Library
Rice Institute
P.O. Box 1892
Houston, TX   77001

Grumman Aircraft Engineering Corporation
Bethpage
Attn: Dr. R. E. Melnik
Long Island, NY   11714

Marquardt Aircraft Corp.
16555 Saticoy Street
Attn: Library
Van Nuys, CA   91409

ARDE Associates
P.O. Box 286
580 Winters Avenue
Attn: Librarian
Paramus, NJ   07652

Aerophysics Company
3500 Connecticut Avenue, N. W.
Attn: Mr. G. D. Boehler
Washington, DC   20003

Aeronautical Research Associates of Princeton
50 Washington Road
Attn: Dr. C. duP. Donaldson
Princeton, NJ   08540

General Research Corporation
5383 Hollister Avenue
P.O. Box 3587
Attn: Technical Information Office
Santa Barbara, CA   93105

DISTRIBUTION (Cont.)

Copies

Sandia Laboratories
Box 5800
Attn: Dr. C. Peterson
       Mr. R. Stearley
       Dr. G. W. Stone
Albuquerque, NM 87115

Hercules Incorporated
Allegany Ballistics Lab.
P.O. Box 210
Attn: Library
Cumberland, MD   21502

General Electric Company
P.O. Box 2500
Attn: Dave Hovis, Room 4109
Daytona Beach, FL   32015

TRW Systems Group
1 Space Park
Attn: Tech. Library/Doc. Acquisitions
Redondo Beach, CA   90278

Stanford Research Institute
333 Ravenswood Avenue
Attn: Dr. G. Abrahamson
Menlo Park, CA   94025

Hughes Aircraft Company
P.O. Box 3310
Attn: Tech. Library, 600-C222
Fullerton, CA   92634

Westinghouse Electric Corp.
Astronuclear Laboratory
P.O. Box 10864
Attn: Library
Pittsburgh, PA   15236

University of Tennessee
Space Institute
Attn: Prof. J. M. Wu
Tullahoma, TN   37388

CONVAIR Division of General Dynamics
Library and Information
P.O. Box 12009
San Diego, CA   92112

DISTRIBUTION (Cont.)

Copies

CONVAIR Division of General Dynamics
P.O. Box 80986
Attn: Dr. J. Raat, Zone 640-02
        Research Library
San Diego, CA 92138

AVCO Missiles Systems Division
201 Lowell Street
Attn: E. E. H. Schurmann
        J. Otis
Wilmington, MA 01887

Chrysler Corporation
Space Division
P.O. Box 29200
Attn: N. D. Kemp 2910
        E. A. Rawls, Dept 2920
New Orleans, LA 70129

General Dynamics
Pomona Division
P.O. Box 2507
Attn: Tech. Doc. Center (6-20)
Pomona, CA 91766

Raytheon Company
Missile Systems Division
Hartwell Road
Attn: D. P. Forsmo
Bedford, MA 01730

TRW Systems Group
Space Park Drive
Attn: M. W. Sweeney, Jr.
Houston, TX 77058

Marine Bioscience Laboratory
513 Sydnor Street
Attn: Dr. A. C. Charters
Ridgecrest, CA 93555

University of California - Los Angeles
Dept. of Mechanics & Structures
Attn: Prof. J. D. Cole
Los Angeles, CA 90024

DISTRIBUTION (Cont.)

Copies

University of Wyoming
University Station
P.O. Box 3295
Attn: Head, Dept. Mech. Eng.
Laramie, WY 82070

Applied Mechanics Review
Southwest Research Institute
8500 Culebra Road
San Antonio, TX 78228

American Institute of Aeronautics and
  Astronautics
Attn: J. Newbauer
New York, NY 10019

Technical Information Services
AIAA
750 Third Avenue
Attn: Miss P. Marshall
New York, NY 10017

Faculty of Aeronautical Systems
University of West Florida
Attn: Dr. R. Fledderman
Pensacola, FL 32504

Space Research Corporation
Chittenden Bank Building
Attn: Library
       J. A. Finkel
North Troy, VT 05859

The Aerospace Corporation
P.O. Box 92957
Attn: R. Hartunion
       W. Mann
       R. Allen
       T. Taylor
       J. Mullen
Los Angeles, CA 90009

DISTRIBUTION (Cont.)

Copies

Notre Dame University
Attn: Dr. T. Muller
       Dr. V. Nee
       Dr. F. Raven
       Dr. R. Nelson
       Dept. of Aero. Engineering
       College of Engineering
       Library
Notre Dame, IN 46556

Prototype Development Association
1740 Garry Avenue
Suite 201
Attn: Mr. J. Dunn
       Mr. M. Sherman
Santa Ana, CA 92705

Systems Research Labs., Inc.
2800 Indian Ripple Road
Attn: Dr. C. Ingram
Dayton, OH 45440

Naval Air Test Facility
Attn: Dr. W. Sule
Lake Hurst, NJ 08733

Chrysler Corp., Defense Div.
Attn: Dr. R. Lusardi
Detroit, MI 48231

TRW
One Space Park
Attn: B. Pearce, Aerodynamics Dept.
Redondo Beach, CA 90278

Army Aviation Systems Command
P.O. Box 209, Main Office
Attn: Dr. L. Lijewski
St. Louis, MO 63166

Air Force Weaons Laboratory
Attn: CAPT Tolman/SAS
Kirtland AFB, NM 87117

California Polytechnic State University
Attn: Dr. J. D. Nicolaides, Head
          Aeronautical Engineering Dept.
San Luis Obispo, CA 93407

DISTRIBUTION (Cont.)

Copies

General Electric Company
3198 Chestnut Street
Attn: John Cassanto
Philadelphia, PA   19101

Acurex Corporation
485 Clyde Avenue
Attn: Joe Hartman
Mt. View, CA   94042

Lockheed Missile & Space
P.O. Box 504
Attn: John Kaku
Sunnyvale, CA   94088

GARD, Inc.
7449 North Natchez Avenue
Attn: Tom Mathieson
Niles, IL   60648

TRW DSSG MI/1409
One Space Park
Attn: C. Wright
Redondo Beach, CA   90278

Systems, Science & Software
P.O. Box 1620
Attn: P. Coleman
La Jolla, CA   92038

Thermo King Corporation
314 W. 90th
Attn: Robert Tessmann
Minneapolis, MN   55420

United Technologies
P.O. Box 358
Attn: K. Nakamura
Sunnyvale, CA   94088

United Technologies - CSD
P.O. Box 358
Attn: Eric C. Huffman
Sunnyvale, CA   94088

DISTRIBUTION (Cont.)

Copies

Sandia Laboratories
Division 5633
Attn: G. F. Wright
Albuquerque, NM 87110.

G. F. M. Claessems
H. Pouwels
National Aerospace Lab.
Anthony Fokker - Weg 2
Amsterdam
The Netherlands

TO AID IN UPDATING THE DISTRIBUTION LIST
FOR NAVAL SURFACE WEAPONS CENTER, WHITE
OAK TECHNICAL REPORTS PLEASE COMPLETE THE
FORM BELOW:

TO ALL HOLDERS OF NSWC TR 79-325
                    by Robert Kavetsky
DO NOT RETURN THIS FORM IF ALL INFORMATION IS CURRENT

A. FACILITY NAME AND ADDRESS (OLD) (Show Zip Code)

NEW ADDRESS (Show Zip Code)

B. ATTENTION LINE ADDRESSES:

C.

☐ REMOVE THIS FACILITY FROM THE DISTRIBUTION LIST FOR TECHNICAL REPORTS ON THIS SUBJECT.

D.

NUMBER OF COPIES DESIRED